signals

MDPI

Article

The Linear Series Decomposition Learner (LSDL): A Multi-Geometric Theory of Signal Structure and Representation

Ejay Nsugbe

Nsugbe Research Labs, Swindon SN1 3LG, UK; ennsugbe@yahoo.com

Abstract

Signal representation underpins modern signal processing, yet many existing methods primarily transform signals into alternative domains without explicitly modelling how informative signal structure evolves during recursive localisation. This paper presents the Linear Series Decomposition Learner (LSDL), a multi-geometric theory of signal structure and representation founded on recursive support localisation. The LSDL is formulated as a recursive localisation operator acting on a fixed amplitude-reference domain, thereby establishing a mathematically rigorous framework for analysing the evolution of signal support across successive localisation levels. Theoretical analysis characterises the fundamental properties of the operator, including support evolution, monotonicity, finite recursion, perturbation stability, and admissible localisation, and it thereby provides a formal foundation for recursive signal decomposition. Building upon this operator-theoretic formulation, the proposed framework establishes that recursive support localisation induces multiple complementary geometries of signal structure. These comprise support geometry, which describes the organisation of retained signal support; discriminative geometry, which characterises class separability under recursive localisation; information geometry, which quantifies entropy redistribution and information concentration; persistence geometry, which models the emergence, evolution, and lifetime of localised signal structures across recursive filtrations; and spectral geometry, which describes recursion-induced reorganisation within the frequency domain. Collectively, these complementary geometries provide a coherent multi-geometric representation that captures structural, statistical, topological, and spectral characteristics within a common mathematical framework. The proposed theory is supported through analytical development and empirical evaluation using synthetic benchmark signals, real-world electromyographic (EMG) datasets, and comparative analyses against established signal representation approaches, including the short-time Fourier transform (STFT), wavelet transforms, empirical mode decomposition (EMD), variational mode decomposition (VMD), and sparse coding. Experimental results demonstrate that recursive support localisation produces interpretable multi-geometric representations while maintaining competitive classification performance and low online computational cost. By establishing recursive support localisation as a principled mechanism through which complementary signal geometries emerge, the LSDL provides a mathematically grounded framework for interpretable signal representation, structural analysis, and representation learning across diverse signal-processing applications.

Check for updates

Academic Editor: Ignacio Bosch Roig

Received: 2 July 2026
Revised: 3 August 2026
Accepted: 11 August 2026
Published: 18 August 2026

Copyright: © 2026 by the author. Licensee MDPI, Basel, Switzerland. This article is an open access article distributed under the terms and conditions of the Creative Commons Attribution (CC BY) license.

Keywords: recursive support localisation; operator-theoretic signal representation; multi-geometric representation; support geometry; information geometry; persistence geometry; spectral geometry; representation learning

1. Introduction

Information extraction of informative structure from complex signals remains a fundamental challenge across signal processing, mechanical systems, biomedical engineering, and intelligent sensing [1–3]. Real-world signals are often characterised by nonstationarity, transient dynamics, nonlinear interactions, and heterogeneous noise, and diagnostically relevant information is frequently concentrated in sparse, localised regions rather than distributed uniformly over time [1–3]. As a result, identifying and characterising informative signals has long been a central objective of modern signal analysis [1–3].

Classical approaches, including Fourier analysis, short-time Fourier transforms, and wavelet decompositions, provide powerful signal representations through transform-domain projections [4–7]. More recently, sparse coding, compressed sensing, and representation-learning methods have sought compact latent descriptions of signal structure [4–7]. These approaches primarily operate in transformed or learned spaces and therefore often provide only indirect insight into how informative signal structure evolves in the original signal domain [4–7]. Consequently, the relationship among signal support, information content, persistence, and spectral organisation remains fragmented across separate analytical domains [4–7].

This motivates an alternative perspective in which signal structure is examined through recursive support evolution [7]. Rather than projecting signals into predefined bases or learned embeddings, recursive localisation progressively contracts signal support, exposing structures that persist under increasingly restrictive localisation criteria [7]. This formulation generates a hierarchy of nested-support representations whose evolution can be studied geometrically, statistically, and spectrally [7].

In this work, we formalise the Linear Series Decomposition Learner (LSDL) as a recursive support-filtration framework [8,9]. The central premise is that recursive amplitude localisation generates an evolving support manifold from which multiple complementary representations emerge [8,9]. Specifically, the framework induces sparse-support geometry, information geometry, persistence geometry, and spectral geometry from a common localisation trajectory, enabling the simultaneous analysis of structural concentration, information organisation, threshold-stable features, and oscillatory behaviour [8,9].

Unlike conventional recursive thresholding procedures, which generally use threshold updates to produce a final segmented, suppressed, or component-isolated signal, the proposed framework assigns representational meaning to the entire threshold trajectory. The LSDL is formulated as a mathematically defined family of support-localisation operators that generate finite, nested-support filtrations. The evolution of these filtrations is then used to quantify support contraction, energetic concentration, informational concentration, perturbation stability, structural persistence, and spectral reorganisation. The resulting geometries therefore arise intrinsically from recursive support evolution rather than from external feature fusion, basis projection, or latent-space optimisation.

The principal contributions of this work are fourfold:

1. We establish the LSDL as a recursive support-filtration operator with finite localisation dynamics and nested-support structures.
2. We introduce a multi-geometric signal representation that unifies support, information, persistence, and spectral geometries.

3. We develop theoretical formulations for robustness, information concentration, persistence stability, and discriminative separability under recursive localisation.
4. We demonstrate through extensive simulations that recursive support filtration can reveal latent signal structure, improve class separability, enhance information concentration, and expose persistent oscillatory organisation.

Collectively, these developments position recursive support localisation as a general signal representation paradigm in which meaningful structure emerges through the evolution of signal support itself. The resulting framework provides an interpretable and computationally efficient route for representing signal structure within a single mathematically coherent formulation.

2. Related Work

Identifying the informative structure in complex signals has been studied extensively in signal processing, machine learning, applied mathematics, and dynamical systems [10]. Existing approaches can be broadly categorised by the representation domain in which signal structure is analysed, including transform-domain methods, sparse representations, information-theoretic domains, topological analyses, and modern representation-learning approaches [10].

2.1. Transform-Domain Signal Representations

Fourier analysis remains one of the foundational tools in signal processing, providing a global frequency-domain description of signal behaviour [11]. Extensions such as the short-time Fourier transform (STFT) and wavelet transforms were introduced to address the limitations of purely global spectral representations by incorporating localised time-frequency analysis [11]. These methods have achieved widespread use in vibration monitoring, biomedical signal analysis, communications, and condition monitoring because they can characterise oscillatory and multiscale phenomena.

Despite their effectiveness, transform-based methods operate through projections onto predefined basis functions. Consequently, the resulting representations primarily describe spectral or time–frequency organisation rather than the evolution of informative support within the original signal domain. By contrast, the LSDL complements rather than replaces transform-domain analysis by examining how signal structure emerges through recursive support localisation in amplitude space [9].

2.2. Sparse Signal Processing and Compressed Representations

Sparse representations have become central to modern signal processing through developments such as compressed sensing, sparse coding, dictionary learning, and related optimisation-based formulations [2,12]. These methods are based on the observation that many signals admit compact descriptions in suitably chosen bases or learned dictionaries [2,12]. Their success has led to important advances in denoising, reconstruction, classification, and feature extraction.

However, sparse representation frameworks are typically reconstruction-based, with sparsity defined relative to an external basis, dictionary, or measurement space. In contrast, the framework presented here examines sparsity directly through support evolution. Rather than seeking sparse coefficients, recursive localisation progressively contracts the signal support itself, allowing sparsity, information concentration, and structural persistence to be analysed within a common support-filtration framework [2,12].

2.3. Information-Theoretic Signal Analysis

Information-theoretic methods provide a complementary perspective by quantifying uncertainty, complexity, and discriminative content through measures such as entropy, mutual information, Kullback–Leibler divergence, and Jensen-Shannon divergence [13,14].

These approaches generally do not prescribe an explicit mechanism by which informative signal support is progressively revealed. In the present study, information-theoretic quantities arise naturally from recursive support localisation, allowing information concentration and discriminative divergence to be interpreted as consequences of support evolution rather than as independent optimisation objectives [13,14].

2.4. Topological and Persistence-Based Approaches

Topological Data Analysis (TDA) and persistent homology have introduced effective methods for characterising structures that remain stable across scales [15,16]. Persistence-based approaches have been applied successfully to time series, dynamical systems, biomedical signals, and complex networks, where stability across scales often has important physical meaning [15,16].

Although persistence methods typically operate on geometric embeddings, simplicial complexes, or reconstructed state spaces, the proposed framework generates persistence directly from recursive amplitude-support filtrations [15,16]. Consequently, persistence is treated not as a separate post-processing step but as an inherent property of support evolution itself. This provides a direct link between localisation dynamics and threshold-stable signal structures [15,16].

2.5. Representation Learning and Latent Signal Geometry

Recent advances in machine learning have increasingly focused on representation learning through deep neural networks, manifold learning, self-supervised learning, and hybrid feature-learning architectures [17,18]. These methods have shown strong performance across numerous signal-analysis tasks by constructing task-specific latent representations.

Despite their predictive success, latent representations often have limited interpretability and may provide only limited insight into the physical organisation of signal structure [17,18]. The proposition here pursues a complementary objective. Rather than learning latent spaces through optimisation, recursive support localisation generates interpretable geometric representations directly from signal organisation [17,18]. The resulting support, information, persistence, and spectral geometries may therefore be viewed as physically grounded latent manifolds induced by recursive support evolution.

2.6. Positioning Relative to Prior LSDL Research

Foundations of the Linear Series Decomposition Learner

The LSDL did not emerge as an isolated signal-processing heuristic but rather as a methodological family developed across a sequence of empirical signal-analysis studies [8,9,19–22]. Its earliest motivating context was acoustic-emission monitoring of particulate and powder systems, in which informative structure was embedded in non-stationary, transient-rich signals and required amplitude-localised decomposition before feature extraction and prediction [8,9,19–22]. Subsequent work extended the same decomposition logic to physiological and biomedical domains, including prosthesis-control biosignals, electromyography–electroencephalography phantom-motion decoding, uterine contraction analysis, labour imminence prediction, depth-of-anaesthesia monitoring, and multimodal sensing [8,9,19–22].

Across these studies, the LSDL was primarily used as an application-driven decomposition tool. The recurring empirical finding was that recursively localising signal regions through amplitude-indexed thresholding could reveal informative support, reduce redundancy, improve feature quality, and enhance downstream classification or prediction [8,9,19–22]. However, the mathematical structure underlying these observations remained dispersed across application-specific implementations. Prior work established the practical utility of the LSDL but did not fully formalise its operator structure, support-filtration dynamics, information-theoretic behaviour, persistence properties, or spectral consequences [8,9,19–22].

The present work therefore reframes the LSDL as a recursive support-filtration framework. Rather than treating the method as a tuned thresholding procedure, we show that the LSDL induces a nested sequence of support sets from which several complementary geometries emerge. These include sparse-support geometry, information geometry, perturbation-stability geometry, persistence geometry, spectral localisation geometry, and fused multi-geometric representations. This provides a theoretical basis for understanding why earlier LSDL applications improved signal interpretability and predictive performance across heterogeneous domains.

Accordingly, the contribution of this paper is not the empirical introduction of the LSDL but the formalisation of its underlying signal-representation theory. The paper unifies prior application-specific uses of the LSDL under a common mathematical framework and establishes recursive support evolution as the central organising principle of the method.

The novelty of the present study should therefore be distinguished from the original empirical introduction of the LSDL. The recursive amplitude-localisation procedure has previously been used as an application-specific decomposition method. The present work, however, formalises this procedure as a family of support-localisation operators and treats the complete recursive trajectory as a signal representation in its own right. Specifically, it establishes explicit upper- and lower-support operators, finite and nested-support filtrations, support-contraction and energy non-expansion properties, robustness-preserving admissibility conditions, and objective-dependent localisation depth. From this common filtration, the study derives support, information, persistence, and spectral geometries and then combines them within a multi-geometric representation.

This formulation also differs from conventional recursive thresholding. In conventional threshold-based procedures, recursion is generally used to obtain a segmented, denoised, or component-isolated output, and the intermediate threshold trajectory carries limited representational significance. In the LSDL, by contrast, the sequence of thresholds and retained-support sets constitutes the primary analytical object. Structure is characterised through how support contracts, how information and energy are redistributed, and how oscillatory organisation changes throughout the filtration. The LSDL is therefore not presented merely as another recursive threshold-selection rule but as a support-filtration framework in which recursive threshold evolution generates multiple complementary and physically interpretable representations of the original signal.

Figure 1 shows an illustrative diagram of this concept, and Table 1 presents a comparison of the LSDL, its prior applications, and the framework proposed in this paper.

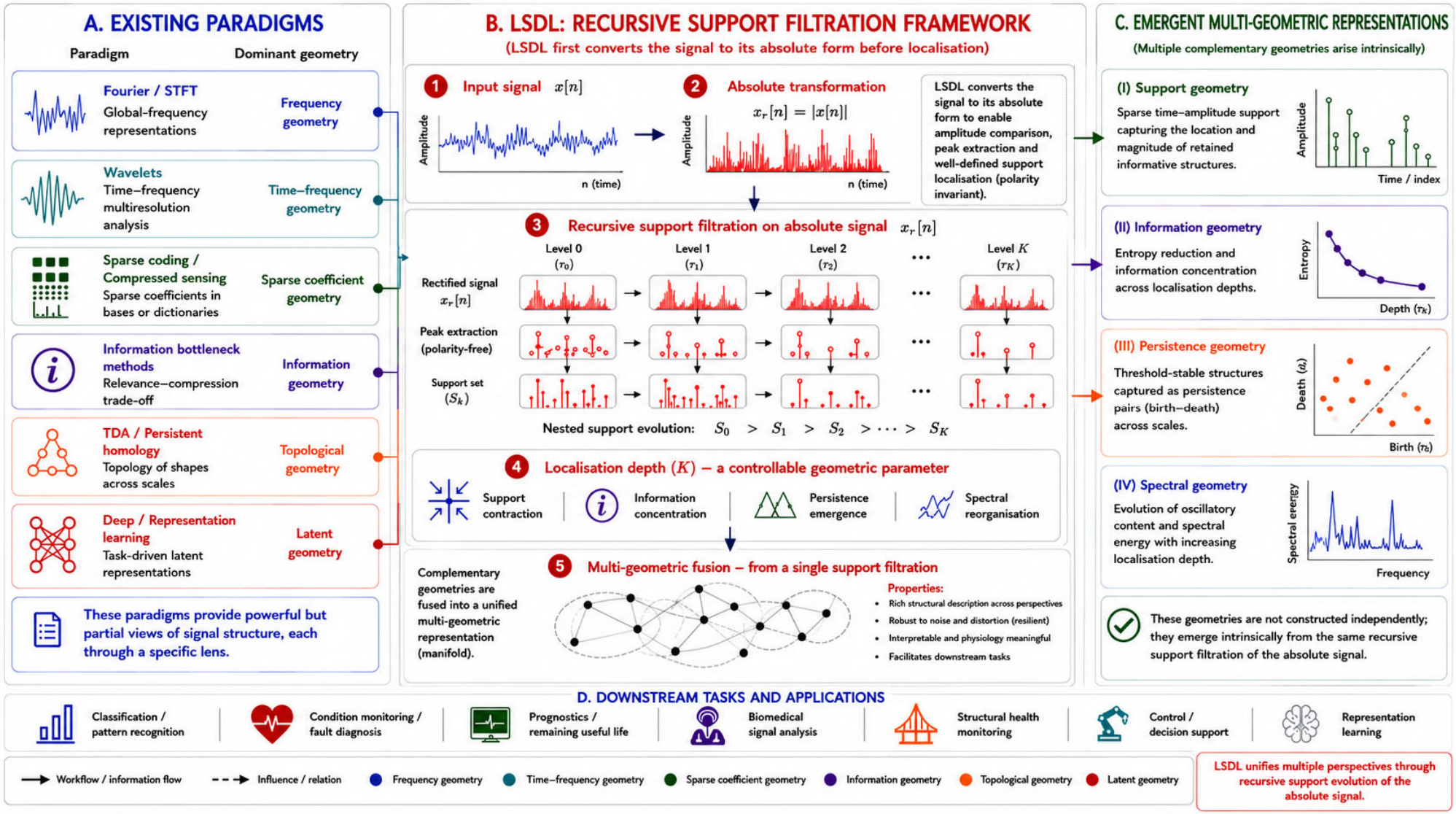


Figure 1. An overview diagram of the LSDL and its architecture. Figure 1 summarises the conceptual progression developed in this study: the left-hand panel situates the LSDL relative to established signal representation paradigms, including Fourier and short-time Fourier analysis, wavelet decomposition, sparse

representation, information-theoretic analysis, topological methods, and learned latent representations. These approaches provide complementary descriptions of signal structure, but they generally operate through separate transform domains, basis systems, topological constructions, or learned embeddings. The central panel illustrates the defining mechanism of the LSDL, in which an input signal is first mapped to a fixed amplitude-reference domain, from which recursively evolving upper-support and lower-support regions are generated. The upper branch progressively retains amplitudes of increasing dominance, whereas the lower branch progressively contracts the positive residual-support region. The complete sequence of thresholds, masks, and retained supports forms the recursive support filtration. This trajectory, rather than only its final output, constitutes the principal analytical object of the proposed framework. The right-hand panel shows how four complementary representations are derived from this common filtration. Support geometry describes contraction, sparsity, and energy concentration; information geometry quantifies entropy and the distribution of information within the retained support; persistence geometry characterises structures that remain stable across localisation depths; and spectral geometry examines recursion-dependent changes in oscillatory organisation. These domains are then evaluated separately and subsequently combined within a multi-geometric representation. The lower part of the figure indicates the intended role of the framework in downstream signal-analysis tasks. The LSDL is not presented as a replacement for all existing transforms or representation-learning methods. Instead, it provides a support-centred analytical layer through which structural, informational, persistent, and spectral properties can be studied within a common recursive trajectory.

Table 1. Comparison of prior related LSDL work.

LSDL-Related Work	Domain	What It Established	Limitation Left Open	What the New Foundations Paper Contributes
Acoustic-emission particle-size and powder-mixture studies [8]	Mechanical/process monitoring	Amplitude-localised decomposition could help isolate informative transient structure in noisy AE signals	Method was application-specific and not yet formalised as a general support-filtration operator	Defines recursive localisation as a general support-evolution process
Gesture recognition using EMG/NIR [22]	Prosthesis control	Demonstrated physiological signal features could support motion decoding	Decomposition theory not yet central	Connects the LSDL to interpretable biosignal representation
Transhumeral phantom-motion decoding [9]	EMG/EEG prosthesis control	Compared LSDL-style time-domain decomposition against raw and wavelet-decomposed signals; showed improved decoding performance	Treated the LSDL largely as a practical decomposition method	Formalises the same process as recursive support filtration

Table 1. *Cont.*

LSDL-Related Work	Domain	What It Established	Limitation Left Open	What the New Foundations Paper Contributes
Uterine contraction signal decomposition [19]	EHG/Toco labour prediction	Applied the LSDL explicitly to contraction signals for preterm and birth-imminency prediction	Application-specific validation without full theory	Explains the LSDL as information localisation over support manifolds
Magnetomyography labour imminency work [20]	Maternal physiological sensing	Extended decomposition logic to low-complexity physiological prediction	Did not generalise decomposition mechanics into formal theory	Adds robustness, admissibility, and support-feasibility concepts
Multiscale depth-of-anaesthesia EEG work [21]	EEG anaesthesia monitoring	Used the LSDL in neural oscillation/state prediction	Frequency behaviour and spectral consequences remained partly unresolved	Adds spectral localisation and oscillatory geometry
Shoulder-girdle/contraction-force prosthesis studies [23]	EMG/Accelerometer/NIR-style prosthesis control	Explored decomposition for force, gesture, and anatomical activation decoding	Did not unify decomposition-depth selection across objectives	Introduces objective-dependent optimality: RI, MI, and classifier accuracy
Current foundations paper	General signal processing	—	—	Converts prior empirical LSDL work into an operator-theoretic, multi-geometric signal representation framework

Taken together, the existing literature demonstrates the practical effectiveness of the LSDL, but it also reveals a common limitation: the absence of a mathematical description. This paper addresses this gap by formalising the decomposition process within a recursive support-localisation framework and by demonstrating its operator-theoretic, geometric, and spectral foundations.

3. Operator-Theoretic Foundations of Recursive Support Localisation

3.1. Overview

The LSDL is a recursive support-filtration approach that localises informative signal structure directly in amplitude-support space [3,4]. Unlike transform-based approaches that rely on harmonic bases or learned dictionaries, the LSDL progressively separates salient and residual signal components through recursive threshold-based localisation [3,4]. All supporting proofs for propositions made can be seen in the Appendices A and B.

Let

$$x = \{x_n\}_{n=1}^{N}$$

denote a discrete-time signal and define its amplitude representation

$$y_n = \mid x_n \mid,$$

where N is the signal length and y_n is the amplitude at sample n.

The maximum amplitude is

$$M = \max_n y_n.$$

The objective is to recursively localise dominant support regions while preserving peak topology and suppressing non-informative support.

3.2. Support-Localisation Operators

Two complementary support sets are defined [9,10].

Upper support is defined as

$$S_\tau^U(y) = \{n : y_n \geq \tau\},$$

which retains amplitudes above threshold τ.

Lower support is defined as

$$S_\tau^L(y) = \{n : y_n < \tau\},$$

which retains amplitudes below threshold τ.

The corresponding localisation operators are

$$L_\tau^U(y) = y \odot \mathbf{1}_{S_\tau^U(y)},$$
$$L_\tau^L(y) = y \odot \mathbf{1}_{S_\tau^L(y)},$$

The upper operator preserves salient-support amplitudes, whereas the lower operator preserves residual-support amplitudes.

Peak topology is subsequently extracted using

$$P_\tau^B(y) = \text{findpeaks}\Big(L_\tau^B(y)\Big), B \in \{U, L\},$$

3.3. Recursive Threshold Filtration

Let

$$x = (x_1, \ldots, x_N)^\top \in \mathbb{R}^N$$

denote a finite discrete signal defined on the index set [9,10,15]

$$\Omega = \{1, \ldots, N\}.$$

The fixed amplitude representation of x is

$$a = \mathcal{A}(x) = (a_1, \ldots, a_N)^\top, a_i = \mid x_i \mid,$$

with maximum amplitude

$$A_{\max} = \parallel x \parallel_\infty = \max_{i \in \Omega} a_i.$$

The vector a is computed once from the original input signal and retained as the common amplitude-reference domain throughout the localisation process. Consequently, thresholds at different recursion depths remain directly comparable and are not redefined from progressively masked intermediate signals.

Let

$$b \in \{U, L\}$$

denote the upper or lower localisation branch. For both branches, initialise the recursively propagated signal as

$$x_0^b = x.$$

Let $\alpha \in (0, 1)$ denote the threshold-update parameter. Given initial thresholds

$$0 \leq \tau_0^L \leq \tau_0^U \leq A_{\max}$$

the upper threshold is updated according to

$$\tau_{k+1}^U = \tau_k^U + \alpha\left(A_{\max} - \tau_k^U\right), k \geq 0,$$

whereas the lower threshold is updated according to

$$\tau_{k+1}^L = (1 - \alpha)\tau_k^L, k \geq 0.$$

The equation produces a non-decreasing upper-threshold sequence satisfying

$$\tau_k^U \uparrow A_{\max},$$

This equation produces a non-increasing lower-threshold sequence satisfying

$$\tau_k^L \downarrow 0.$$

At recursion depth k, the upper support is defined by

$$S_k^U = \left\{i \in \Omega : a_i \geq \tau_k^U\right\},$$

and the lower support is defined by

$$S_k^L = \left\{i \in \Omega : 0 < a_i \leq \tau_k^L\right\}.$$

The exclusion of $a_i = 0$ from the lower branch ensures that zero-valued samples introduced by previous masking operations are not interpreted as a retained residual signal structure.

The corresponding binary masks are

$$m_k^U(i) = 1_{\{a_i \geq \tau_k^U\}},$$

and

$$m_k^L(i) = 1_{\{0 < a_i \leq \tau_k^L\}},$$

or, in general branch notation,

$$m_k^b(i) = 1_{\{i \in S_k^b\}}, b \in \{U, L\}.$$

The recursively localised signal is then defined by

$$x_k^b = x_{k-1}^b \odot m_k^b, k = 1, \ldots, K,$$

where $\odot$ denotes elementwise multiplication.

Component wise, the upper-branch recursion is

$$\left[x_k^U\right]_i = \left[x_{k-1}^U\right]_i \mathbf{1}_{\{a_i \geq \tau_k^U\}},$$

whereas the lower-branch recursion is

$$\left[x_k^L\right]_i = \left[x_{k-1}^L\right]_i \mathbf{1}_{\{0 < a_i \leq \tau_k^L\}}.$$

Thus, the signal entering recursion level k is the output x_{k-1}^b retained from the preceding level. However, support membership at every level is evaluated using the fixed original amplitude vector $a = |\, x \,|$.

3.3.1. Reference-Conditioned Localisation Operator

To distinguish the signal being masked from the signal defining the amplitude-reference domain, define the localisation operator as [9,15]

$$\mathcal{L}_\tau^b(z; x),$$

where z is the current recursively propagated signal; x is the fixed original reference signal; and τ is the threshold applied at the current depth.

For the upper branch,

$$\left[\mathcal{L}_\tau^U(z; x)\right]_i = z_i \mathbf{1}_{\{|x_i| \geq \tau\}},$$

and for the lower branch,

$$\left[\mathcal{L}_\tau^L(z; x)\right]_i = z_i \mathbf{1}_{\{0 < |x_i| \leq \tau\}}.$$

The recursive update is therefore written precisely as

$$x_k^b = \mathcal{L}_{\tau_k^b}^b\left(x_{k-1}^b; x\right).$$

This notation removes the ambiguity that would arise from writing only

$$\mathcal{L}_{\tau_k^b}^b(x_{k-1}^b),$$

which could incorrectly suggest that the threshold support is recomputed from the amplitude distribution of the intermediate signal.

3.3.2. Cumulative-Support Representation

A repeated substitution yields

$$x_k^b = x \odot m_1^b \odot m_2^b \odot \cdots \odot m_k^b.$$

Define the cumulative mask

$$\bar{m}_k^b = \bigodot_{j=1}^{k} m_j^b,$$

so that

$$x_k^b = x \odot \bar{m}_k^b.$$

The support of the cumulative mask is

$$\bar{S}_k^b = \bigcap_{j=1}^{k} S_j^b.$$

As the upper thresholds are non-decreasing,

$$\tau_{k+1}^U \geq \tau_k^U,$$

the upper supports satisfy

$$S_{k+1}^U \subseteq S_k^U.$$

Likewise, because the lower thresholds are non-increasing,

$$\tau_{k+1}^L \leq \tau_k^L,$$

the lower supports satisfy

$$S_{k+1}^L \subseteq S_k^L.$$

For either branch,

$$S_{k+1}^b \subseteq S_k^b.$$

Consequently,

$$\bar{S}_k^b = \bigcap_{j=1}^{k} S_j^b = S_k^b,$$

and therefore

$$\bar{m}_k^b = m_k^b.$$

It follows that the recursive representation may equivalently be written as

$$x_k^b = x \odot m_k^b.$$

Hence,

$$x_k^b = \mathcal{L}_{\tau_k^b}^b\left(x_{k-1}^b; x\right) = \mathcal{L}_{\tau_k^b}^b(x; x) = x \odot m_k^b$$

under the stated monotonic threshold conditions.

The first equality is the sequential computational form, in which the output from recursion depth $k-1$ is passed to depth k. The second and third equalities give the cumulative analytical form, in which the depth-k signal is expressed directly as a masked version of the original input.

The sequential form describes the implemented localisation process, whereas the cumulative form is used in subsequent theoretical analysis because it makes support contraction, energy behaviour and persistence across localisation depth explicit.

3.3.3. Absorption Property of Nested Localisation Operators

For the upper branch,

$$\left[\mathcal{L}^{U}_{\tau_k^U}\left(\mathcal{L}^{U}_{\tau_{k-1}^U}(x;x);x\right)\right]_i = x_i \mathbf{1}_{\{a_i \geq \tau_{k-1}^U\}} \mathbf{1}_{\{a_i \geq \tau_k^U\}}.$$

Since

$$\tau_k^U \geq \tau_{k-1}^U,$$

the condition $a_i \geq \tau_k^U$ implies $a_i \geq \tau_{k-1}^U$. Therefore,

$$\mathbf{1}_{\{a_i \geq \tau_{k-1}^U\}} \mathbf{1}_{\{a_i \geq \tau_k^U\}} = \mathbf{1}_{\{a_i \geq \tau_k^U\}},$$

and hence

$$\mathcal{L}^{U}_{\tau_k^U} \circ \mathcal{L}^{U}_{\tau_{k-1}^U} = \mathcal{L}^{U}_{\tau_k^U}.$$

Similarly, for the lower branch,

$$\left[\mathcal{L}^{L}_{\tau_k^L}\left(\mathcal{L}^{L}_{\tau_{k-1}^L}(x;x);x\right)\right]_i = x_i \mathbf{1}_{\{0 < a_i \leq \tau_{k-1}^L\}} \mathbf{1}_{\{0 < a_i \leq \tau_k^L\}}.$$

Since

$$\tau_k^L \leq \tau_{k-1}^L,$$

the condition $0 < a_i \leq \tau_k^L$ implies $0 < a_i \leq \tau_{k-1}^L$. Therefore,

$$\mathbf{1}_{\{0 < a_i \leq \tau_{k-1}^L\}} \mathbf{1}_{\{0 < a_i \leq \tau_k^L\}} = \mathbf{1}_{\{0 < a_i \leq \tau_k^L\}},$$

and hence

$$\mathcal{L}^{L}_{\tau_k^L} \circ \mathcal{L}^{L}_{\tau_{k-1}^L} = \mathcal{L}^{L}_{\tau_k^L}.$$

More generally,

$$\mathcal{L}^{b}_{\tau_k^b} \circ \mathcal{L}^{b}_{\tau_{k-1}^b} \circ \cdots \circ \mathcal{L}^{b}_{\tau_1^b} = \mathcal{L}^{b}_{\tau_k^b}$$

for $b \in \{U, L\}$.

The prior equation is the absorption property of the nested localisation operators, and it establishes formally that recursively applying all preceding masks produces the same depth-k signal as applying the cumulative depth-k mask directly to the original signal.

An algorithmic flow and pseudocode for the LSDL recursive support localisation can be seen in Algorithm 1.

Algorithm 1. LSDL Recursive Support Localisation [9,10,20,21]

Input: Signal $\mathbf{x} \in \mathbb{R}^N$; branch $b \in \{U, L\}$; initial threshold $\tau_0^{(b)}$; update parameter α; maximum recursion depth $K_{\max}$; minimum support size $m_{\min}$; convergence tolerance ε_τ.
Output: Thresholds $\left\{\tau_k^{(b)}\right\}$, supports $\left\{\mathcal{S}_k^{(b)}\right\}$, and localised signals $\left\{\mathbf{x}_k^{(b)}\right\}$.

Compute
$a \leftarrow |x|$,
$a\max \leftarrow \max i$ ai
Initialise
$x - 1(b) \leftarrow x$
for $k = 0,\ldots, K\max$ do
    if $b = U$ then
        $Sk(b) \leftarrow \{i: ai \geq \tau k(b)\}$
    else
        $Sk(b) \leftarrow \{i: 0 < ai \leq \tau k(b)\}$
    end if
    Construct the binary mask
$mk,i(b) =$
$\{1, \quad$ if $i \in Sk(b)$
$0, \quad$ otherwise$\}$
    Localise the signal
$xk(b) \leftarrow xk - 1(b) \odot mk(b)$
    Store $\tau k(b)$, $Sk(b)$, $xk(b)$
    if $|Sk(b)| < m\min$ then
        break
    end if
    if $k \geq 1$ and
$Sk(b) = Sk - 1(b)$ and
$|\tau k(b) - \tau k - 1(b)| \leq \varepsilon\tau$ then
        break
    end if
    if $b = U$ then
        $\tau k + 1(U) \leftarrow \tau k(U) + \alpha(a\max - \tau k(U))$
    else
        $\tau k + 1(L) \leftarrow (1 - \alpha)\tau k(L)$
    end if
end for
return $\{\tau k(b), Sk(b), xk(b)\}$

3.4. Structural Properties of the Recursive Localisation Operators [24,25]

The recursive localisation mechanism is now characterised formally. Let

$$x = (x_1, \ldots, x_N)^\top \in \mathbb{R}^N$$

denote a finite discrete signal and let

$$a = \mathcal{A}(x) = (|\, x_1 \,|, \ldots, |\, x_N \,|)^\top \in \mathbb{R}^N_{\geq 0}$$

be its non-negative amplitude representation. Define

$$A_{\max} = \| \, x \, \|_\infty = \max_{1 \leq i \leq N} |\, x_i \,|.$$

The index set of the signal is

$$\Omega = \{1, \ldots, N\}.$$

For any threshold $\tau \in [0, A_{\max}]$, define the upper and lower retained-support sets by

$$S^U(\tau) = \{i \in \Omega : a_i \geq \tau\},$$

and

$$S^L(\tau) = \{i \in \Omega : 0 < a_i \leq \tau\}.$$

The exclusion of zero-amplitude samples from $S^L(\tau)$ prevents locations that carry no signal energy from being interpreted as residual signal structure. If zero-valued samples are retained in the numerical implementation, the same nesting results hold, but the lower-support cardinality includes the fixed zero-amplitude set and therefore does not necessarily converge to zero.

The corresponding localisation operators are defined component wise as

$$\left[\mathcal{L}^U_\tau(x)\right]_i = x_i \mathbf{1}_{\{a_i \geq \tau\}},$$

and

$$\left[\mathcal{L}^L_\tau(x)\right]_i = x_i \mathbf{1}_{\{0 < a_i \leq \tau\}},$$

where $\mathbf{1}_{\{.\}}$ denotes the indicator function. Equivalently, these operators may be written as diagonal support projections,

$$\mathcal{L}^b_\tau(x) = P^b_\tau x, b \in \{U, L\},$$

where

$$P^b_\tau = \operatorname{diag}\left(\mathbf{1}_{\{1 \in S^b(\tau)\}}, \ldots, \mathbf{1}_{\{N \in S^b(\tau)\}}\right).$$

For a fixed threshold, P^b_τ is an orthogonal coordinate projection satisfying

$$(P^b_\tau)^2 = P^b_\tau, (P^b_\tau)^\top = P^b_\tau.$$

Thus, the nonlinearity of the LSDL does not arise from the masking operation conditional on a fixed support but from the data-dependent construction and recursive evolution of the threshold and its associated support.

3.4.1. Assumptions Governing the Localisation Trajectory [9,15,20]

Let

$$\mathcal{T}^U = \left\{\tau^U_0, \tau^U_1, \ldots, \tau^U_K\right\}$$

and

$$\mathcal{T}^L = \left\{\tau^L_0, \tau^L_1, \ldots, \tau^L_K\right\}$$

denote the upper- and lower-threshold trajectories, respectively, over a finite recursion horizon

$$K \in \mathbb{N}.$$

The structural results below are established under the following assumptions.

Assumption 1. *Finite signal domain.*

The signal has finite length $N < \infty$, and every signal amplitude a_i is finite.

Assumption 2. *Common amplitude domain.*

Both localisation branches operate on the same fixed amplitude representation $a = \mathcal{A}(x)$ throughout the recursion. The signal is therefore not re-normalised independently at each depth unless that normalisation is incorporated explicitly into the threshold definition.

Assumption 3. *Monotonic upper-threshold trajectory.*

The upper threshold is non-decreasing:

$$0 \leq \tau_k^U \leq \tau_{k+1}^U \leq A_{\max}, k = 0, \ldots, K-1.$$

Assumption 4. *Monotonic lower-threshold trajectory.*

The lower threshold is non-increasing:

$$0 \leq \tau_{k+1}^L \leq \tau_k^L \leq A_{\max}, k = 0, \ldots, K-1.$$

Assumption 5. *Increasing localisation restrictiveness.*

A deeper recursion level corresponds to a more restrictive retention criterion. Consequently, upper localisation retains progressively higher-amplitude samples, whereas lower localisation retains progressively smaller subsets of the positive residual-amplitude region.

These assumptions are satisfied by the recursive threshold trajectories used in this study. In particular, the upper recursion advances towards $A_{\max}$, whereas the lower recursion advances towards zero. The resulting branches are therefore directionally different in amplitude space but equivalent in their set-theoretic effect: both generate progressively contracted retained supports.

At recursion depth k, write

$$S_k^U = S^U(\tau_k^U), S_k^L = S^L(\tau_k^L),$$

and

$$x_k^U = \mathcal{L}_{\tau_k^U}^U(x), x_k^L = \mathcal{L}_{\tau_k^L}^L(x).$$

The trajectories

$$\mathcal{F}^U = \left(S_0^U, S_1^U, \ldots, S_K^U\right)$$

and

$$\mathcal{F}^L = \left(S_0^L, S_1^L, \ldots, S_K^L\right)$$

are referred to as the upper- and lower-support filtrations.

Proposition 1. *Nested-support contraction.*

Under Assumptions 1–5, the upper and lower LSDL support trajectories form decreasing filtrations on Ω:

$$S_{k+1}^U \subseteq S_k^U, S_{k+1}^L \subseteq S_k^L, k = 0, \ldots, K-1.$$

Consequently,

$$|\, S_{k+1}^U \,| \leq |\, S_k^U \,|, |\, S_{k+1}^L \,| \leq |\, S_k^L \,|,$$

and the corresponding indicator masks satisfy the component-wise order relations

$$\mathbf{1}_{S_{k+1}^U} \preceq \mathbf{1}_{S_k^U}, \mathbf{1}_{S_{k+1}^L} \preceq \mathbf{1}_{S_k^L},$$

where $\preceq$ denotes the standard partial order on $\{0,1\}^N$.

Equivalently, the associated diagonal projection matrices satisfy

$$P_{k+1}^U P_k^U = P_k^U P_{k+1}^U = P_{k+1}^U,$$

and

$$P_{k+1}^L P_k^L = P_k^L P_{k+1}^L = P_{k+1}^L.$$

Thus, localisation at depth $k+1$ is invariant to prior localisation at depth k: once a sample has been removed from a branch, it cannot re-enter that branch at a later depth.

It follows that

$$\mathcal{K}_{\text{adm}} \subseteq \{0,1,\ldots,K\}$$

denote the non-empty set of admissible localisation depths, and let

$$J : \mathcal{K}_{\text{adm}} \to \mathbb{R}$$

be a specified empirical evaluation criterion. A selected localisation depth is defined by

$$k^* \in \arg\max_{k \in \mathcal{K}_{\text{adm}}} J(k).$$

As $\mathcal{K}_{\text{adm}}$ is finite and non-empty, the argmax set is non-empty, and this is a finite-search property rather than a substantive convergence or optimality theorem. It does not imply that k^* is unique, that it is optimal outside the evaluated trajectory, or that it generalises to unseen data. Where J is data-dependent, k^* must be selected within the training or validation procedure to avoid optimistic bias.

3.4.2. Experimental Validation

The proposed operator-theoretic framework was evaluated using the benchmark sunspot signal over twenty recursive localisation iterations, as can be seen in Figure 2.

Upper-Branch Dynamics

The upper localisation branch progressively concentrates signal structure into increasingly sparse salient-support regions.

The observed behaviour includes

- Monotonic threshold convergence toward the signal maximum;
- Progressive reduction in support density;
- Simplification of peak topology;
- Monotonic reduction in localised energy.

These observations are consistent with the theoretical support-contraction and energy non-expansion properties.

Lower-Branch Dynamics

The lower localisation branch progressively removes the residual-support structure.

The observed behaviour includes

- Threshold convergence toward zero;
- Progressive contraction of residual support;
- Extinction of residual peak topology;
- Elimination of residual-support energy.

The lower branch therefore acts as a residual-support suppression mechanism complementary to the upper branch. Figure 3 shows a series of diagrams of the lower-branch recursive localisation dynamics.

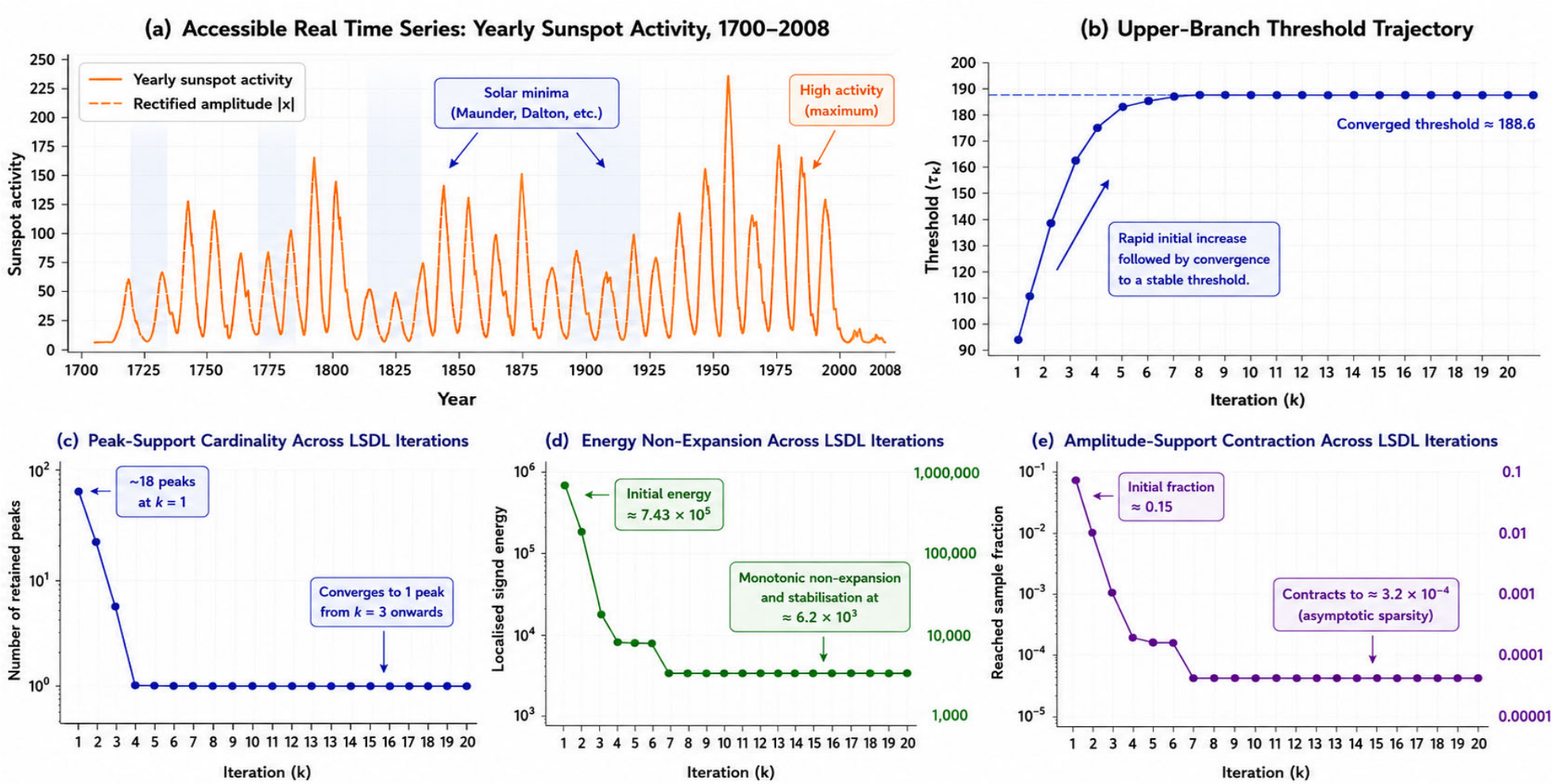


Figure 2. Upper-branch recursive localisation dynamics for the benchmark sunspot signal. (**a**) Input signal and rectified amplitude representation. (**b**) Upper-threshold evolution. (**c**) Peak-support cardinality. (**d**) Localised energy. (**e**) Retained-support density. The recursive localisation process progressively concentrates signal structure into increasingly sparse salient-support regions while exhibiting threshold convergence, support contraction, peak-topology simplification, and energy non-expansion.

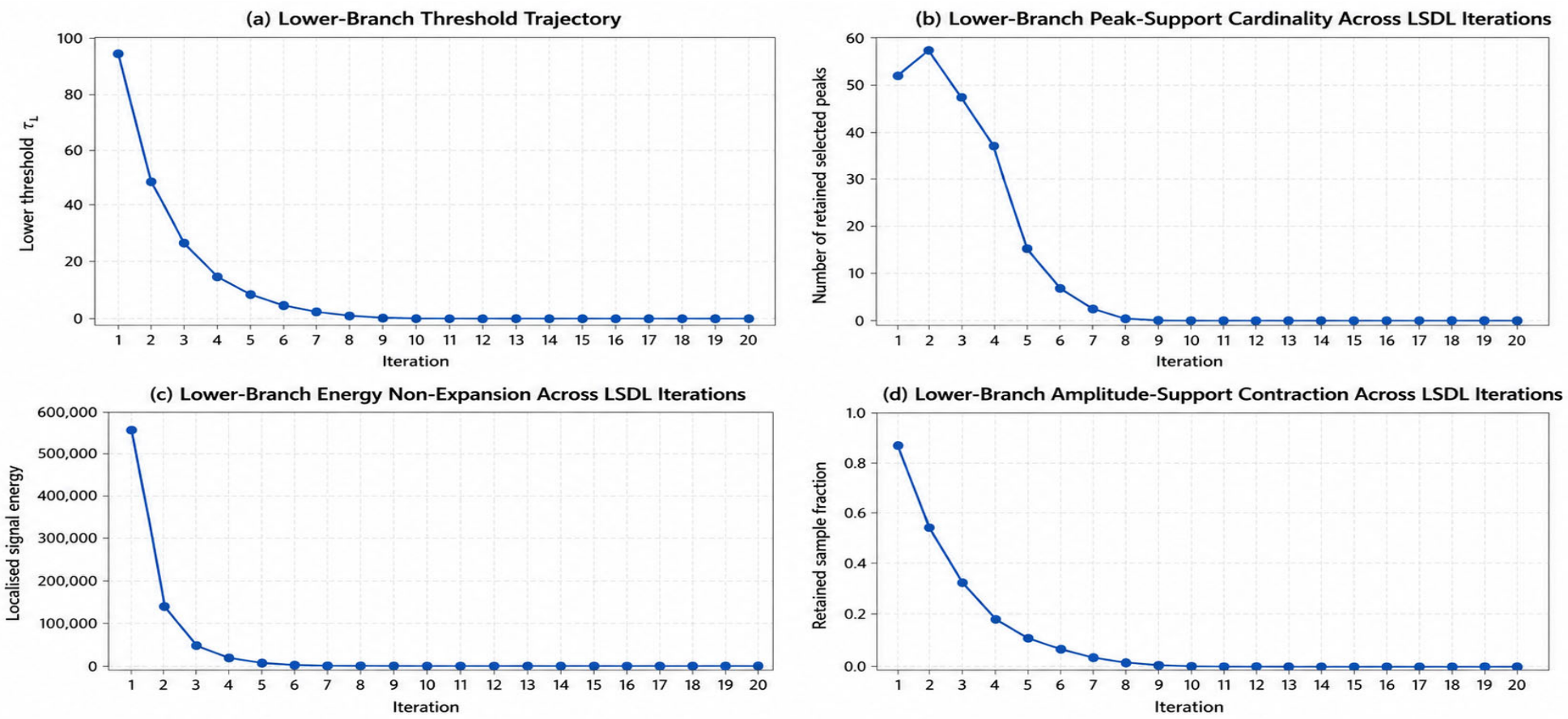


Figure 3. Lower-branch recursive localisation dynamics. (**a**) Lower branch threshold trajectory. (**b**) Lower branch peak support cardinality across LSDL iterations. (**c**) Lower branch energy non-expansion across LSDL iterations. (**d**) Lower branch amplitude support contraction across LSDL iterations. The recursive localisation process progressively contracts residual support, extinguishes peak topology, and removes residual-support energy as the threshold converges towards zero.

Generalisation to Physiological Electromyographic Signals

To demonstrate that the recursive localisation framework generalises beyond the illustrative benchmark signal, the proposed operator was further evaluated using a publicly available physiological electromyography (EMG) recording from the PhysioNet Examples of Electromyograms database. The selected recording corresponds to a healthy participant performing a sustained contraction of the tibialis anterior muscle and was sampled at 4 kHz after acquisition with a high-fidelity clinical EMG system. Unlike the benchmark sunspot series, this dataset represents a real biological signal characterised by broadband neuromuscular activity, transient motor-unit action potentials, and stochastic amplitude fluctuations. Consequently, it provides a substantially different signal morphology for assessing whether the theoretical properties of the recursive localisation operator remain valid under realistic physiological conditions.

Figure 4 illustrates the evolution of the recursive localisation process for the EMG signal. Consistent with the benchmark analysis, the upper branch shows monotonic threshold growth and converges rapidly toward the dominant signal amplitudes, whereas the lower branch shows monotonic threshold decay toward zero. This behaviour mirrors the convergence characteristics previously observed for the sunspot signal, indicating that the adaptive threshold-update mechanism is determined by the underlying support-selection process rather than by the specific signal domain.

The evolution of support density exhibits the same nested-support behaviour predicted by Propositions 1 and 2. As the upper threshold increases, progressively fewer samples satisfy the upper-support criterion, producing a sparser salient-support representation. Conversely, the lower-support region contracts steadily as the threshold approaches zero, eventually resulting in the complete extinction of residual support. The monotonic contraction observed in both branches closely follows the trends obtained for the benchmark signal and provides empirical evidence that the recursive support filtration behaves consistently across substantially different classes of time series.

Similarly, the retained energy trajectories exhibit behaviour analogous to the benchmark validation. The upper branch progressively concentrates signal energy into an increasingly compact set of dominant activations, whereas the lower branch rapidly loses residual energy until extinction. Although the absolute energy values differ from those observed for the sunspot series owing to the distinct statistical characteristics of physiological EMG, the qualitative monotonic behaviour remains unchanged. This agreement supports the theoretical non-expansion property of energy established in proposition and demonstrates that the recursive localisation mechanism preserves its fundamental energy concentration behaviour independently of signal modality.

Finally, the peak-cardinality trajectories further reinforce the consistency of the framework. The progressive reduction in the number of retained peaks reflects the same topological simplification previously observed for the benchmark signal, with increasingly sparse representations emerging as recursion proceeds. Importantly, despite the considerably greater complexity and stochastic variability of the EMG waveform, the recursive localisation process exhibits the same structural evolution as that obtained from the benchmark analysis.

Collectively, these results provide additional evidence that the proposed recursive localisation framework is signal-agnostic and reproduces the same convergence, support contraction, energy concentration, and topological simplification behaviours on an independent physiological biosignal. Rather than constituting a second validation study, this experiment demonstrates the robustness and generalisability of the theoretical framework across markedly different signal domains, thereby strengthening confidence that the recursive localisation operator captures intrinsic structural properties of one-dimensional signals rather than characteristics specific to the benchmark example.

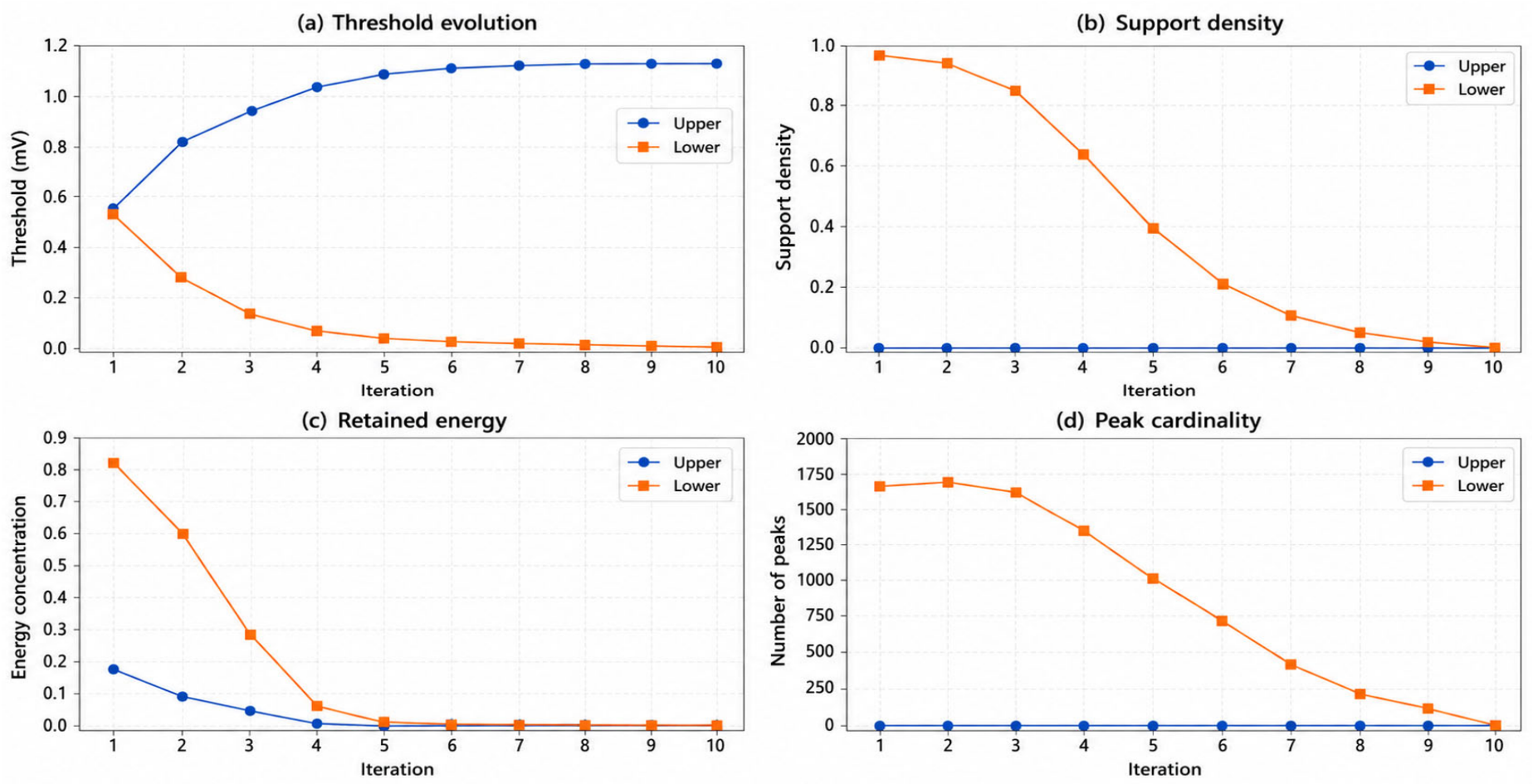


Figure 4. Recursive localisation trajectories for a healthy physiological EMG recording from the PhysioNet Examples of Electromyograms database. The signal was acquired from the tibialis anterior muscle of a healthy participant and analysed using the proposed recursive localisation framework. The upper branch demonstrates monotonic threshold growth with progressively contracting salient support, while the lower branch exhibits monotonic threshold decay leading to complete residual-support extinction. Corresponding reductions in support density, retained energy and peak cardinality closely mirror the behaviours observed for the benchmark sunspot signal, illustrating the consistency and signal-independent nature of the proposed recursive support-filtration framework.

3.4.3. Sensitivity Analysis of the Recursive Threshold Parameter

To investigate the practical behaviour of the proposed recursive threshold formulation, a sensitivity analysis was conducted using the publicly available EMG Data for Gestures dataset from the UCI Machine Learning Repository [26]. A binary classification task was selected to isolate the effect of the recursive threshold scaling parameter and to avoid additional variability associated with multiclass decision boundaries. Specifically, the analysis examined discrimination between Fist and Wrist Extension, which represent two physiologically distinct voluntary muscle activation patterns commonly used in myoelectric control studies.

The dataset includes recordings from 36 participants acquired with an eight-channel Myo armband. Signals were segmented into 40-sample windows with 50% overlap, corresponding to a 20-sample stride. To support a balanced evaluation while keeping computational demands manageable, 10 evenly distributed windows were selected from each gesture for every participant, yielding 720 analysis windows that were evenly divided between the two movement classes. Classification performance was evaluated using participant-grouped five-fold cross-validation with a standardised shrinkage Linear Discriminant Analysis (LDA) classifier.

The recursive threshold scaling parameter was evaluated over

$$\alpha \in \{0.25, 0.40, 0.50, 0.60, 0.75\},$$

thereby spanning progressively weaker to stronger recursive threshold updates.

Recursive localisation was applied independently to the upper and lower branches until one of two operational conditions was satisfied. Localisation terminated when either the retained support contained no more than one sample or the support mask remained unchanged across successive recursive iterations. Analysis of all recursive trajectories showed that these two conditions accounted for virtually all stopping events, whereas the maximum recursion depth and threshold tolerance served only as safety mechanisms and were not activated in the reported experiments. Consequently, the reported localisation depths represent the effective number of recursive localisation levels reached before support stabilisation.

As shown in Table 2, participant-averaged classification performance differed across the investigated scaling values. Mean balanced accuracy was highest at $\alpha = 0.25$, reaching 0.669 ± 0.123, and was closely followed by the conventional value $\alpha = 0.50$, which achieved 0.660 ± 0.125. Performance then declined progressively at larger scaling values, reaching its lowest mean balanced accuracy of 0.619 ± 0.110 at $\alpha = 0.75$.

The corresponding F1 results showed a somewhat different pattern. The highest mean F1 score was obtained at the conventional setting of $\alpha = 0.50$, with a value of 0.638 ± 0.148, whereas $\alpha = 0.25$ produced a similar value of 0.634 ± 0.160. Mean F1 subsequently decreased to 0.598 ± 0.132 at $\alpha = 0.75$. This pattern suggests that $\alpha = 0.50$ provided the most favourable balance between the two classes, despite $\alpha = 0.25$ yielding the highest mean balanced accuracy.

Increasing α reduced the upper-branch localisation depth from 2.916 to 2.119, indicating faster support contraction. Upper retained energy also decreased from 0.800 at $\alpha = 0.25$ to 0.530 at $\alpha = 0.75$, while lower-branch retained energy approached zero at the highest scaling value. Peak density similarly declined in both branches. Thus, larger values of α produced stronger and faster localisation, but this greater selectivity was not accompanied by improved classification performance.

Table 2. Sensitivity of LSDL behaviour to the recursive threshold scaling parameter α in the binary EMG exercise.

α	Balanced Accuracy	F1 Score	Upper Localisation Depth (Levels)	Lower Localisation Depth (Levels)	Upper Retained Energy	Lower Retained Energy	Upper Peak Density	Lower Peak Density
0.25	0.669 ± 0.123	0.634 ± 0.160	2.916	1.853	0.800	0.0120	0.856	0.491
0.40	0.640 ± 0.124	0.615 ± 0.160	2.731	2.331	0.674	0.0158	0.741	0.475
0.50	0.660 ± 0.125	0.638 ± 0.148	2.597	2.550	0.608	0.0149	0.681	0.388
0.60	0.633 ± 0.115	0.612 ± 0.144	2.406	2.622	0.574	0.0063	0.672	0.272
0.75	0.619 ± 0.110	0.598 ± 0.132	2.119	2.547	0.530	0.0010	0.638	0.147

Classification metrics are reported as participant-level mean $\pm$ standard deviation across 36 participants. Localisation variables summarise recursive behaviour across the analysed windows and channels. Retained energy is the proportion of original signal energy remaining at the terminal localisation level. Peak density is the number of detected peaks relative to retained-support size.

Overall, the results indicate that moderate scaling values provide the most appropriate operating range. The conventional value $\alpha = 0.50$ yielded the highest participant-averaged F1 score and classification performance close to the maximum balanced accuracy, while maintaining intermediate localisation depth, retained energy, and peak density. It may therefore be interpreted as a balanced compromise between aggressive support contraction and preservation of discriminative signal structure. A similar monotonic trend was observed in the structural characteristics of the recursively localised signals. As per Table 2 and Figure 5, increasing the recursive threshold scaling parameter progressively reduced the effective localisation depth of the upper branch while increasing the corresponding depth of the lower branch up to approximately $\alpha = 0.60$, after which a slight stabilisation was observed. These complementary patterns indicate that larger scaling values accelerate contraction of the upper support while delaying convergence within the lower support. Consistent with this behaviour, upper retained energy decreased monotonically from 0.800 at $\alpha = 0.25$ to 0.530 at $\alpha = 0.75$, whereas lower retained energy remained comparatively small across all operating points before approaching zero at the largest scaling value. Peak density likewise declined in both branches, indicating progressive simplification of the retained signal morphology as recursive threshold progression became increasingly aggressive.

Despite these substantial changes in recursive localisation behaviour, downstream classification performance remained comparatively stable across the investigated operating range. Mean participant-level balanced accuracy decreased only modestly from 0.669 ± 0.123 at $\alpha = 0.25$ to 0.619 ± 0.110 at $\alpha = 0.75$, while the highest mean F1 score was obtained at the conventional setting of $\alpha = 0.50$ (0.638 ± 0.148). These findings suggest that the historical midpoint recursion provides an effective compromise between preserving discriminative signal structure and achieving sufficient recursive localisation. Increasing the threshold scaling parameter beyond this operating point removes progressively more signal energy and structural complexity without producing corresponding improvements in classification performance.

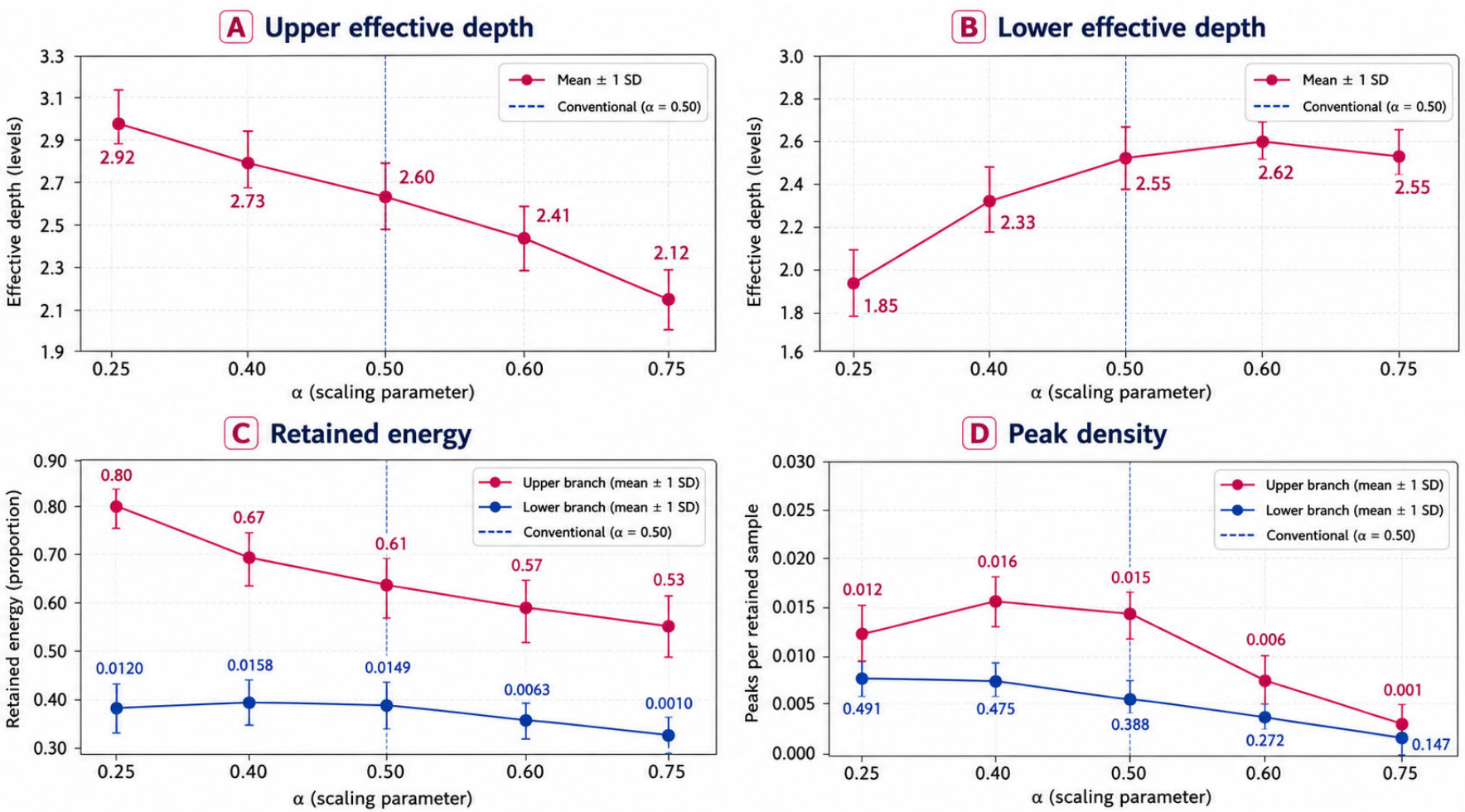


Figure 5. Sensitivity of recursive localisation behaviour to the threshold scaling parameter (α). Mean $\pm$ standard deviation across 36 participants is shown for (**A**) upper effective depth, (**B**) lowereffective depth, (**C**) retained energy, and (**D**) peak density. The dashed vertical line denotes the conventional operating point ($\alpha = 0.50$). Increasing α produces progressively more aggressive recursive localisation, characterised by reduced upper-branch localisation depth, lower retained energy and decreased peak density, while the lower branch exhibits a complementary increase in localisation depth before stabilisation. Collectively, these results demonstrate that the recursive threshold scaling parameter provides direct control over the localisation dynamics and structural complexity of the recursively localised signal.

Statistical analysis further supported the observed sensitivity of the recursive threshold scaling parameter (α). A Friedman test identified a statistically significant effect of α on participant-level balanced accuracy (Friedman $\chi^2(4) = 10.86$, $p = 0.028$, Kendall's $W = 0.075$), whereas the corresponding effect on F1 score did not reach statistical significance (Friedman $\chi^2(4) = 9.43$, $p = 0.051$, Kendall's $W = 0.066$). To control the family-wise error rate, post hoc Wilcoxon signed-rank comparisons between the conventional operating point ($\alpha = 0.50$) and the remaining scaling values were adjusted using the Holm procedure. Following multiplicity correction, none of the pairwise comparisons remained statistically significant. The largest participant-level difference was observed between $\alpha = 0.75$ and $\alpha = 0.50$ for balanced accuracy (raw $p = 0.017$; Holm-adjusted $p = 0.067$; rank-biserial correlation $= -0.483$), corresponding to a moderate effect size despite not satisfying the adjusted significance criterion. These findings indicate that variation in α exerts a measurable global influence on localisation dynamics and downstream classification performance, while providing no evidence that any individual scaling value is statistically superior to the conventional setting after correction for multiple comparisons. Consequently, the historical choice of $\alpha = 0.50$ is best interpreted as a robust and practically balanced operating point that provides stable discriminative performance while preserving favourable localisation characteristics, rather than as a statistically unique optimum.

The participant-level trajectories shown in Figure 5 provide additional insight into these aggregate statistics. Although individual participants exhibited varying degrees of sensitivity to recursive threshold progression, the overall trends were highly consistent across the cohort. Increasing α systematically reduced upper-branch localisation depth and retained energy and peak density, while also altering the localisation characteristics of the lower branch in a predictable manner. Consequently, the primary effect of α is not to change classification performance itself but to regulate the recursive localisation process in a systematic way. These observations support interpreting α as a physically meaningful control parameter that governs recursive signal localisation rather than as a classifier hyperparameter alone, with the conventional choice of $\alpha = 0.50$ representing a balanced operating point between localisation selectivity and the preservation of informative signal structure.

3.5. Discussion

It can be seen that the LSDL is a recursive nonlinear support-filtration framework that operates directly in amplitude-support space.

The upper branch serves as a salient-support concentration operator, progressively isolating dominant signal structures. In contrast, the lower branch serves as a residual-support extinction operator, progressively removing weak-support components.

Together, these complementary localisation processes generate hierarchical support filtrations that exhibit

1. Threshold convergence;
2. Support contraction;
3. Peak-topology simplification;
4. Energy non-expansion.

Theoretical properties and experimental observations are closely consistent, establishing the mathematical basis on which the subsequent information-theoretic, persistence, spectral, and multi-geometric developments of the LSDL framework are built.

4. Sparse Informative Support Geometry

4.1. Overview

Having established the operator-theoretic foundations of recursive support localisation, attention now shifts to the geometry generated by the evolving retained support. Rather than treating localisation only as a recursive masking procedure, the retained support is viewed as a geometric object whose organisation, density, and energy distribution change systematically with localisation depth. This perspective provides a basis for analysing sparse-support structure and its related geometric properties [2,16,18].

Let

$$y = | x |,$$

and define the localised signal at recursion depth k as

$$y^{(k)} = L_{\tau_k}(y).$$

The corresponding support set is

$$S_k = \mathrm{supp}(y^{(k)}) = \left\{ n : y_n^{(k)} \neq 0 \right\}.$$

The objective is to quantify how recursive localisation alters support geometry, energy concentration, sparsity, and information density.

4.2. Support Geometry

For the upper branch,

$$S_k^U = \left\{ n : y_n \geq \tau_k^U \right\},$$

and for the lower branch,

$$S_k^L = \left\{ n : y_n < \tau_k^L \right\}.$$

The support density is defined as

$$\rho_k = \frac{| S_k |}{N},$$

where N is the signal length and $| S_k |$ is the number of retained-support samples.

Recursive localisation induces nested-support sequences

$$S_{k+1}^B \subseteq S_k^B, B \in \{U, L\},$$

implying monotonic support contraction.

4.3. Peak Geometry [9,10]

Let

$$P_k = P_{\tau_k}(y^{(k)})$$

denote the peak-support set.

The number of retained peaks is

$$m_k = | P_k |.$$

Peak density is defined as

$$\eta_k = \frac{| P_k |}{| S_k |},$$

which measures the degree to which the retained support is concentrated around local maxima.

4.4. Energy Concentration [3,4]

The total signal energy is

$$E_0 = \| y \|_2^2.$$

The retained localised energy is

$$E_k = \| y^{(k)} \|_2^2.$$

The energy concentration ratio is

$$C_k = \frac{E_k}{E_0}.$$

To quantify energy concentration relative to support size, localisation gain is defined as

$$G_k = \frac{C_k}{\rho_k}.$$

Values of

$$G_k > 1$$

indicate that the retained support contains disproportionately large amounts of signal energy relative to its size.

4.5. Information and Sparsity Measures

Support entropy is defined as [19]

$$H_k = -\sum_{n \in S_k} p_n^{(k)} \log p_n^{(k)},$$

where

$$p_n^{(k)} = \frac{y_n^{(k)}}{\sum_{i \in S_k} y_i^{(k)}}.$$

Support sparsity is quantified using the Hoyer sparsity index:

$$\Psi_k = \frac{\sqrt{|\, S_k \,|} - \frac{\|y^{(k)}\|_1}{\|y^{(k)}\|_2}}{\sqrt{|\, S_k \,|} - 1}.$$

Values approaching one indicate a highly sparse-support structure.

4.6. Fundamental Property

Proposition 2. *Monotonic Support Contraction.*

For both localisation branches,

$$\rho_{k+1}^B \leq \rho_k^B, B \in \{U, L\}.$$

Thus, recursive localisation produces progressively smaller support manifolds.

4.7. Experimental Validation

The support-geometry framework was evaluated using the benchmark sunspot signal over twenty recursive localisation iterations.

Support Density Contraction

Support density decreased monotonically in both localisation branches.

For the upper branch,

$$\rho_1^U = 0.1489, \rho_{20}^U = 0.0032.$$

For the lower branch,

$$\rho_1^L = 0.8511, \rho_{20}^L = 0.0097.$$

These results provide direct empirical validation of Proposition 2.

Figure 6 shows a plot of the support density contraction of the upper and lower thresholds.

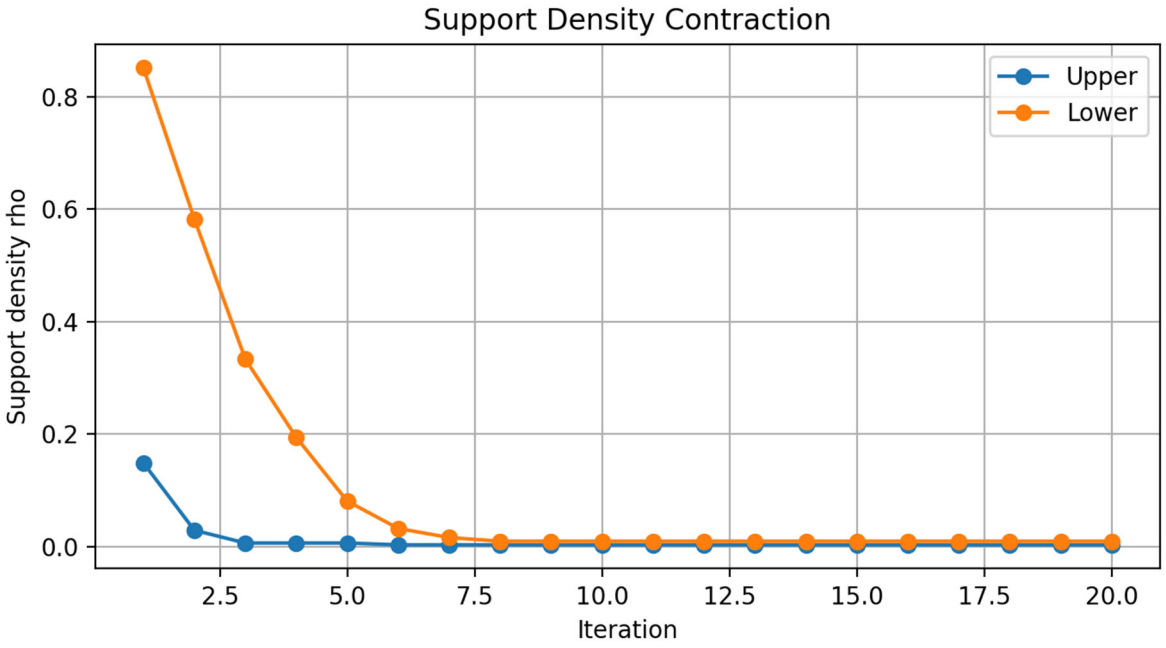


Figure 6. Support density evolution for upper and lower localisation branches. Support density decreases monotonically with recursion depth in both branches, confirming the progressive contraction of retained support and validating the sparse-support geometry formulation. Energy concentration and localisation gain.

The upper branch increasingly concentrated signal energy within progressively smaller support regions.

Maximum localisation gain reached

$$G_{\max} = 8.81,$$

indicating strong energetic concentration within retained support.

In contrast, the lower branch exhibited substantially smaller localisation gains

$$G_{\max} = 0.49,$$

consistent with progressive residual-support extinction. Figure 7 shows the energy concentration and localisation gains across various recursion depth.

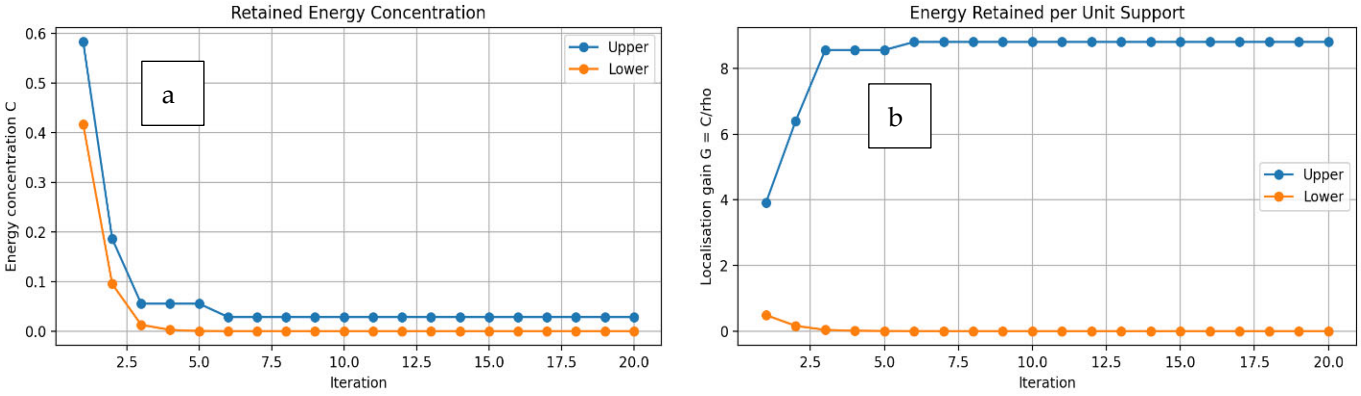


Figure 7. Energy concentration and localisation gain across recursion depth. (**a**) Retained Energy concentration ratio C_k, showing the proportion of signal energy retained within the localised support. (**b**) Energy Retained per Unit Support. Increasing localisation gain indicates progressively more informative and energetically concentrated support regions. Support entropy and sparsity.

Support entropy decreased with recursion depth, while sparsity increased. The upper branch reached

$$\Psi_{\max} = 1.00,$$

indicating near-complete geometric sparsification.

The lower branch remained substantially less sparse,

$$\Psi_{\max} = 0.19.$$

These results support the hypothesis that recursive localisation progressively concentrates informative signal structure into sparse-support regions. Figure 8 shows a support entropy and geometric sparsity evolution.

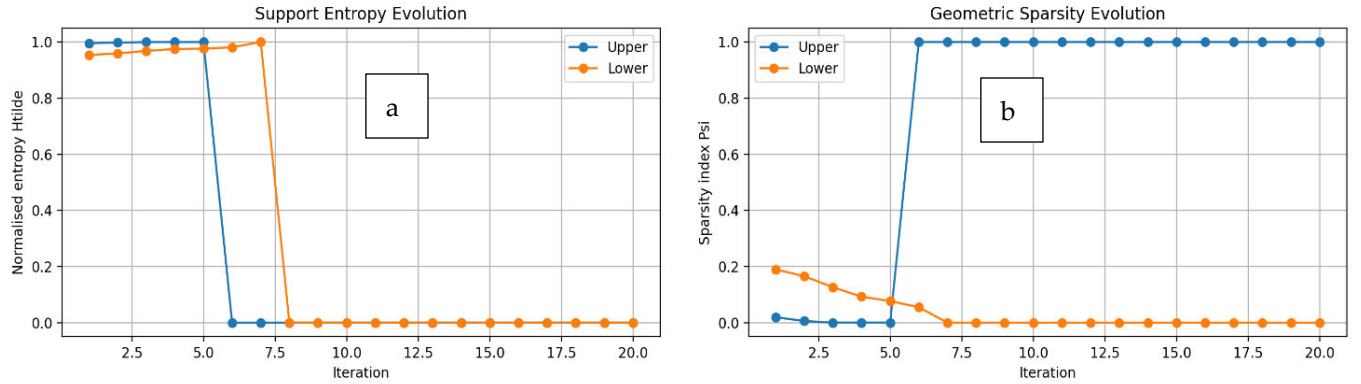


Figure 8. Information-theoretic and sparsity characteristics of retained support. (**a**) Support entropy evolution H_k, characterising the distribution of retained amplitudes within the support. (**b**) Geometric Sparsity Evolution, Hoyer sparsity index Ψ_k, quantifying geometric sparsity. The upper branch exhibits decreasing entropy and increasing sparsity, consistent with the concentration of informative signal structure.

Representative Support Geometry

Figure 9 illustrates representative support manifolds at successive localisation depths.

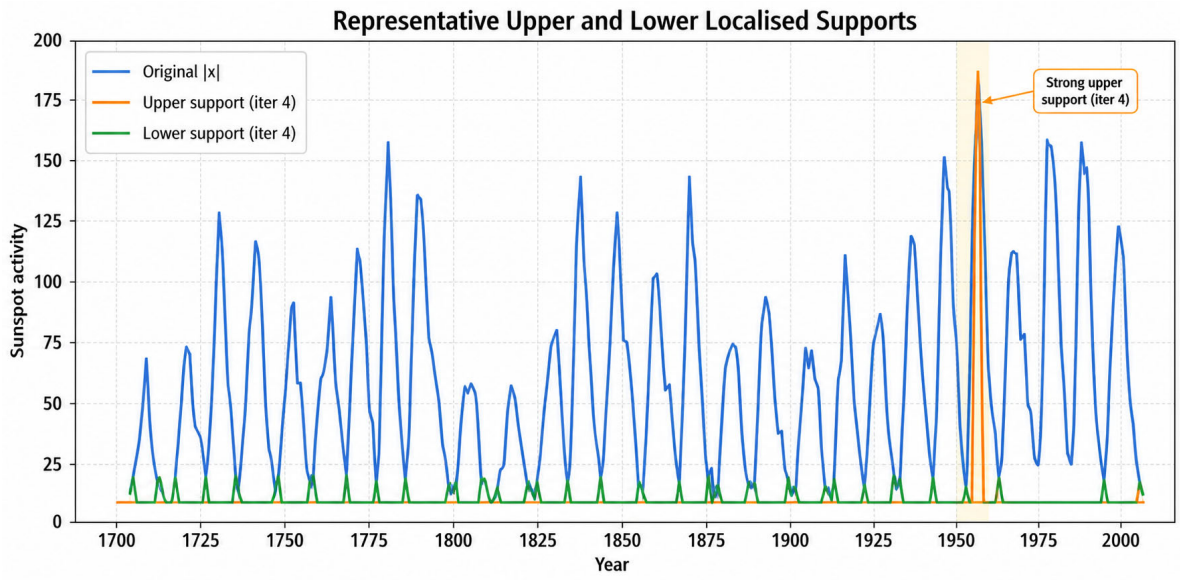


Figure 9. Representative support manifolds generated by recursive localisation. Successive localisation depths produce progressively contracted support regions. The upper branch concentrates salient signal structure into sparse informative supports, whereas the lower branch progressively extinguishes residual-support structure.

Progressive support contraction is accompanied by increasing concentration around dominant signal structures in the upper branch and progressive extinction of residual-support structure in the lower branch. Figure 9 shows a representative support manifold generated by recursive localisation.

4.8. Discussion

The results establish that recursive support localisation induces a well-defined support geometry characterised by contraction, increasing sparsity, decreasing entropy, and increasing localisation gain.

For the salient-support branch,

$$\rho_k^U \downarrow, H_k^U \downarrow, \Psi_k^U \uparrow, G_k^U \uparrow,$$

demonstrating progressive concentration of the informative signal structure.

Conversely,

$$\rho_k^L \downarrow, C_k^L \downarrow, E_k^L \to 0,$$

indicating systematic residual-support extinction.

The resulting support manifold

$$\mathcal{M}_k = (S_k, P_k, \rho_k, C_k, H_k, \Psi_k, G_k)$$

provides a geometric representation of localisation dynamics and forms the foundation for the persistence, information-theoretic, and multiscale developments introduced in subsequent stages of the framework.

5. Perturbation Stability of Recursive Support Localisation

5.1. Overview

The practical usefulness of any signal representation depends not only on how well it describes the signal but also on how resilient it is to realistic perturbations. After characterising the geometry of recursively localised support, the next issue is the stability

of these structures when the underlying signal is affected by noise or temporary disturbances. This section therefore investigates the perturbation robustness of the proposed localisation framework [3,4].

The objective is to determine whether recursive support localisation preserves informative signal structure when the input signal is perturbed.

Let

$$y = |\, x \,|$$

denote the reference amplitude representation and let

$$\widetilde{y} = y + \varepsilon$$

denote a perturbed observation, where ε represents an additive perturbation process.

The corresponding localised supports are

$$S_k = \mathrm{supp}(L_{\tau_k}(y))$$

and

$$\widetilde{S}_k = \mathrm{supp}(L_{\tau_k}(\widetilde{y})).$$

The question is how closely the perturbed support geometry reproduces the reference support geometry.

5.2. Stability Measures

Support Similarity

Support preservation is quantified using the Jaccard similarity coefficient [27,28]

$$J_k = \frac{|\, S_k \cap \widetilde{S}_k \,|}{|\, S_k \cup \widetilde{S}_k \,|}.$$

Values approaching one indicate near-identical support recovery.

Peak Survival

Peak preservation is quantified by

$$R_k = \frac{|\, P_k \cap \widetilde{P}_k \,|}{|\, P_k \,|},$$

where P_k and $\widetilde{P}_k$ denote the peak-support sets extracted from the reference and perturbed signals, respectively.

Energy Deviation

Robustness of retained energy is quantified as

$$D_k = \frac{|\, E_k - \widetilde{E}_k \,|}{E_k},$$

where E_k and $\widetilde{E}_k$ denote localised energies before and after perturbation.

Stability Score

A composite stability measure is defined as

$$\Sigma_k = \frac{J_k + R_k + (1 - D_k)}{3},$$

which jointly evaluates support preservation, peak preservation, and energetic consistency.

5.3. Fundamental Property

The practical utility of recursive support localisation depends on the stability of the retained support under small perturbations. This section shows that bounded additive perturbations do not change support membership when the perturbation remains below the corresponding threshold margin. Consequently, the localisation operator demonstrates local robustness to additive signal disturbances.

Let

$$y = x + \eta$$

be a perturbed signal satisfying

$$\| \eta \|_\infty \leq \varepsilon.$$

Let the localisation threshold τ be fixed and applied to both x and y. For the upper-support operator,

$$S_x^U(\tau) = \{i : \mid x_i \mid \geq \tau\}, S_y^U(\tau) = \{i : \mid y_i \mid \geq \tau\}.$$

Then

$$S_x^U(\tau) \triangle S_y^U(\tau) \subseteq B_\varepsilon(\tau),$$

where

$$B_\varepsilon(\tau) = \{i : \mid\mid x_i\mid - \tau \mid \leq \varepsilon\}$$

and $\triangle$ denotes the symmetric difference.

Proof. By the reverse triangle inequality,

$$\mid \mid y_i \mid - \mid x_i \mid \mid \leq \mid y_i - x_i \mid = \mid \eta_i \mid \leq \varepsilon.$$

Suppose first that

$$\mid x_i \mid > \tau + \varepsilon.$$

Then,

$$\mid y_i \mid \geq \mid x_i \mid - \varepsilon > \tau,$$

so i belongs to both upper-support sets. Conversely, if

$$\mid x_i \mid < \tau - \varepsilon,$$

then

$$\mid y_i \mid \leq \mid x_i \mid + \varepsilon < \tau,$$

so i belongs to neither support set. Therefore, membership can differ only when

$$\mid\mid x_i \mid - \tau \mid \leq \varepsilon.$$

Hence,

$$S_x^U(\tau) \triangle S_y^U(\tau) \subseteq B_\varepsilon(\tau).$$

□

5.4. Experimental Validation

The perturbation-stability framework was evaluated using bounded Gaussian noise, bounded uniform noise, and sparse impulsive disturbances over multiple perturba-

tion levels. Figure 10 shows the results of representative perturbations applied to the benchmark signals.

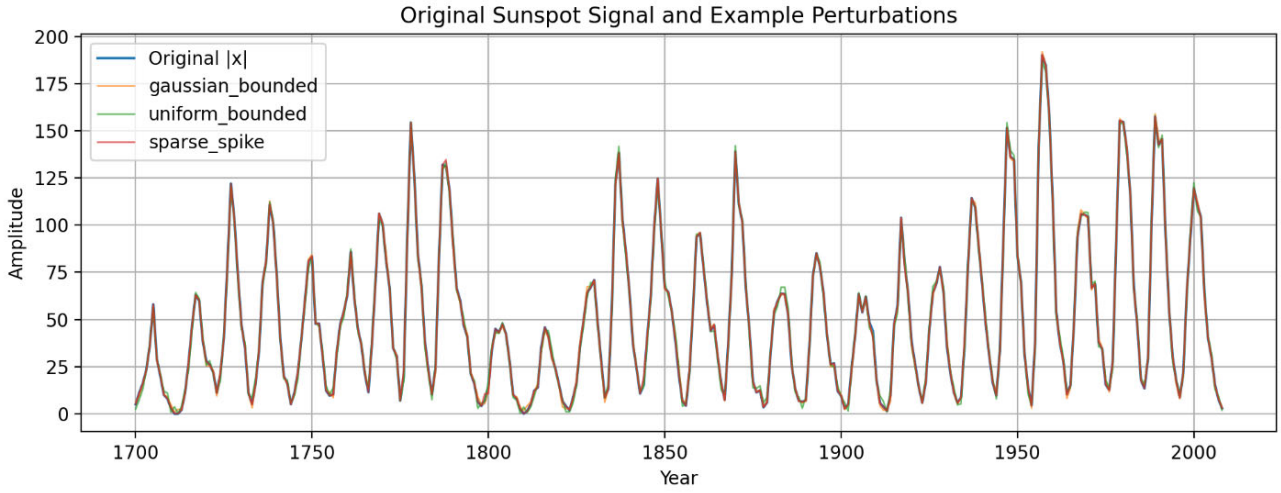


Figure 10. Representative perturbations applied to the benchmark signal. The original signal and corresponding perturbed observations generated under increasing noise levels. Despite progressive degradation of the raw signal, the dominant support structure remains visually preserved, motivating the perturbation-stability analysis performed in subsequent figures.

Support Preservation

Support similarity remained high across all perturbation regimes.

The Jaccard coefficient decreased gradually with increasing perturbation magnitude, indicating progressive but controlled support deformation. Figure 11 shows the results of a support similarity under perturbations.

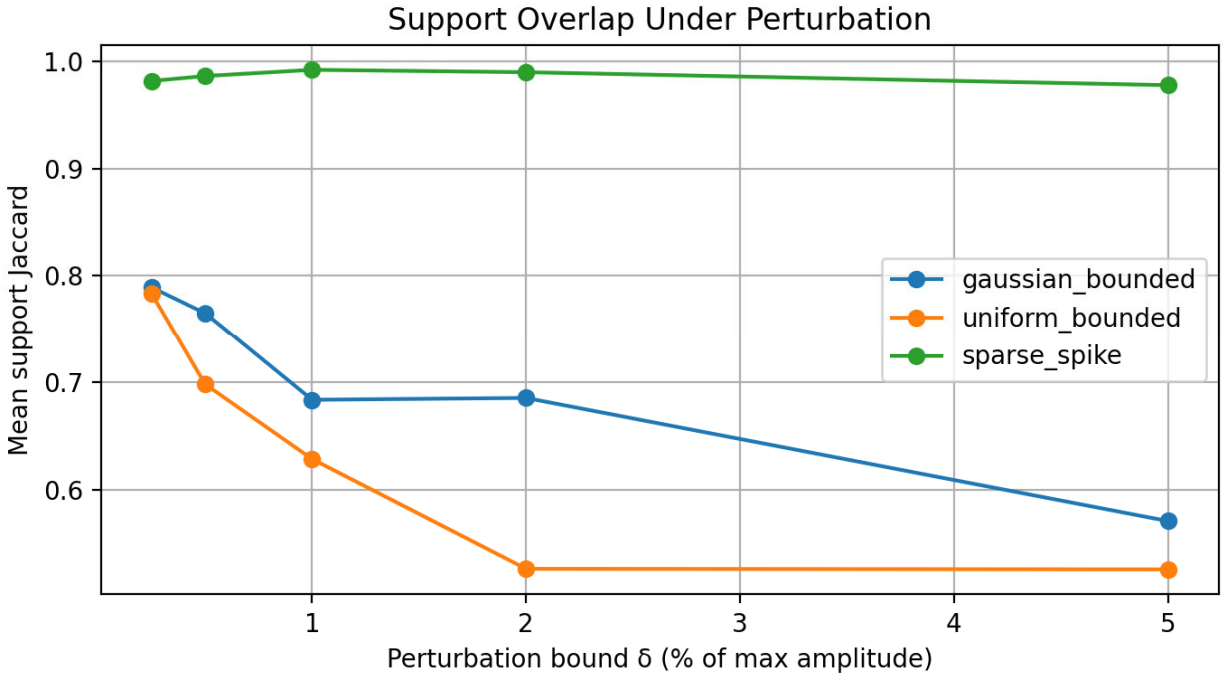


Figure 11. Support similarity under perturbation. Jaccard similarity coefficient J_k between the reference support and perturbed support as a function of perturbation magnitude. Similarity remains high across increasing noise levels, indicating that recursive support localisation preserves the underlying support geometry under bounded disturbances.

Peak Preservation and Energy Stability

Peak topology exhibited strong robustness to perturbation. Although energetic deviations increased with noise magnitude, the dominant support structure remained largely preserved. Figure 12 shows the plots of perturbation effects on peak topology and localised energy.

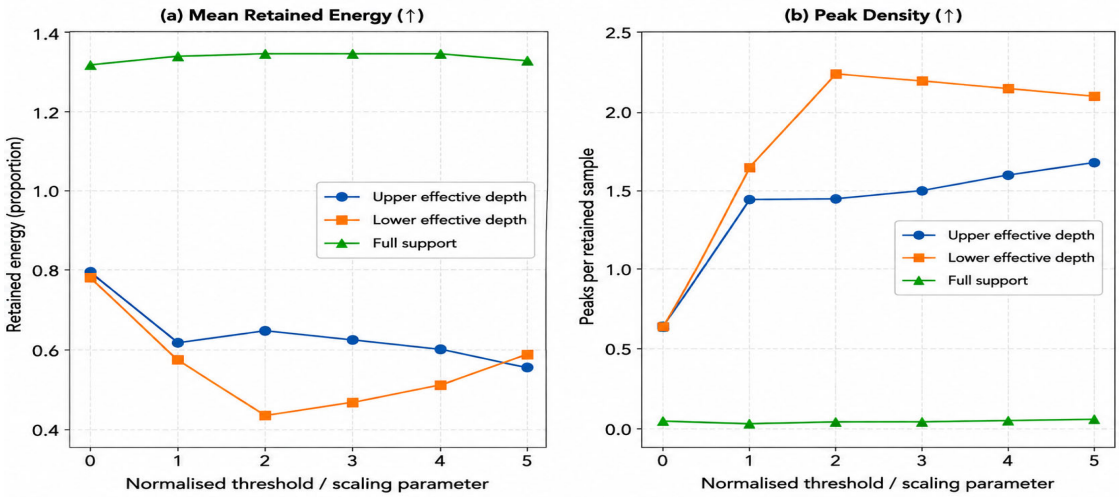


Figure 12. Perturbation effects on peak topology and localised energy. (**a**) Peak-survival ratio R_k, quantifying preservation of peak-support topology under increasing perturbation levels. (**b**) Energy-deviation ratio D_k, measuring the relative difference between localised energies obtained from the reference and perturbed signals. Although energetic deviations increase with perturbation magnitude, the dominant peak-support structure remains substantially preserved.

Composite Stability Behaviour

The composite stability score decreases smoothly with perturbation magnitude rather than collapsing abruptly, indicating graceful degradation of localisation performance. Figure 13 shows the result of the composite perturbation-stability analysis.

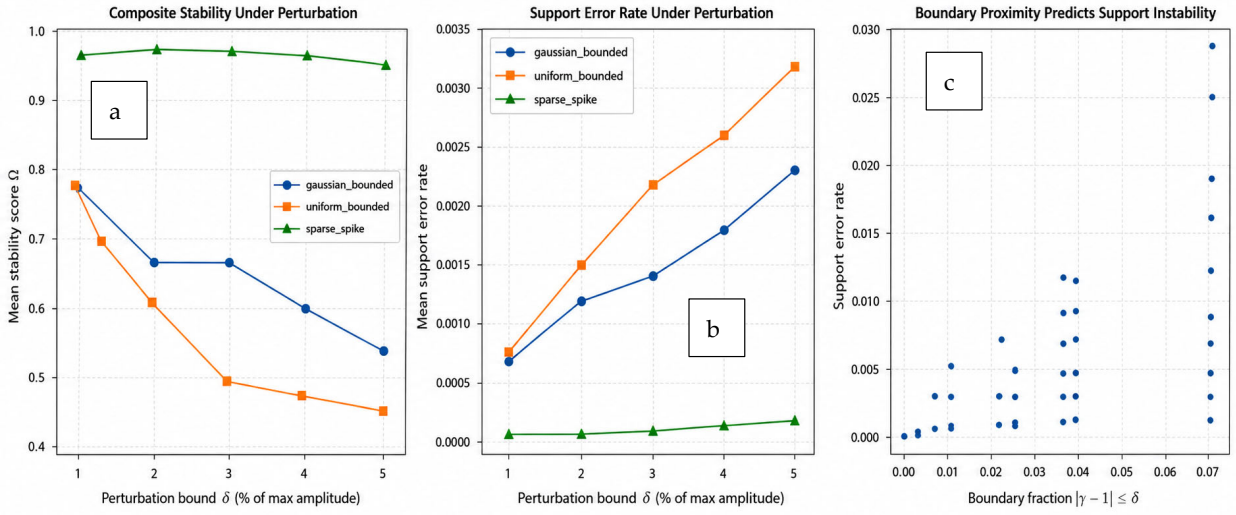


Figure 13. Composite perturbation-stability analysis. (**a**) Composite stability score Σ_k, combining support similarity, peak preservation, and energy consistency. (**b**) Support-error rate as a function of perturbation magnitude. (**c**) Relationship between localisation-boundary fraction and support error. The results show that support degradation occurs gradually rather than catastrophically and that localisation errors remain concentrated near support boundaries, supporting the perturbation-stability proposition.

5.5. Discussion

The experiments reflect that recursive support localisation exhibits substantial robustness under bounded perturbations. Support similarity remains high, peak topology is largely preserved, and support errors are concentrated near threshold boundaries rather than being distributed throughout the support manifold. This behaviour is consistent with the theoretical expectation that bounded perturbations primarily affect samples located near localisation boundaries.

Taken together, the LSDL support manifold is not only sparse and informative (Step 2) but also stable under realistic perturbations. This robustness provides the basis for the persistence and multiscale analyses developed in later stages of the framework.

6. Discriminative Separability and Class Geometry

6.1. Overview

Beyond structural organisation and robustness, an important question is whether recursive support localisation also improves the discriminative arrangement of signal representations. This section examines how recursive localisation changes class geometry within feature space and whether these developing representations enhance class separability while still maintaining enough support for dependable feature extraction.

Let

$$x_i^{(c)} \in \mathbb{R}^N$$

denote the i-th signal belonging to class c, where

$$c \in \{1, \ldots, C\}$$

and C denotes the number of classes.

The corresponding rectified signal is

$$y_i^{(c)} = | \, x_i^{(c)} \, |.$$

6.2. LSDL Feature Embedding [2]

At localisation depth k, recursive localisation produces

$$y_{i,k}^{(c)} = L_{\tau_k}\left(y_i^{(c)}\right)$$

together with the associated peak-support representation

$$P_{i,k}^{(c)} = P_{\tau_k}\left(y_{i,k}^{(c)}\right).$$

A feature embedding map

$$\phi_k : \mathbb{R}^N \to \mathbb{R}^d$$

is then used to construct an LSDL feature vector

$$z_{i,k}^{(c)} = \phi_k\left(y_{i,k}^{(c)}, P_{i,k}^{(c)}\right),$$

where d denotes the feature-space dimension.

Typical LSDL feature representations include support density, energy concentration, localisation gain, peak density, entropy, sparsity, retained energy, and peak-support cardinality.

Thus, recursive localisation induces a feature-space mapping

$$x_i^{(c)} \mapsto z_{i,k}^{(c)}.$$

6.3. Robustness-Admissible Localisation

Excessive localisation may generate highly sparse supports that are statistically fragile. To prevent this, only localisation depths retaining sufficient support are considered admissible.

Let

$$\widetilde{S}_k$$

denote the median retained-support cardinality across all signals at localisation depth k.

A localisation depth is admissible if

$$\widetilde{S}_k \geq S_{\min},$$

where $S_{\min}$ denotes the minimum robustness-preserving support floor.

The admissible localisation set is therefore

$$\mathcal{A} = \left\{ k : \widetilde{S}_k \geq S_{\min} \right\}.$$

Throughout this study,

$$S_{\min} = 30.$$

This constraint prevents pathological over-localisation while maintaining sufficient support for reliable feature estimation.

6.4. Class Geometry [29]

For each class c, define the class centroid

$$\mu_{c,k} = \frac{1}{N_c} \sum_{i=1}^{N_c} z_{i,k}^{(c)},$$

where N_c denotes the number of samples belonging to class c.

The global centroid is

$$\mu_k = \frac{1}{N} \sum_{c=1}^{C} \sum_{i=1}^{N_c} z_{i,k}^{(c)},$$

where

$$N = \sum_{c=1}^{C} N_c.$$

Class compactness is quantified by the within-class scatter matrix

$$S_{W,k} = \sum_{c=1}^{C} \sum_{i=1}^{N_c} \left(z_{i,k}^{(c)} - \mu_{c,k} \right) \left(z_{i,k}^{(c)} - \mu_{c,k} \right)^T.$$

Class separation is quantified by the between-class scatter matrix

$$S_{B,k} = \sum_{c=1}^{C} N_c (\mu_{c,k} - \mu_k)(\mu_{c,k} - \mu_k)^T.$$

6.5. Discriminative Separability [30]

Class separability is quantified using a Fisher-style discriminative ratio

$$\Lambda_k = \frac{\mathrm{tr}(S_{B,k})}{\mathrm{tr}(S_{W,k}) + \varepsilon},$$

where $\mathrm{tr}(\cdot)$ denotes the matrix trace and $\varepsilon > 0$ prevents numerical instability.

Large values of

$$\Lambda_k$$

indicate strong class separability characterised by large between-class distances and compact within-class structure.

To assess the contribution of localisation, a raw-feature baseline is defined as

$$\Lambda_0.$$

The primary Step-4 hypothesis is that there exists at least one admissible localisation depth satisfying

$$\exists k \in \mathcal{A} : \Lambda_k > \Lambda_0.$$

6.6. Optimal Discriminative Localisation

The optimal robustness-admissible localisation depth is defined as

$$k^\star = \arg\max_{k \in \mathcal{A}} \Lambda_k.$$

The corresponding threshold

$$\tau^\star = \tau_{k^\star}$$

defines the optimal discriminative LSDL representation

$$z_i^\star = \phi_{k^\star}(L_{\tau^\star}(\mid x_i \mid)).$$

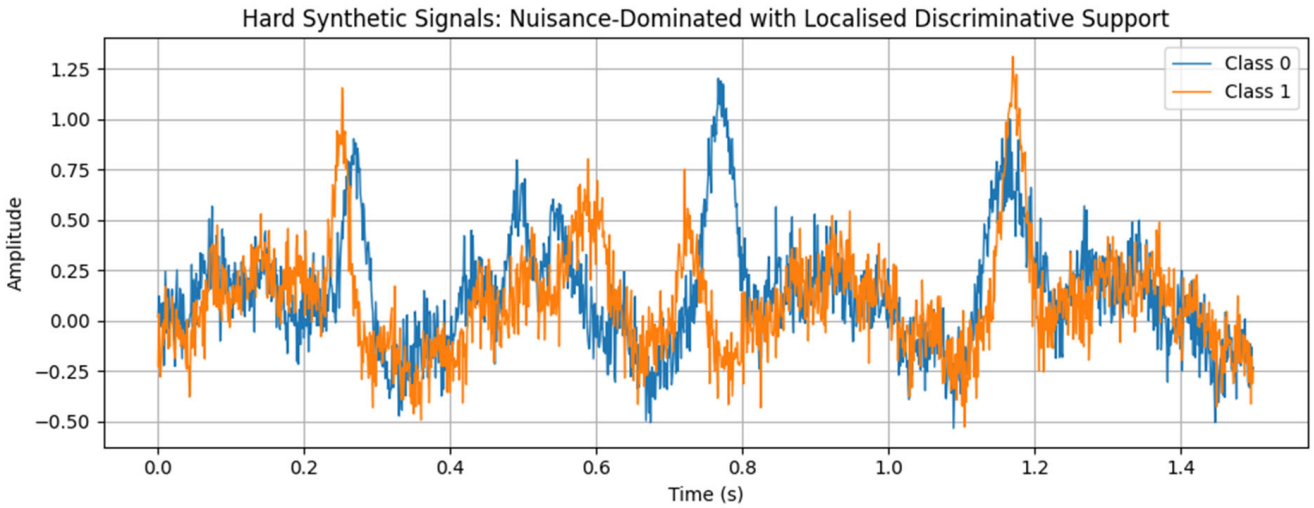
This formulation directly links localisation depth to discriminative class geometry while enforcing robustness-preserving support constraints.

6.7. Experimental Validation

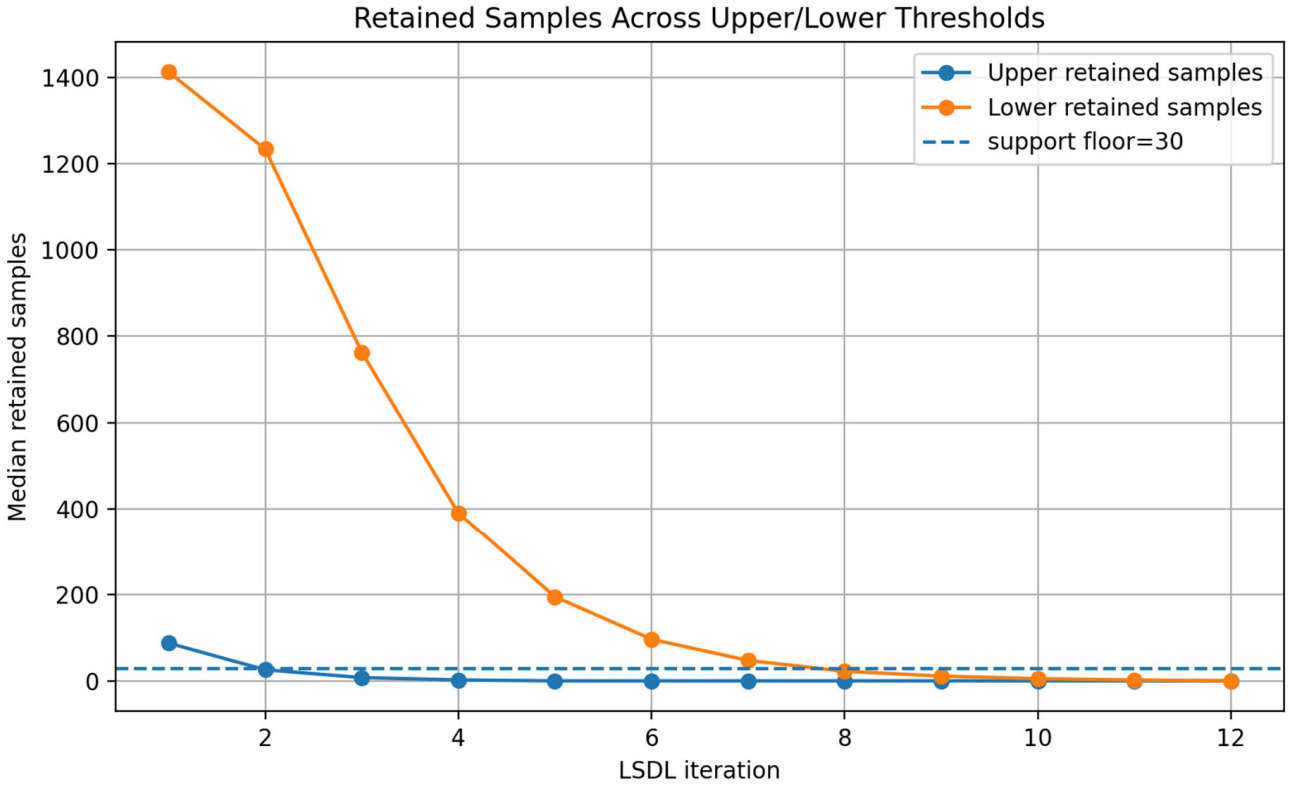
The discriminative localisation framework was evaluated using class-labelled signals over the complete localisation trajectory. An image of the contrasted pair of signals can be seen below in Figure 14a,b, which show the retained number of samples. As part of the generation of the synthetic signal, both comprise dominant nuisance components with low frequency oscillatory drift with a strong inclusion of Gaussian noise, with narrow Gaussian-shaped transients at varied time locations. The mathematical representation of this is as follows:

$$x_c(t) = n_c(t) + \sum_{j=1}^{J_c} A_c, j \exp\left[-\frac{(t - \mu_{c,j})^2}{2\sigma_{c,j}^2} \right] + \varepsilon_c(t)$$

where $x_c(t)$ denotes the observed signal for channel c at time t; $n_c(t)$ is the underlying baseline (background) signal; J_c is the total number of Gaussian components in channel c; $A_{c,j}$ is the amplitude of the j-th Gaussian component; $\mu_{c,j}$ is its temporal centre (mean location); $\sigma_{c,j}$ is its standard deviation, which determines the spread (width) of the component; $\exp(\cdot)$ denotes the exponential function; and $\varepsilon_c(t)$ represents additive residual noise or modelling error.



(**a**)



(**b**)

Figure 14. (**a**) Hard synthetic signals; (**b**) robustness-admissible support cardinality across localisation depth. Median retained-support size as a function of localisation threshold. The support floor $S_{\min}$ defines the admissible localisation region used for discriminative analysis. Thresholds producing support cardinalities below the support floor are excluded to prevent statistically fragile feature estimation and pathological over-localisation.

The discriminative analysis employed 11 structural descriptors extracted from the retained support, namely, retained-support cardinality, support density, retained peak count, peak density, retained energy, energy concentration, energy density, support entropy, normalised entropy, sparsity, and localisation gain. Classification was performed using Linear Discriminant Analysis (LDA), with model performance evaluated using five-fold cross-validation.

Support-Floor Admissibility

The retained-support cardinality decreases monotonically with localisation depth. The robustness-preserving support floor identifies the admissible region in which localisation remains statistically reliable.

Separability Evolution

Class separability initially increases as non-discriminative support is removed and subsequently decreases once localisation becomes excessively aggressive.

This behaviour reveals the existence of an optimal robustness-admissible localisation depth. Figure 15 shows the discriminative separability under recursive localisation results.

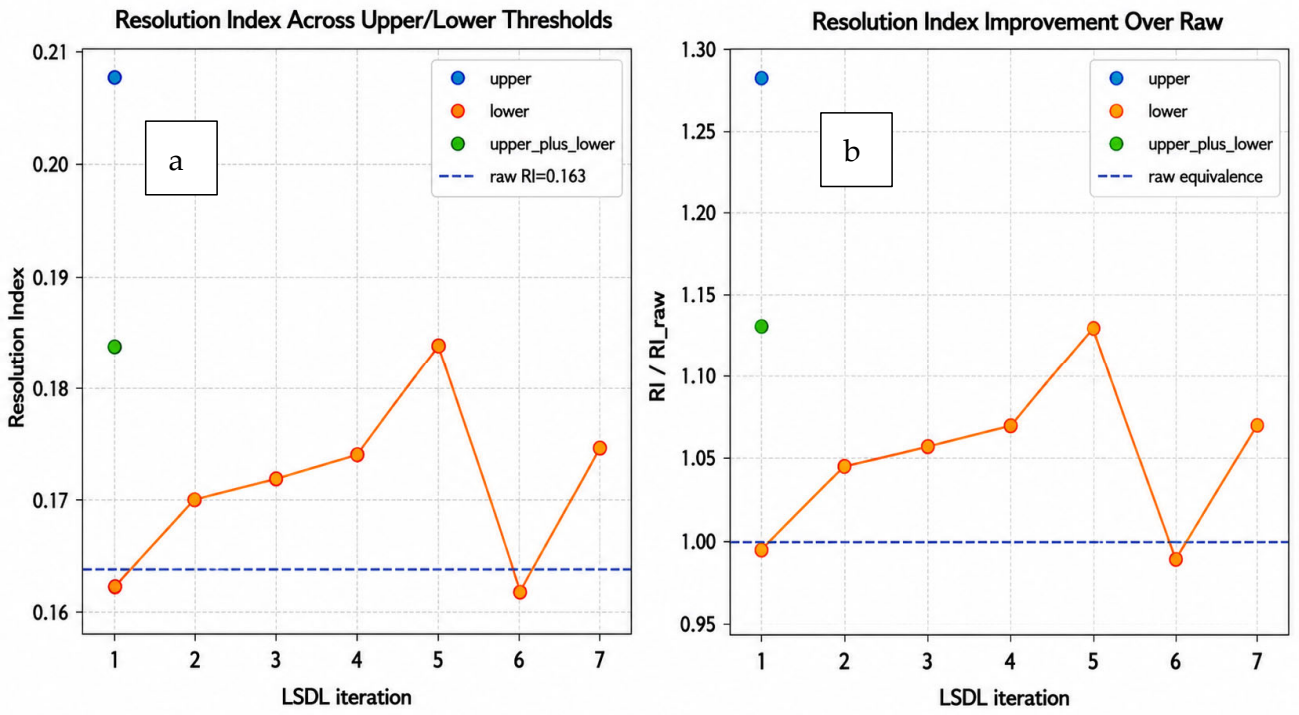


Figure 15. Discriminative separability under recursive localisation. (**a**) Resolution Index (RI) representing class separation relative to within-class spread across localisation depths. (**b**) Relative improvement in separability compared with the raw-feature baseline. The optimal discriminative localisation depth occurs at the admissible threshold, maximising class separability while preserving the required support floor.

Feature-Space Geometry

Visualisation of the embedded feature space demonstrates that recursive localisation contracts within-class structure while preserving or enhancing between-class separation.

The optimal localisation depth yields the clearest class geometry. Figure 15 shows the class geometry before and after recursive localisation.

Classification Performance

Classification performance follows the same trend observed in the separability metric.

Maximum classification accuracy occurs at the robustness-admissible localisation depth corresponding to the peak separability score. Figures 16 and 17 shows the classification performance and localisation trajectory.

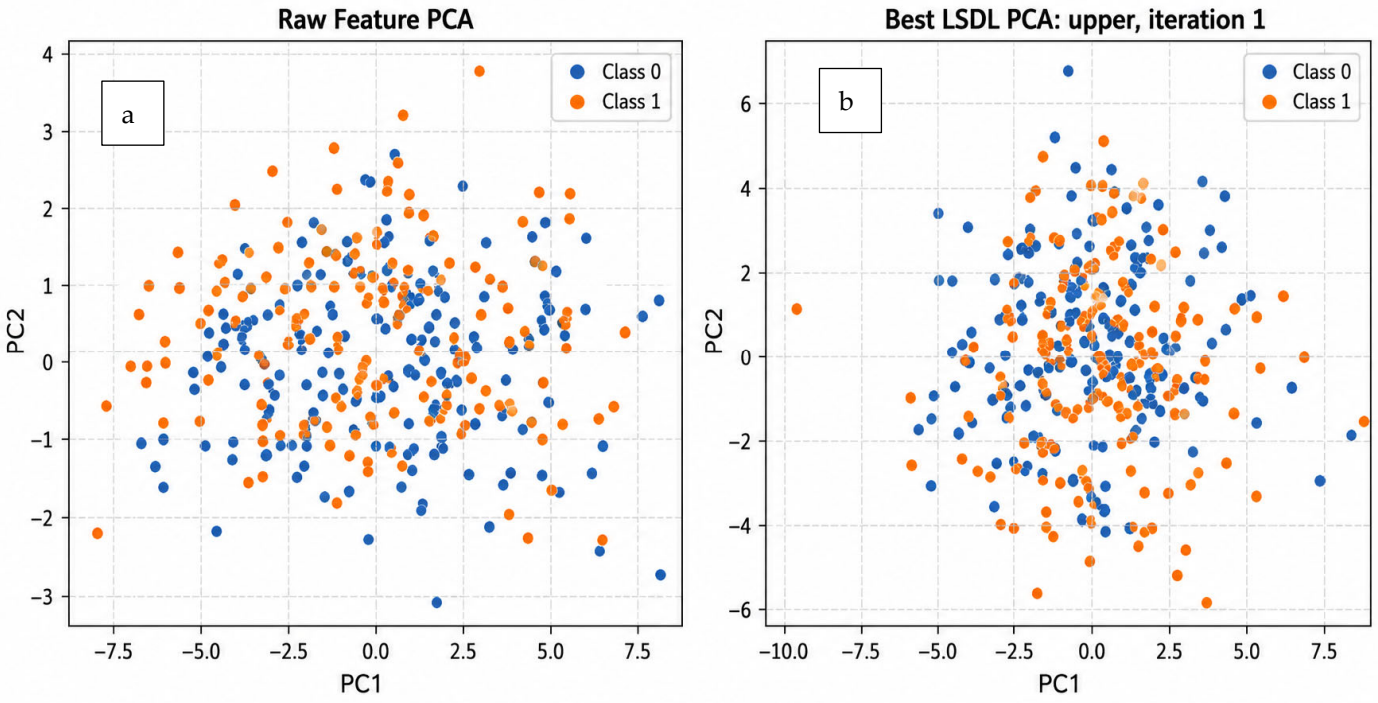


Figure 16. Class geometry before and after recursive localisation. Principal Component Analysis (PCA) projections of the feature space. (**a**) Raw-signal representation. (**b**) Optimal LSDL representation at the robustness-admissible localisation depth. Recursive localisation produces increased class compactness and improved separation of class centroids within feature space.

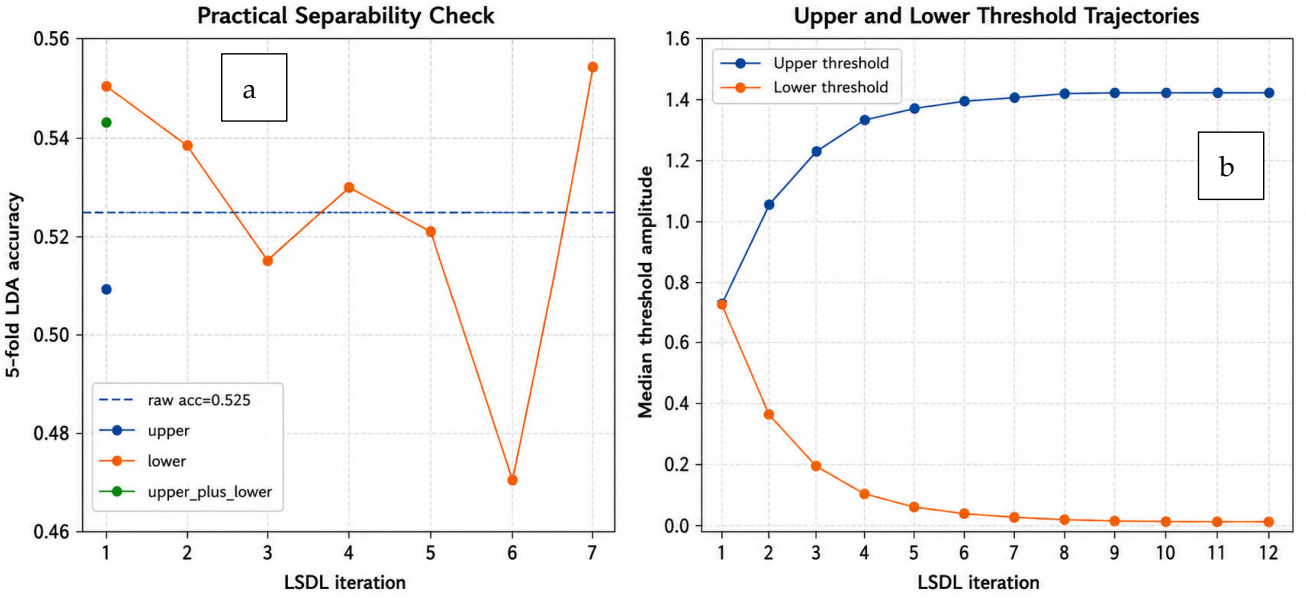


Figure 17. Classification performance and localisation trajectory. (**a**) LDA classification accuracy across localisation depths. (**b**) Corresponding threshold trajectory. The optimal admissible localisation depth maximises classification performance while maintaining sufficient retained support for robust feature estimation.

6.8. Discussion

The results indicate that recursive support localisation can improve class geometry when applied within a robustness-preserving admissible region. As localisation proceeds, non-discriminative support is removed, resulting in reduced within-class scatter and increased between-class separation. However, excessive localisation eventually reduces

retained support below the level required for robust feature estimation, which motivates the introduction of the support-floor constraint.

The observed existence of an optimal admissible localisation depth supports the central hypothesis that recursive support localisation can improve discriminative structure relative to the raw representation while preserving sufficient support for statistical robustness.

Consequently, the LSDL may be interpreted not only as a support-localisation framework but also as a discriminative representation-learning mechanism that enhances class geometry through robustness-constrained support concentration.

7. Information Localisation and Information Geometry

7.1. Overview

Geometric concentration by itself does not necessarily indicate information concentration. Another equally important issue is how recursive localisation reshapes informational content as the retained support becomes smaller. This section therefore examines the changes in entropy, information density, and class-relevant information during the recursive localisation process [14,19]. Specifically, it considers whether recursive localisation progressively concentrates informational content within the retained support as localisation proceeds. Rather than focusing on energy concentration alone, the analysis characterises how information evolves over the support manifold under recursive support contraction.

Let

$$y^{(k)} = L_{\tau_k}(y)$$

denote the localised signal at recursion depth k, with support

$$S_k = \mathrm{supp}(y^{(k)}).$$

The objective is to quantify how entropy, information concentration, and class information relationships evolve throughout recursive localisation.

7.2. Support Entropy [19]

Using the normalised support weights introduced in Step 2,

$$p_n^{(k)} = \frac{y_n^{(k)}}{\sum_{i \in S_k} y_i^{(k)}},$$

support entropy is

$$H_k = -\sum_{n \in S_k} p_n^{(k)} \log p_n^{(k)}.$$

Large values indicate diffuse information distributed across many support elements, whereas small values indicate concentrated information.

7.3. Information Concentration [19]

Define information concentration as

$$I_k = 1 - \frac{H_k}{H_0},$$

where H_0 denotes the entropy of the original signal support.

Values approaching one indicate progressive concentration of information into fewer support elements.

7.4. Energy–Information Coupling [19]

To examine whether energy concentration corresponds to information concentration, define

$$\Omega_k = C_k I_k,$$

where

$$C_k = \frac{E_k}{E_0}$$

is the energy concentration ratio from Step 2.

Large values of

$$\Omega_k$$

indicate that localisation simultaneously concentrates energy and information.

7.5. Information Density [19]

Information concentration alone does not account for support size.

Define information density

$$D_k = \frac{I_k}{\rho_k},$$

where ρ_k is support density.

Information density quantifies the amount of information retained per unit support.

7.6. Class Information Measure [14]

For labelled data, information preservation can be quantified through mutual information.

Let

$$Y$$

denote class labels and

$$Z_k$$

denote the feature representation generated by localisation depth k.

The mutual information between features and class labels is

$$MI_k = I(Z_k; Y).$$

Larger values indicate that localisation retains greater class-relevant information.

7.7. Distributional Class Separation [14]

Class-distribution separation is quantified using Jensen–Shannon divergence

$$JS_k.$$

Higher divergence indicates stronger separation between class information distributions.

7.8. Information-Localisation Hypothesis

The central hypothesis is

$$H_k \downarrow, I_k \uparrow, D_k \uparrow, MI_k \uparrow,$$

over an admissible localisation region.

This would indicate that recursive support localisation progressively concentrates informative structure rather than merely removing samples.

7.9. Experimental Validation

Information Concentration

Support entropy decreases monotonically while information concentration increases.

This demonstrates progressive concentration of informative signal structure into a shrinking support manifold. Figure 18 shows entropy and information concentration dynamics.

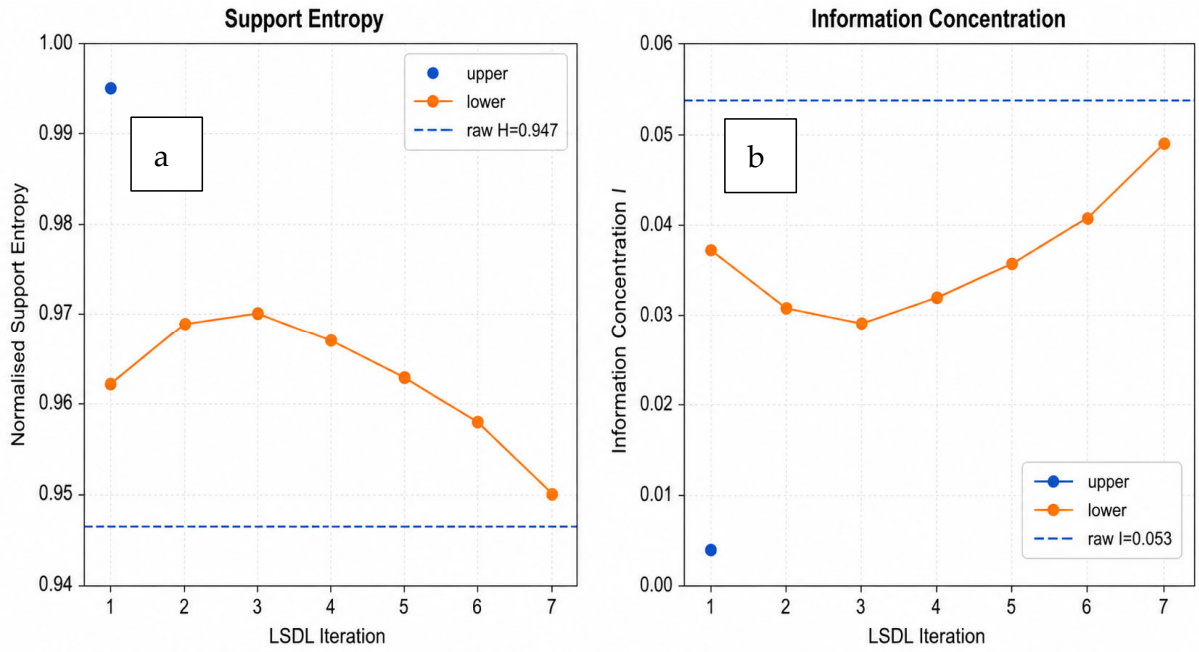


Figure 18. Entropy and information concentration dynamics. (**a**) Support entropy H_k as a function of localisation depth. Entropy decreases progressively as recursive localisation concentrates retained support into increasingly compact regions. (**b**) Information concentration I_k, defined relative to the entropy of the original signal support. Increasing information concentration indicates that informative signal structure becomes progressively localised within a shrinking support manifold. Together, these results demonstrate that recursive localisation concentrates information rather than merely reducing support cardinality.

Energy–Information Coupling

Energy concentration and information concentration evolve together across localisation depth.

This indicates that informative structure remains coupled to dominant energetic support regions. Figure 19 shows the results for the energy–information-localisation dynamics.

Class-Relevant Information

Mutual information initially increases with localisation depth before eventually declining as excessive localisation removes informative support.

An optimal information-localisation depth therefore exists. Figures 18–20 shows the mutual-information-localisation analysis results.

Information-Geometric Class Separation

The results for the information-geometric class separation can be seen in Figure 21, where Jensen–Shannon divergence increases over the admissible localisation region, demonstrating improved separation of class information distributions.

The corresponding feature-space representation exhibits enhanced class geometry relative to the raw baseline.

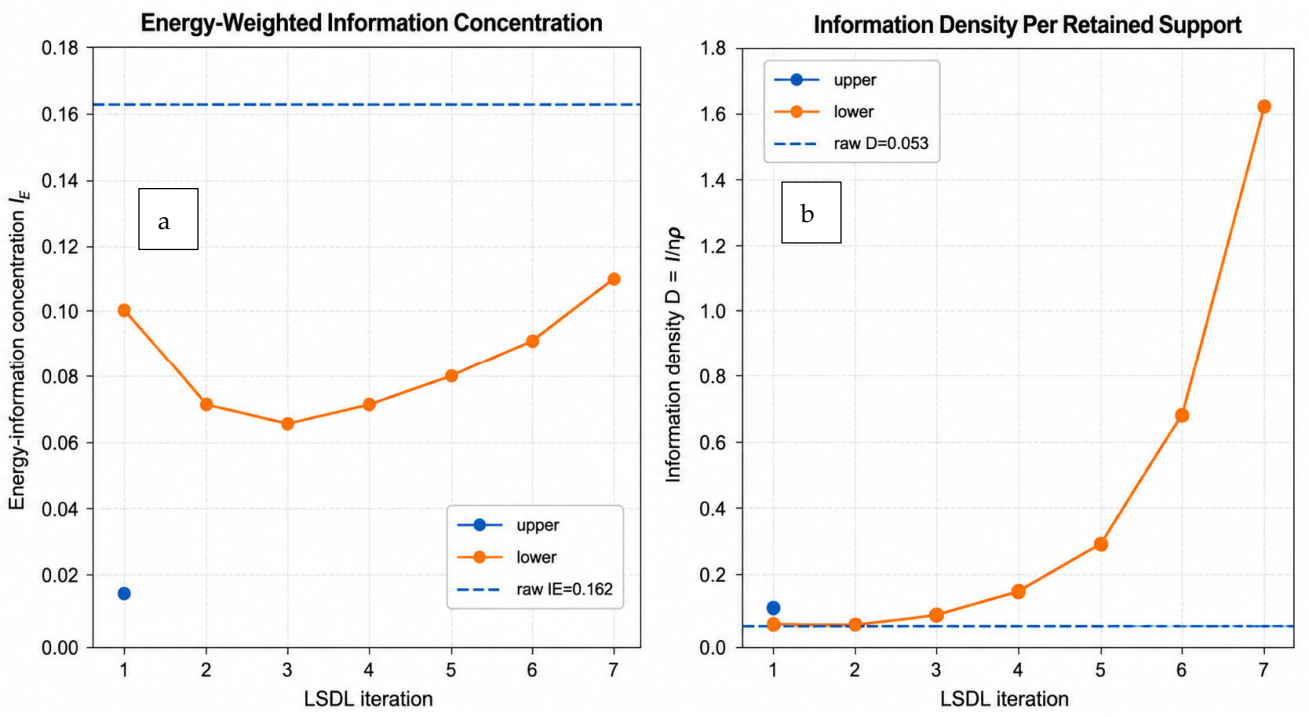


Figure 19. Energy–information-localisation dynamics. (**a**) Energy–information concentration measure Ω_k, quantifying the joint localisation of energetic and informational signal content. (**b**) Information density D_k, representing information concentration normalised by retained-support density. The results demonstrate that recursive localisation increasingly concentrates informative structure within progressively smaller support regions while maintaining strong coupling between energetic and informational content.

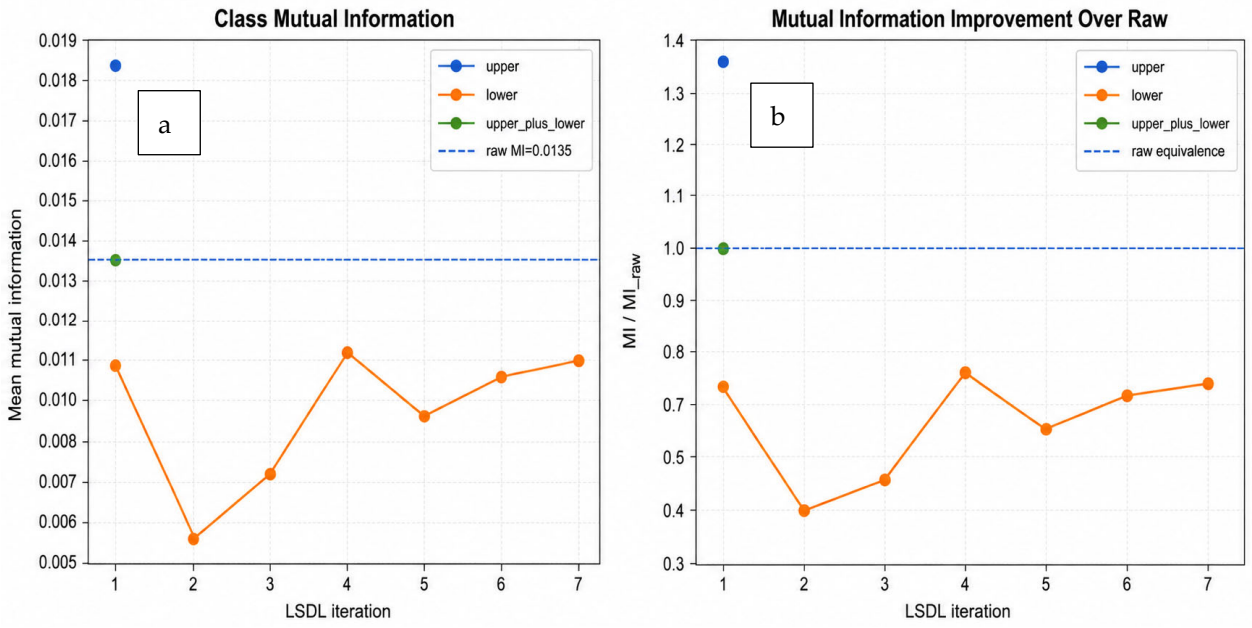


Figure 20. Mutual-information-localisation analysis. (**a**) Mutual information MI_k between localisation-derived feature representations and class labels across localisation depth. (**b**) Relative mutual-information improvement with respect to the raw-feature baseline. Mutual information initially increases as non-informative support is removed and subsequently declines under excessive localisation, indicating the existence of an optimal information-localisation depth that maximises class-relevant information retention.

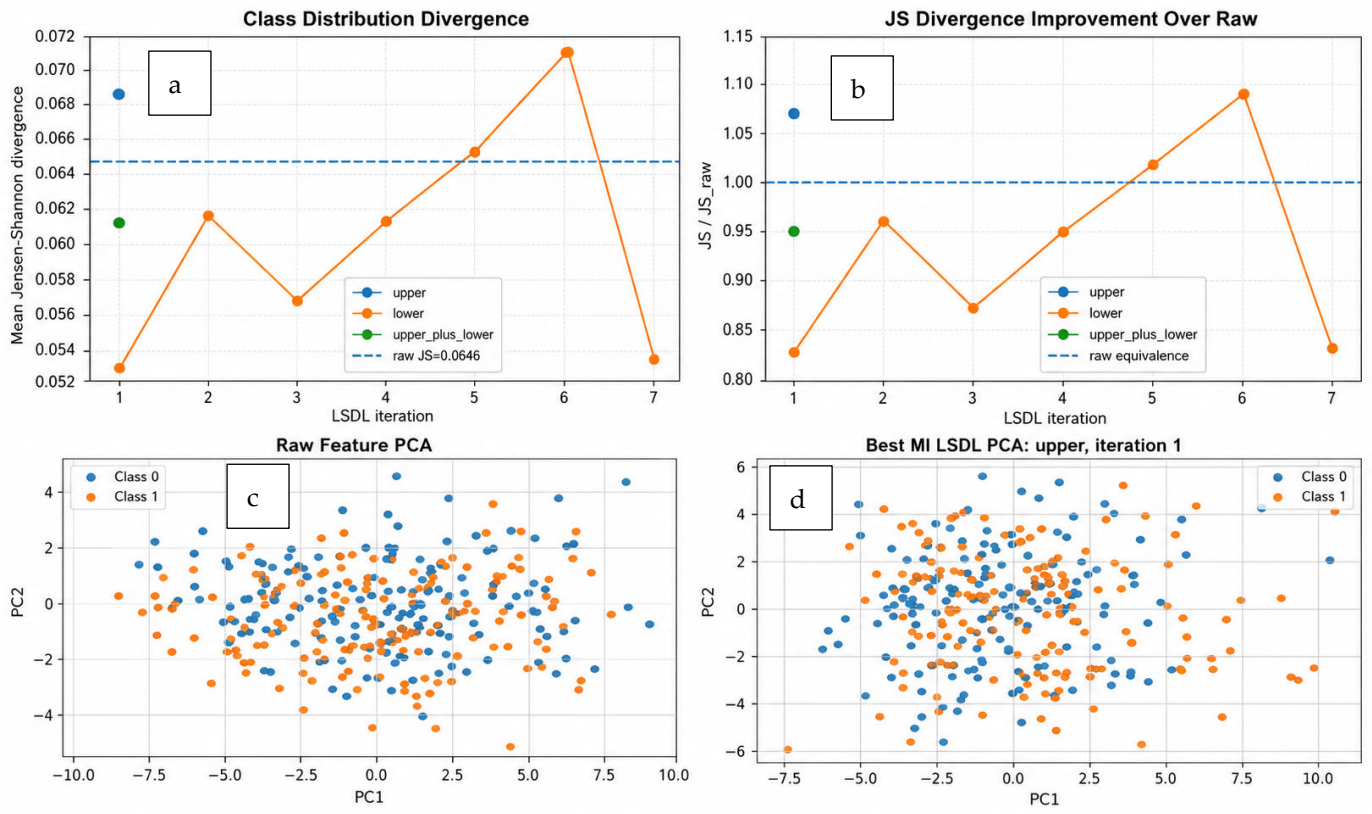


Figure 21. Information-geometric class separation. (**a**) Jensen–Shannon divergence between class distributions. (**b**) Relative improvement in distributional separation compared with the raw baseline. (**c**) Principal Component Analysis (PCA) projection of the raw-feature space. (**d**) PCA projection at the optimal information-localisation depth. Localisation increases distributional separation and improves class geometry within feature space.

7.10. Discussion

It can be seen that recursive support localisation does more than concentrate energy. As localisation progresses, entropy decreases, information density increases, and class-relevant information becomes increasingly concentrated within the retained-support regions. The observed increases in mutual information and Jensen–Shannon divergence indicate that localisation improves the informational structure available for discrimination. Consequently, the LSDL support manifold may be interpreted as an information-localisation process that concentrates informative signal content into progressively smaller support regions. This interpretation provides the information-theoretic basis for the persistence and topological developments introduced in the subsequent stage of the framework. The information Geometric Separation results can be seen in Figure 21.

8. Persistence Filtration and Persistent Signal Structures

8.1. Overview

Recursive support localisation naturally produces a hierarchy of nested-support sets whose development extends beyond any single localisation depth. This leads to the question of which structures remain stable across the filtration and whether this persistence captures meaningful signal organisation beyond instantaneous amplitude alone [12,17].

The LSDL naturally induces a filtration over amplitude-support space because recursive threshold evolution generates nested-support sets. Persistent structures are therefore identified by their survival across localisation depth rather than their amplitude at a single threshold.

8.2. Filtration Structure [12,17]

For the upper branch,

$$S_1^U \supseteq S_2^U \supseteq \cdots \supseteq S_K^U$$

and for the lower branch,

$$S_1^L \supseteq S_2^L \supseteq \cdots \supseteq S_K^L.$$

Together, these define a bidirectional amplitude-threshold filtration.
At localisation depth k, the peak-support set is

$$P_k = P_{\tau_k}\left(y^{(k)}\right).$$

8.3. Persistence Lifetime [12,17]

A peak is tracked across successive localisation depths.
The birth depth is

$$b(p) = \min\{k : p \in P_k\},$$

and the death depth is

$$d(p) = \max\{k : p \in P_k\}.$$

The persistence lifetime is

$$l(p) = d(p) - b(p) + 1.$$

Large values of $l(p)$ correspond to threshold-stable structures, whereas short lifetimes indicate transient support features.

8.4. Persistence Energy [12,17]

The amplitude trajectory of a persistent peak is

$$a_p(k).$$

Persistence energy is defined as

$$\pi_E(p) = \sum_{k=b(p)}^{d(p)} a_p(k)^2.$$

Unlike amplitude alone, persistence energy jointly measures survival duration and energetic significance across the filtration.

8.5. Persistence Entropy and Concentration [12,17]

Normalised persistence weights are

$$r_p = \frac{\pi_E(p)}{\sum_q \pi_E(q)}.$$

Persistence entropy is

$$H_\Pi = -\sum_p r_p \log r_p.$$

Persistence concentration is

$$I_\Pi = 1 - \frac{H_\Pi}{\log \mid P \mid}.$$

Low entropy and high concentration indicate that a small number of persistent structures dominate the filtration.

8.6. Class-Conditioned Persistence Geometry [12,17]

Persistence features are represented by

$$\psi(x) = \left[l_{\max}, \bar{l}, \sum_p \pi_E(p), H_\Pi, I_\Pi, \mid P \mid \right].$$

Class separability is quantified through

$$\Lambda_\Pi = \frac{\mathrm{tr}(S_{B,\Pi})}{\mathrm{tr}(S_{W,\Pi}) + \varepsilon}.$$

This tests whether persistence itself carries discriminative information.

8.7. Persistence Hypothesis

The central hypothesis is

$$\exists p : l(p) \text{largeand} \pi_E(p) \text{ large},$$

and that persistence-derived representations improve class geometry:

$$\Lambda_\Pi > \Lambda_0.$$

Thus, persistent structures are not merely high-amplitude structures; rather, they are structures that survive across localisation scale.

8.8. Experimental Validation

Filtration Dynamics

The recursive threshold trajectory generates progressively contracted support manifolds while preserving a subset of persistent structures. Figure 22 shows the results of the filtration dynamics across localisation depth.

Persistence-Based Separability

The results in Figure 23 show that separability based on persistence features exceeds the raw-feature baseline across a range of admissible localisation depths. Twelve dimensional persistence descriptors were extracted from the signals: number of tracks; maximum lifetime; mean lifetime; lifetime standard deviation; total persistence energy; maximum persistence energy; mean persistence energy; total amplitude persistence; persistence entropy; persistence concentration; long-track fraction; and lifetime–energy correlation.

Figure 23 indicates that the LSDL largely preserves the discriminative information available in the original signal. Classification performance remains comparable with the raw representation across the evaluated recursive configurations, although the magnitude and direction of change depend on the selected branch and recursion level.

The results therefore do not support a general claim that recursive localisation consistently improves classification accuracy. Instead, they indicate that appropriately selected LSDL representations can maintain competitive classification performance while reducing the signal to a localised subset of its amplitude support. Poorly matched or overly deep recursive configurations may remove discriminative signal components and consequently reduce performance.

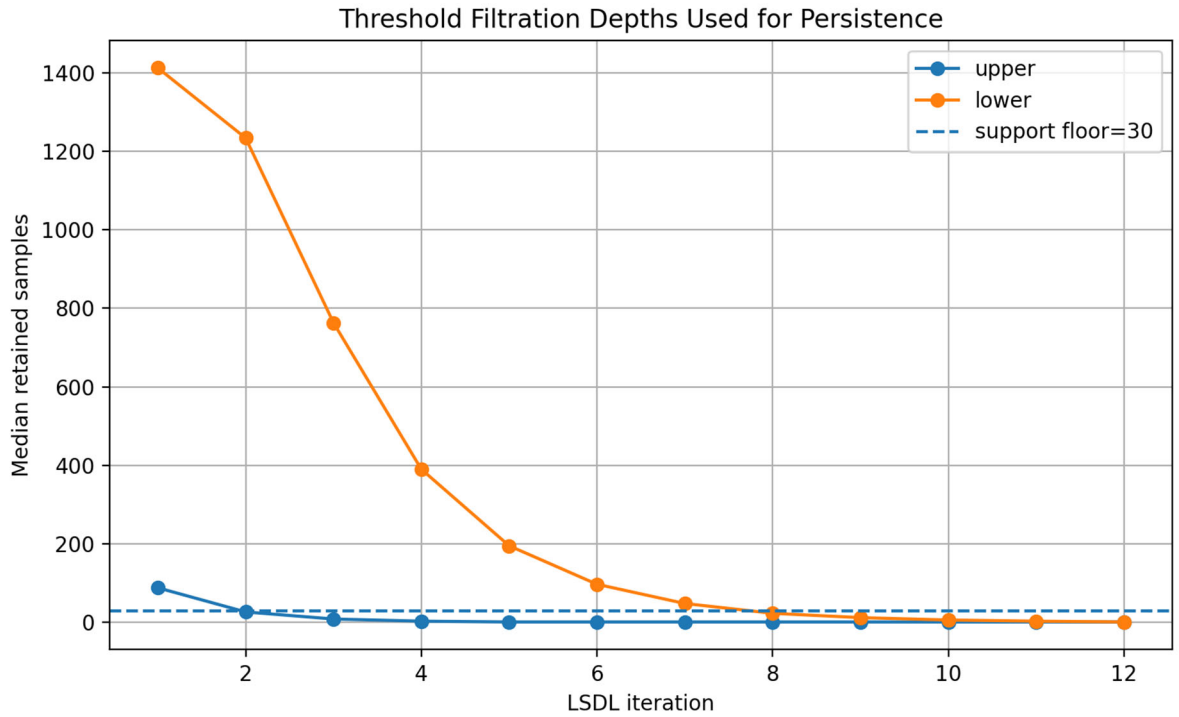


Figure 22. Persistence filtration across localisation depth. Evolution of retained-support structure throughout recursive threshold localisation. Persistent signal structures survive across multiple localisation depths, whereas transient structures disappear rapidly from the filtration.

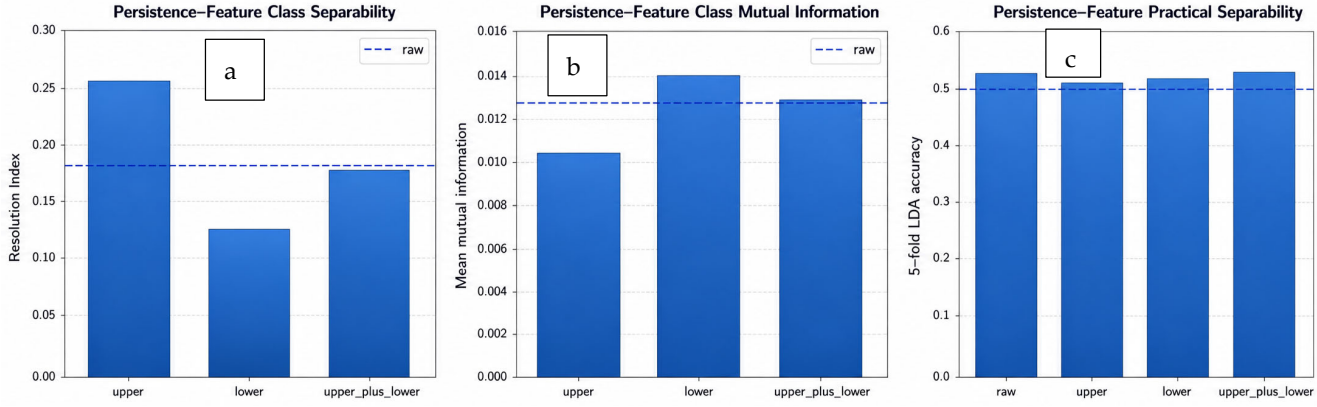


Figure 23. Persistence-driven discriminative performance. (**a**) Resolution Index based on persistence features. (**b**) Mutual information between persistence features and class labels. (**c**) LDA classification accuracy. This figure demonstrates that persistence-derived features yield classification performance comparable to the raw representation. While substantial gains in classification accuracy are not observed, persistence features maintain predictive performance while providing enhanced structural interpretability through lifetime, persistence energy, and concentration descriptors. This suggests that persistence primarily captures stable signal organisation rather than directly maximising discriminative accuracy.

Persistence Feature Distributions

The results in Figure 24 show that persistent structures exhibit class-dependent behaviour.

Differences emerge in mean persistence lifetime, total persistence energy, persistence concentration, and long-track prevalence.

Persistence Geometry

The results in Figure 25 show that the persistence features produce a more discriminative representation than the raw-feature space.

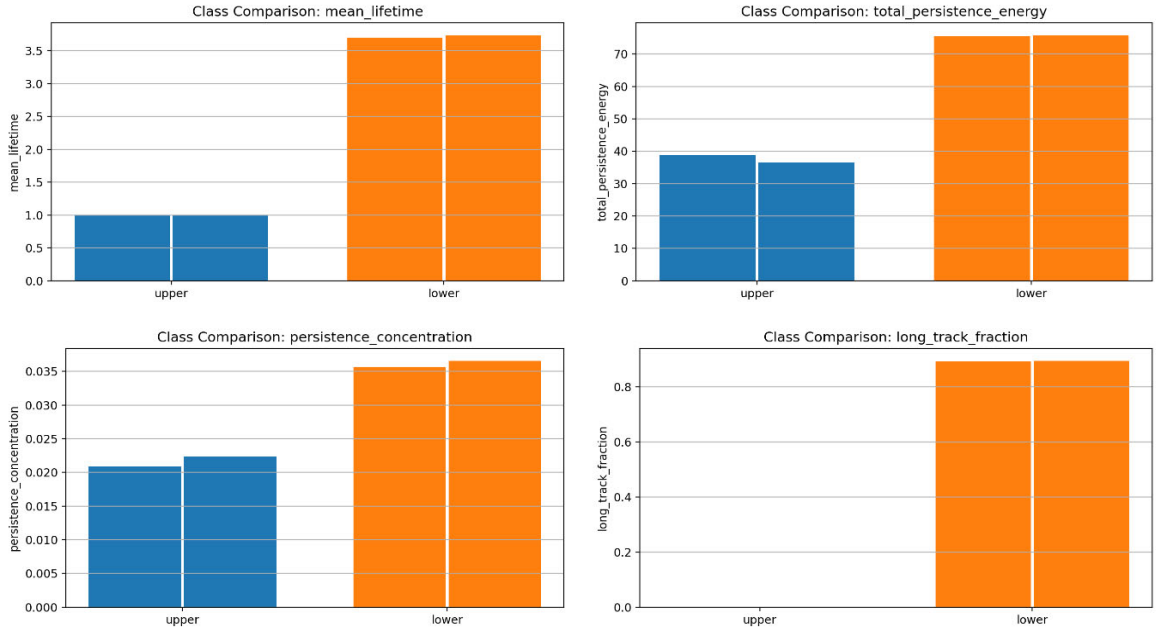


Figure 24. Class-conditioned persistence statistics. Comparison of persistence-derived feature distributions between classes. Persistent structures exhibit class-dependent differences in lifetime, energy, concentration, and long-track prevalence, indicating that persistence carries discriminative information.

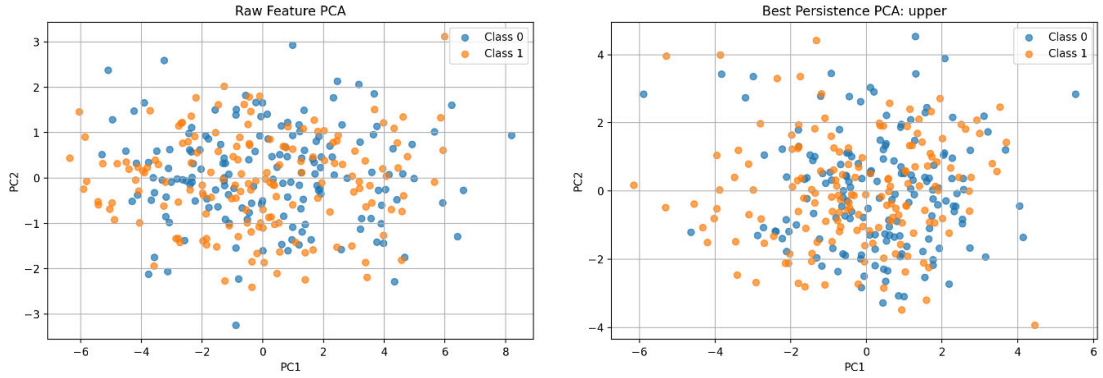


Figure 25. Persistence feature-space geometry. Principal Component Analysis (PCA) projections of the feature space before and after persistence-based localisation. Persistence features produce increased class compactness and improved class separation relative to the raw representation.

8.9. Discussion

The results demonstrate that recursive localisation naturally induces a persistence filtration over amplitude-support space. Signal structures can therefore be characterised by their survival across localisation depth rather than by amplitude at a single threshold.

Persistent structures exhibit greater stability, carry discriminative information, and produce improved feature-space geometry relative to the raw representation. Consequently, the LSDL may be interpreted as a persistence-based signal representation framework in which informative structures are identified through threshold survival across the localisation scale.

9. Spectral Localisation and Oscillatory Geometry

9.1. Overview

Although recursive localisation is carried out directly in amplitude space, its consequences also extend to the frequency domain. This section examines how gradual support contraction rearranges oscillatory structure and alters spectral representations, offering a complementary frequency-domain interpretation of the localisation process [1,3,4,6].

The LSDL may be interpreted as a spectral localisation framework because recursive amplitude localisation alters the distribution of spectral power across frequency space. Rather than merely selecting amplitude-support regions, localisation may concentrate oscillatory information into progressively more coherent spectral structures.

9.2. Localised Spectral Representation [1,3,4]

Let

$$X(\omega) = \mathcal{F}(x)$$

denote the Fourier representation of a signal x.

For the localised signal

$$y^{(k)} = L_{\tau_k}(y),$$

the corresponding localised spectrum is

$$X^{(k)}(\omega) = \mathcal{F}\left(y^{(k)}\right),$$

with spectral-power density

$$P_k(\omega) = \mid X^{(k)}(\omega) \mid^2.$$

This defines a sequence of spectra indexed by localisation depth.

9.3. Spectral Entropy and Information Concentration [19]

Normalised spectral power is

$$p_k(\omega) = \frac{P_k(\omega)}{\sum_\omega P_k(\omega)}.$$

Spectral entropy is

$$H_{\Omega,k} = -\sum_\omega p_k(\omega) \log p_k(\omega).$$

The normalised spectral entropy is

$$\widetilde{H}_{\Omega,k} = \frac{H_{\Omega,k}}{\log \mid \Omega \mid}.$$

Spectral information concentration is defined as

$$I_{\Omega,k} = 1 - \widetilde{H}_{\Omega,k}.$$

Low entropy and high information concentration indicate coherent oscillatory structure rather than diffuse broadband activity.

9.4. Spectral Localisation Gain [1,3,4]

Define spectral support

$$\Omega_k = \{\omega : P_k(\omega) > \varepsilon\}.$$

Spectral-support density is

$$\rho_{\Omega,k} = \frac{\mid \Omega_k \mid}{\mid \Omega \mid}.$$

The spectral localisation gain is

$$G_{\Omega,k} = \frac{I_{\Omega,k}}{\rho_{\Omega,k}}.$$

https://doi.org/10.3390/signals7040083

This quantity mirrors the amplitude-space localisation gain introduced in Step 2 and measures oscillatory information concentration relative to spectral-support size.

9.5. Dominant-Frequency Persistence [1,3,4]

The dominant oscillatory component is

$$\omega_k^\star = \arg\max_\omega P_k(\omega).$$

Tracking

$$\omega_1^\star, \omega_2^\star, \ldots, \omega_K^\star$$

across localisation depth defines oscillatory persistence.

Persistent oscillatory structures satisfy

$$\omega_k^\star \approx \omega^\star$$

over multiple localisation depths.

9.6. Spectral Class Geometry

For class-labelled signals, define the spectral feature representation [2,3]

$$\zeta_k(x_i^{(c)}) = [H_{\Omega,k}, I_{\Omega,k}, G_{\Omega,k}, \omega_k^\star].$$

Class separability is quantified by

$$\Lambda_{\Omega,k} = \frac{\mathrm{tr}(S_{B,\Omega,k})}{\mathrm{tr}(S_{W,\Omega,k}) + \varepsilon}.$$

This evaluates whether localisation improves oscillatory class geometry.

9.7. Spectral Localisation Hypothesis

The central hypothesis is

$$\exists k^\star : I_{\Omega,k^\star} > I_{\Omega,0}$$

and/or

$$\Lambda_{\Omega,k^\star} > \Lambda_{\Omega,0}.$$

Thus, recursive localisation is expected to improve spectral organisation and oscillatory separability.

9.8. Experimental Validation

Spectral Information Concentration

The results in Figure 26 show that the recursive localisation reduces spectral entropy and increases the oscillatory information concentration. The feature extraction done as part of this section spans the following: total spectral power, low-frequency power ratio, mid-frequency power ratio, high-frequency power ratio, normalised spectral entropy, spectral information concentration, spectral-support density, dominant frequency, dominant-frequency power ratio, spectral centroid, retained spectral-power ratio, spectral concentration gain, spectral flatness and oscillatory peak-power ratio.

Figure 26 illustrates branch-dependent changes in spectral entropy across the recursive decomposition levels. The lower branch shows an increase in spectral entropy as recursion progresses, indicating that spectral energy becomes more widely distributed across the frequency domain. This behaviour reflects reduced spectral concentration and suggests that the lower branch does not consistently isolate a progressively narrower spectral structure.

Instead, the recursive retention of lower-amplitude signal components can produce a more dispersed spectral representation.

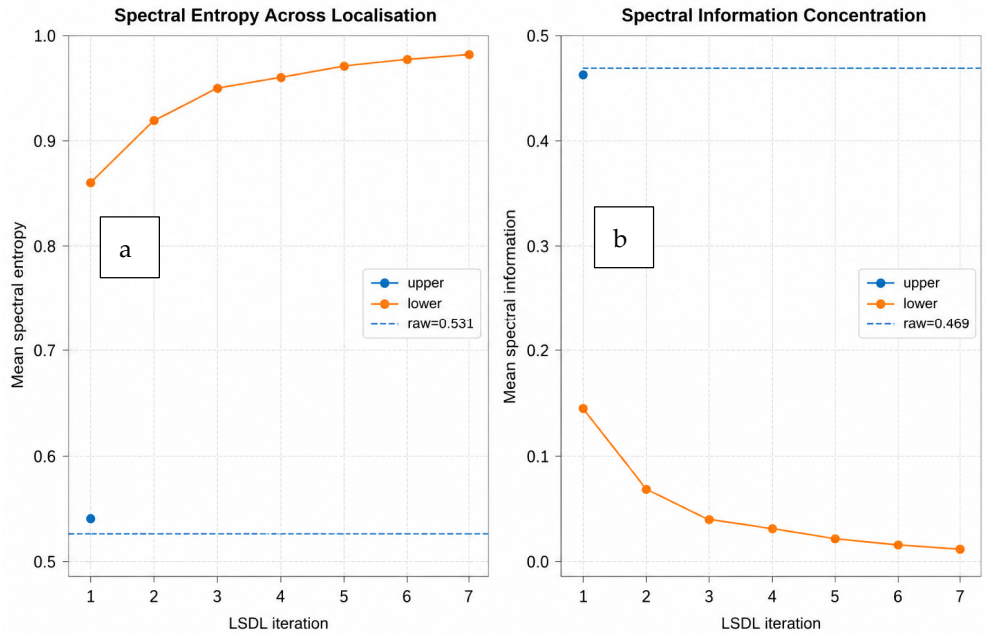


Figure 26. Spectral entropy and oscillatory information concentration. (**a**) Spectral entropy $H_{\Omega,k}$ across localisation depth. Entropy decreases as recursive localisation suppresses diffuse broadband structure and concentrates spectral power into increasingly coherent oscillatory components. (**b**) Spectral information concentration $I_{\Omega,k}$, showing the corresponding increase in oscillatory organisation. Together, these results demonstrate the progressive concentration of spectral information under recursive localisation.

The upper and lower branches should therefore not be interpreted as showing equivalent spectral behaviour. Whereas the upper branch preferentially retains larger-amplitude signal components and may preserve dominant spectral structures, the lower branch retains progressively weaker-amplitude components whose spectral content can be more broadly distributed. The observed changes therefore indicate branch-specific spectral reorganisation rather than a universal increase in spectral concentration.

Spectral Class Geometry

Figure 27 shows that separability improves across a range of admissible localisation depths.

Oscillatory Persistence

Figure 28 shows that the dominant-frequency trajectories reveal whether coherent oscillatory modes survive localisation.

Figure 28 shows that dominant-frequency behaviour depends on recursion depth. Relatively modest changes are observed at earlier recursive levels, suggesting that the principal frequency component can initially be preserved during support localisation. However, more pronounced dominant-frequency shifts occur at later recursion levels, particularly as the retained support becomes increasingly limited.

These results indicate that frequency preservation is conditional rather than uniform across the recursive sequence. Earlier levels retain a broader portion of the original signal structure, whereas deeper recursion can suppress components that contribute to the original dominant frequency and reveal alternative spectral components. Consequently, the recursive process should be interpreted as progressively modifying the spectral representation rather than maintaining complete frequency stability.

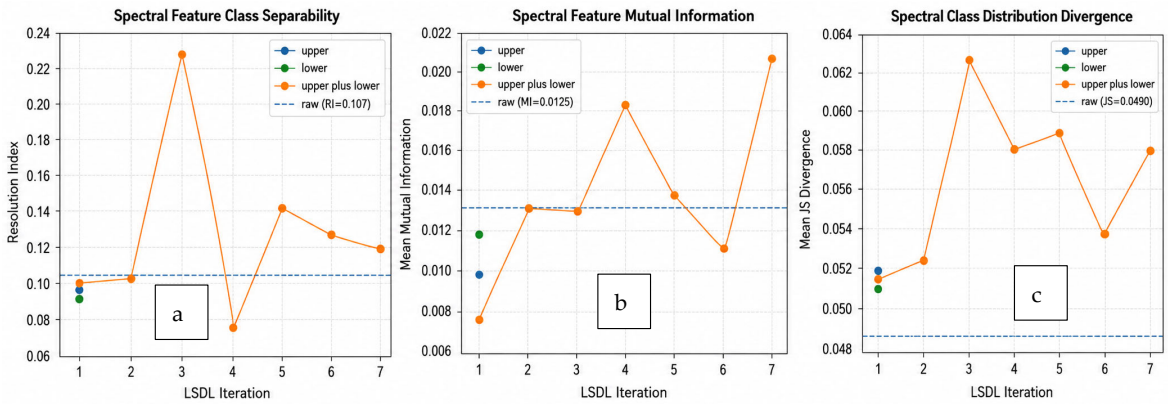


Figure 27. Oscillatory class geometry under recursive localisation. (**a**) Resolution Index computed from spectral features. (**b**) Mutual information between spectral representations and class labels. (**c**) Jensen–Shannon divergence between class-specific spectral distributions. Improvements in these measures indicate that recursive localisation enhances oscillatory class geometry and increases the discriminative structure of spectral representations.

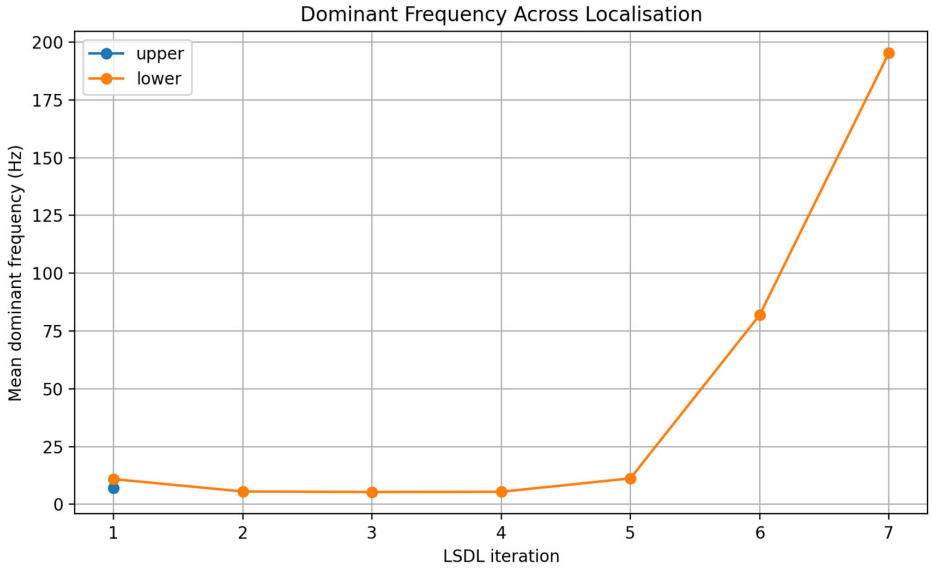


Figure 28. Dominant-frequency persistence across localisation depth. Evolution of the dominant oscillatory component $\omega_k^\star$ under recursive localisation. Stable trajectories indicate persistent oscillatory structure, whereas large shifts would imply spectral reorganisation. The persistence of dominant frequencies provides evidence that localisation preserves coherent rhythmic modes while suppressing diffuse spectral content.

Practical Classification Performance

Figure 29 shows that the spectral localisation features are evaluated through downstream classification and feature-space geometry.

The recursive support localisation reorganises oscillatory structure as well as amplitude structure, can be seen from the results Spectral entropy decreases, oscillatory information concentration increases, and the dominant oscillatory modes remain stable across localisation depth. These findings indicate that the LSDL is not only an amplitude selection framework but also a mechanism for recursive spectral reorganisation. Consequently, localisation may improve oscillatory class geometry by suppressing diffuse broadband structure while preserving coherent rhythmic components. This interpretation is particularly relevant for physiological systems, in which pathology is often associated with oscillatory dysregulation, spectral redistribution, and rhythmic instability rather than amplitude changes alone.

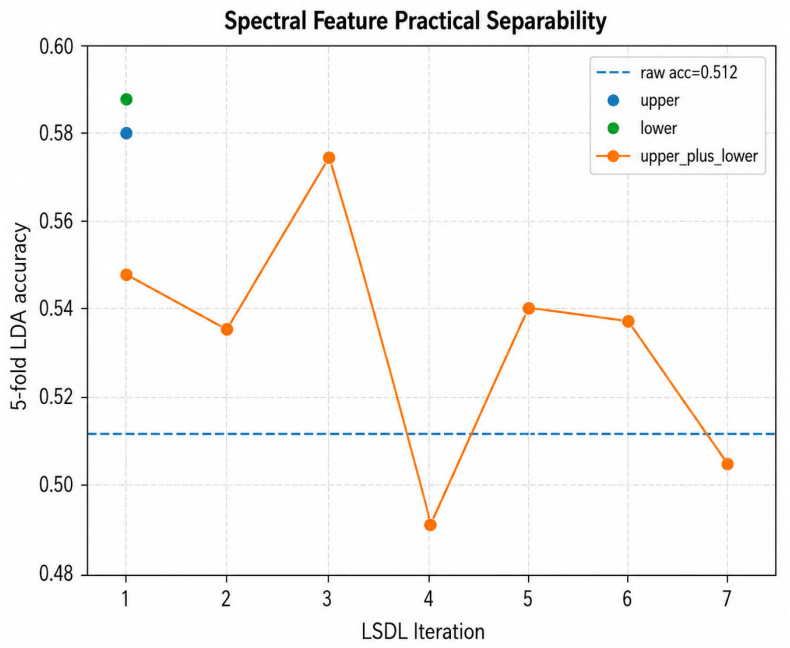


Figure 29. Spectral localisation performance and feature-space organisation. Linear Discriminant Analysis (LDA) classification accuracy using spectral-localisation features across localisation depth.

10. Cross-Geometric Fusion and Unified LSDL Representation

The preceding sections show that recursive localisation produces several complementary representations of signal structure instead of one descriptive geometry. The final stage combines these structural, informational, persistence, and spectral viewpoints into a unified multi-geometric representation derived from a shared recursive support filtration

$$\Phi_T, \Phi_I, \Phi_P, \Phi_\Omega$$

corresponding to

- Time/amplitude geometry;
- Information geometry;
- Persistence geometry;
- Spectral geometry.

The purpose of Step 8 is to formalise how these geometries are fused into a unified representation manifold. Rather than treating localisation as a thresholding procedure, Step 8 interprets the LSDL as a multi-geometric representation-learning framework.

10.1. Unified Representation [2]

At localisation depth k, define

$$\Psi_k = \left[\Phi_T^{(k)}, \Phi_I^{(k)}, \Phi_P^{(k)}, \Phi_\Omega^{(k)}\right].$$

This forms the multi-geometric latent representation.

For upper and lower localisation branches,

$$\Psi_k^U, \Psi_k^L,$$

the fused representation becomes

$$\Psi_k^{fusion} = \left[\Psi_k^U, \Psi_k^L\right].$$

The upper branch captures dominant salient structure, whereas the lower branch captures residual latent structure.

10.2. Geometry-Dependent Optimality

Different objectives induce different optimal localisation depths:

$$k^{\star}_{RI} = \arg\max RI(\Psi_k),$$
$$k^{\star}_{MI} = \arg\max MI(\Psi_k),$$
$$k^{\star}_{clf} = \arg\max C(\Psi_k).$$

Consequently,

$$k^{\star}_{RI} \neq k^{\star}_{MI} \neq k^{\star}_{clf}$$

may naturally occur.

This is not a failure of localisation but evidence that the fused manifold contains multiple geometric structures that become optimal under different objectives.

10.3. Unified Representation Proposition

The following proposition concerns common-filtration construction of the LSDL representation. Let

$$\left\{\mathcal{L}^{b}_{k}(x) : b \in \{U, L\}, k \in \mathcal{K}_{\text{adm}}\right\}$$

be a finite family of well-defined localised signals generated by the upper and lower support-filtration operators. Let

$$\phi_A, \phi_I, \phi_P, \phi_S$$

denote finite-valued feature maps representing, respectively, time–amplitude/support, information, persistence and spectral geometry. Then, for every admissible depth k, the concatenated representation

$$\Phi_k(x) = \left[\phi_A(\mathcal{L}_k(x)), \phi_I(\mathcal{L}_k(x)), \phi_P(\left\{\mathcal{L}_j(x)\right\}_{j\leq k}), \phi_S(\mathcal{L}_k(x))\right]$$

is a well-defined finite-dimensional representation derived from a common support-filtration trajectory.

The recursion horizon and signal length are finite; therefore, each localised signal contains finitely many samples, and each admissible trajectory contains finitely many support sets. By assumption, each geometric map returns a finite-valued vector on its stated domain. Their finite concatenation is therefore well defined and finite-dimensional. Since every component is computed from either the localised signal at depth k or its preceding filtration trajectory, all components share the same underlying support-filtration construction. This proposition establishes only the mathematical construction and common origin of the multi-geometric representation. It does not imply that concatenating geometries necessarily improves separability, mutual information, or predictive accuracy. Such improvement depends on the signal distribution, localisation depth, feature normalisation, sample size, classifier, and validation procedure, and is therefore evaluated empirically in Section 10.4.

10.4. Experimental Validation

In this section, a multi-geometric representation approach is adopted across four complimentary feature families spanning structural/time–amplitude, information, spectral and persistence, yielding 11, six, 14 and 12 features, respectively. While including the LDA, additional classification models were utilised in this section, including RBF Support Vector Machine; Extra Trees; and Random Forest.

The results shown in Figures 30–32 show the aftermath and therein the results for the various experimental validations.

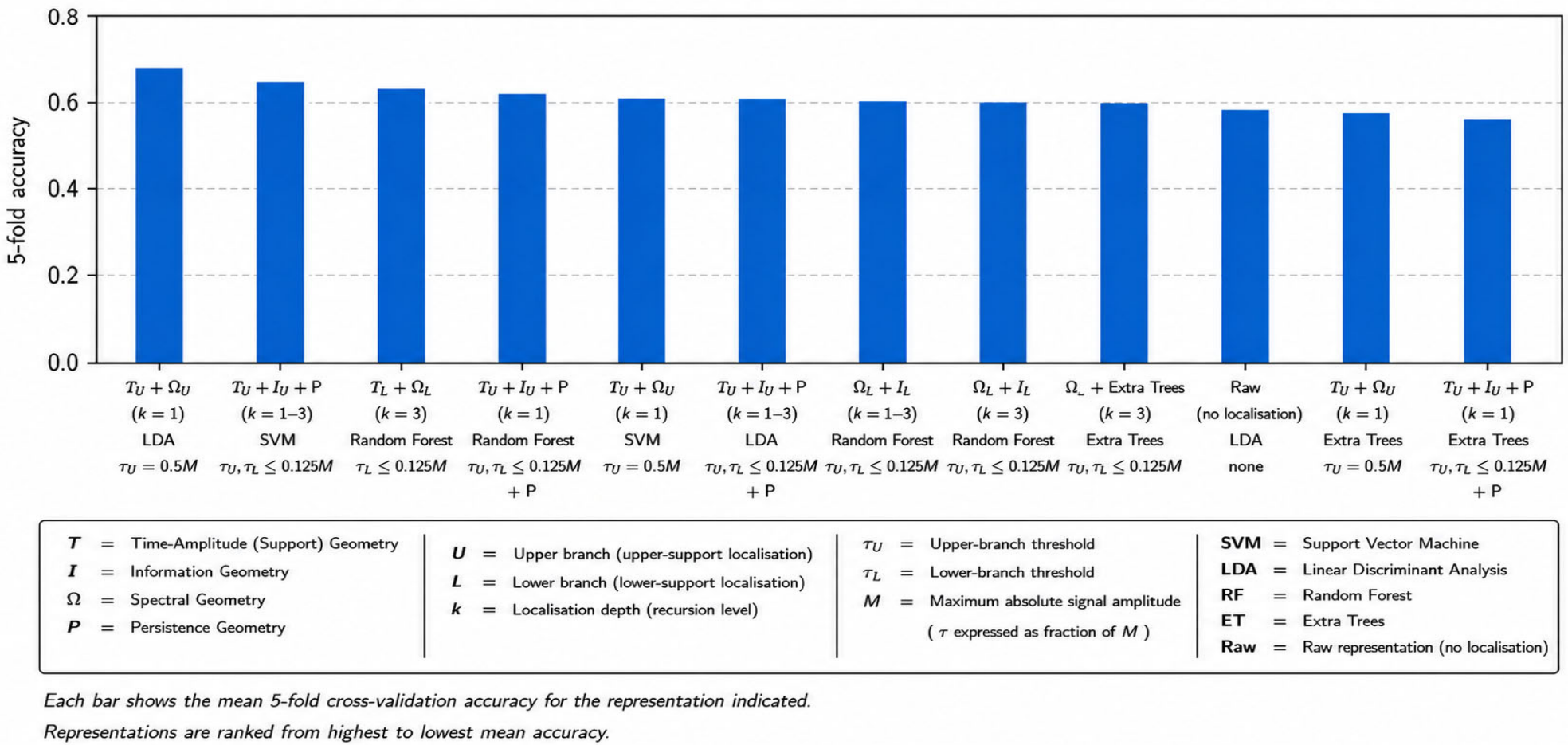


Figure 30. Highest-performing multi-geometric LSDL representations obtained under five-fold cross-validation. Representations are ranked according to classification performance and illustrate the contribution of different geometric combinations to discriminative capability. The results demonstrate that fusion of complementary geometries generally outperforms individual geometric domains.

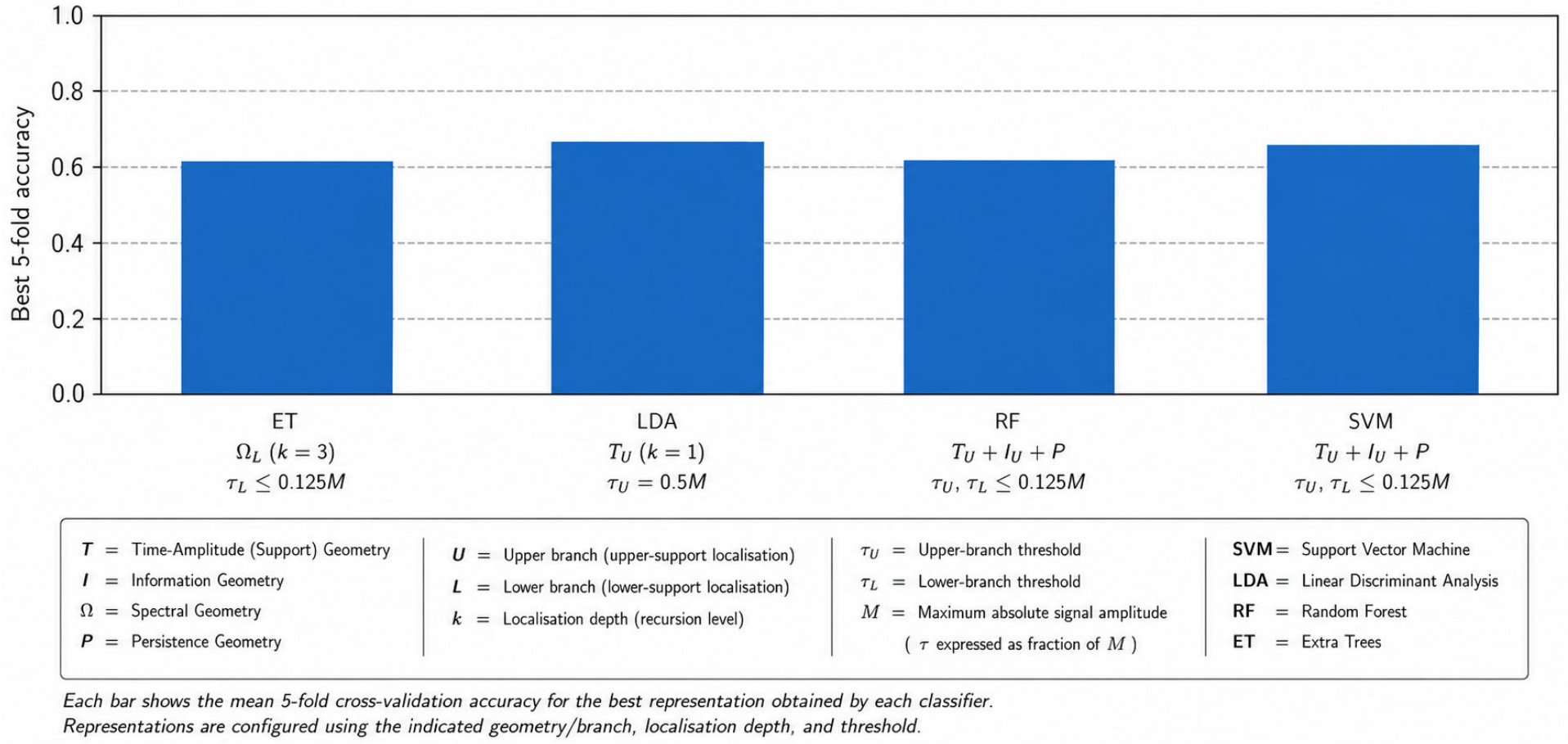


Figure 31. Optimal multi-geometric representation for each classifier family. Different classifiers favour different localisation regimes and geometric combinations, demonstrating geometry-dependent optimality. The absence of a universal optimum supports the hypothesis that the LSDL generates nonlinear latent manifolds with multiple discriminative operating points.

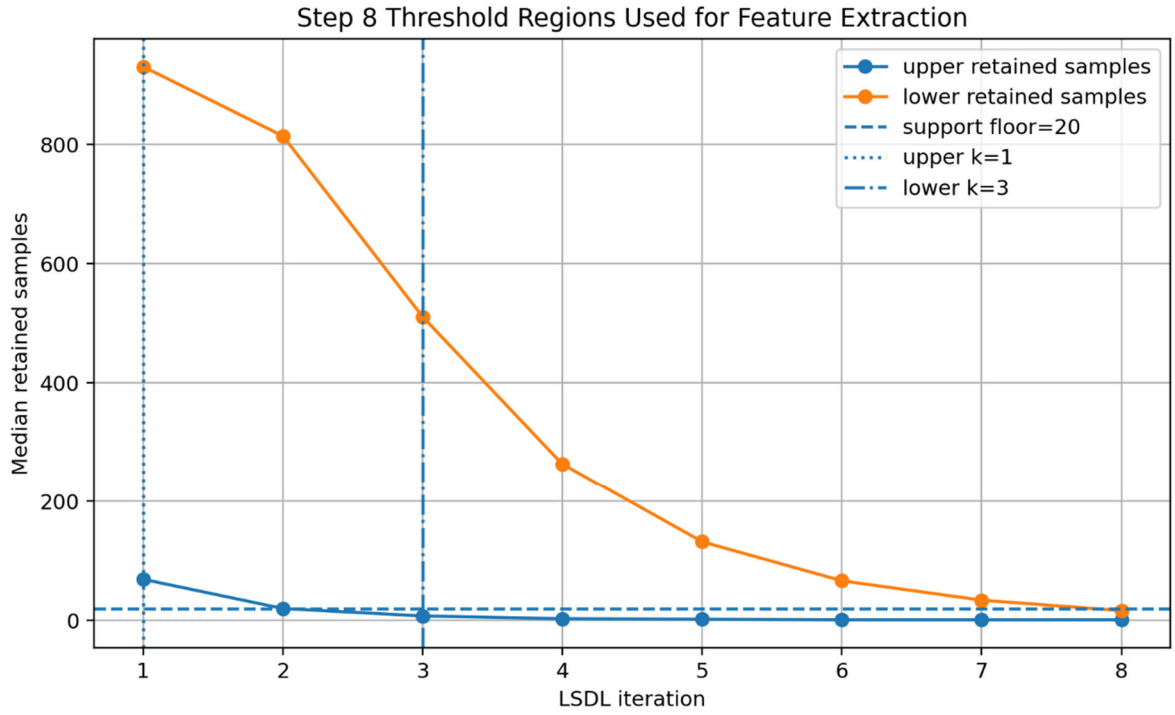


Figure 32. Support-feasible localisation regions. Retained-support cardinality as a function of localisation depth together with admissible threshold regions. Optimisation is restricted to support-feasible localisation depths to prevent geometric degeneration caused by excessive support contraction.

11. Relationship to Existing Representation Approaches

11.1. STFT and Wavelet Representations

The short-time Fourier transform (STFT) and wavelet transforms are among the most widely used signal representations. Both methods seek to characterise non-stationary signals through localised spectral analysis [1,3,4,6].

For the STFT,

$$X(t,\omega) = \int x(\tau) w(\tau - t) e^{-j\omega\tau} d\tau,$$

where $w(\cdot)$ denotes a sliding analysis window. The resulting representation provides a time-frequency decomposition whose resolution is constrained by the chosen window length.

Wavelet transforms address this limitation by employing multiscale basis functions [5–8],

$$W(a,b) = \frac{1}{\sqrt{a}} \int x(t) \psi\left(\frac{t-b}{a}\right) dt,$$

allowing adaptive localisation in both time and scale.

Both approaches primarily characterise spectral-temporal geometry. However, neither directly models information concentration, persistence structure, or support topology. In contrast, the spectral geometry developed in Step 7 arises naturally from recursive support localisation and remains coupled to the underlying support manifold.

11.2. EMD and VMD

Empirical mode decomposition (EMD) and variational mode decomposition (VMD) decompose signals into oscillatory modes [31,32].

EMD iteratively extracts intrinsic mode functions (IMFs),

$$x(t) = \sum_{m=1}^{M} \mathrm{IMF}_m(t) + r(t),$$

where $r(t)$ denotes the residual component.

VMD formulates decomposition as a constrained variational optimisation problem, producing band-limited modes with improved robustness and spectral separation.

Both EMD and VMD focus on oscillatory structure and have proven valuable for analysing physiological and mechanical systems. However, they operate primarily in the spectral domain and do not explicitly incorporate information geometry, persistence geometry, or recursive support evolution.

In contrast, the LSDL does not decompose the signal into modes. Instead, it recursively reorganises the support structure, allowing oscillatory geometry to emerge as one projection within a broader multi-geometric representation.

11.3. Sparse Coding

Sparse coding assumes that signals admit a sparse representation in an overcomplete dictionary [11,17],

$$x \approx D\alpha,$$

where D denotes a dictionary and α is a sparse coefficient vector.

The optimisation problem is typically written as

$$\min_{\alpha} \parallel x - D\alpha \parallel_2^2 + \lambda \parallel \alpha \parallel_1 .$$

Sparse coding has strong theoretical links to compressed sensing, feature extraction, and representation learning.

Conceptually, sparse coding and the LSDL share an interest in sparse structure. However, sparse coding defines sparsity through coefficient activation within a learned basis, whereas the LSDL defines sparsity through recursive support filtration. Consequently, sparsity in the LSDL remains directly interpretable in the original signal domain rather than in a transformed coefficient space.

11.4. Topological Data Analysis and Persistence

Topological Data Analysis (TDA) seeks to characterise shape through persistent topological features [13,18].

Given a filtration

$$\mathcal{F}_1 \subseteq \mathcal{F}_2 \subseteq \cdots \subseteq \mathcal{F}_K,$$

topological features are tracked across scale through persistence diagrams and barcodes.

Persistence is quantified through birth and death parameters,

$$(b_i, d_i),$$

yielding lifetime

$$l_i = d_i - b_i.$$

Step 6 demonstrated that the LSDL naturally induces a filtration through recursive threshold evolution,

$$S_1 \supseteq S_2 \supseteq \cdots \supseteq S_K.$$

Consequently, persistence geometry arises intrinsically within the LSDL without requiring explicit simplicial-complex construction. This establishes a conceptual connection between support filtration and topological persistence while remaining computationally simpler for one-dimensional signals.

11.5. Information Bottleneck Theory

The Information Bottleneck (IB) framework seeks representations that maximise task-relevant information while compressing irrelevant structure.

Formally,

$$\max I(Z;Y) - \beta I(Z;X),$$

where

- X denotes the input;
- Y denotes the target variable;
- Z denotes the compressed representation.

The objective is to preserve predictive information while discarding nuisance variation. The information-localisation framework developed in Step 5 is conceptually related. Recursive localisation progressively removes diffuse support and increases information concentration and class-relevant mutual information. However, unlike the IB, the LSDL does not require optimisation over latent variables. Instead, information concentration emerges through recursive support evolution.

11.6. Deep Representation Learning

Modern deep-learning methods construct latent representations through multilayer nonlinear transformations [2],

$$z_L = f_L \circ f_{L-1} \circ \cdots \circ f_1(x).$$

These methods have achieved state-of-the-art performance across numerous domains, but they often suffer from limited interpretability. The latent geometries learned by deep networks are generally implicit and difficult to analyse directly. In contrast, each stage of the LSDL framework produces explicitly interpretable geometric quantities, including support density, entropy, localisation gain, persistence lifetime, spectral concentration, and class geometry.

Accordingly, the LSDL may be viewed as an interpretable representation-learning framework whose latent manifold is generated analytically through recursive support filtration rather than learned through optimisation.

11.7. LSDL as a Multi-Geometric Support-Filtration Framework

The preceding sections reveal that existing representation methods generally focus on a single geometric viewpoint. In contrast, the LSDL generates multiple geometries from a common support-filtration process [18].

The unified representation may be written as

$$\Psi_{LSDL} = [\Phi_T, \Phi_I, \Phi_P, \Phi_\Omega],$$

where

- Φ_T denotes time–amplitude geometry;
- Φ_I denotes information geometry;
- Φ_P denotes persistence geometry;
- Φ_Ω denotes spectral geometry.

Consequently, the LSDL is most appropriately viewed not as a thresholding algorithm but as a multi-geometric support-filtration framework for representation learning.

https://doi.org/10.3390/signals7040083

11.8. Benchmark Comparison Results

To evaluate the effectiveness of the proposed LSDL approach, a controlled benchmark comparison was conducted against six widely used EMG signal representations: raw time-domain signals, STFT, DWT, EMD, VMD, and sparse coding. All competing methods were evaluated through an identical experimental pipeline to ensure that performance differences resulted solely from the signal representation rather than from downstream processing. The experiments used the UCI EMG Data for Gestures dataset, which was segmented into 1 s windows of 200 samples without overlap. Each analysis window therefore consisted of an 8×200 multichannel EMG segment. A common processing pipeline was applied to every signal representation, and after transformation, identical feature extraction, classifier design, and evaluation procedures were used across all methods to provide a controlled comparison.

Classification used LDA, and performance was assessed with grouped cross-validation to prevent windows from the same gesture repetition from appearing in both the training and testing partitions. Where participant-specific optimisation was required, as for the LSDL and wavelet, parameter selection was performed through an independent validation stage before final evaluation. To ensure that comparisons reflected differences in signal representation rather than feature engineering, an identical feature vector was extracted from every representation. Conventional time-domain descriptors were computed independently for each channel, comprising Mean Absolute Value (MAV), Root Mean Square (RMS), Waveform Length (WL), Zero Crossings (ZC), Slope Sign Changes (SSC), and Willison Amplitude (WAMP).

The resulting channel-wise feature vectors were concatenated to form the final representation provided to the LDA classifier.

The baseline representation utilised the original segmented EMG windows directly, without signal decomposition or transformation, before feature extraction. Twenty-four candidate decompositions were evaluated during participant-specific optimisation, comprising both upper and lower recursive branches across threshold levels T1 to T12. After optimisation, the selected decomposition was fixed and applied to all subsequent test windows. Time–frequency representations were generated using a 64-sample Hann window with 50% overlap. Spectral coefficients were reconstructed into a one-dimensional representation before extraction of the common feature set. For the wavelet method, the signals were decomposed using the Daubechies-4 (db4) mother wavelet, and five candidate reconstruction regions (A4, D4, D3, D2, and D1) were evaluated during participant-specific optimisation. The optimal reconstruction level was then fixed before testing. The EMD was performed using the classical sifting procedure until convergence, and the leading IMFs were retained for feature extraction with identical downstream processing. VMD employed a fixed five-mode decomposition (K = 5) with identical optimisation parameters across all participants, and feature extraction was subsequently performed on the reconstructed decomposition. For sparse coding, sparse representations were generated using an overcomplete learned dictionary. Sparse coefficients were estimated using Orthogonal Matching Pursuit (OMP) before identical feature extraction and classification. The results in Table 3 shows a summary of the overall classification accuracy obtained from each representation.

The LSDL achieved the highest overall classification performance, with a mean accuracy of $81.01 \pm 0.11\%$. This result marginally exceeded that of the raw signal representation and also outperformed all conventional decomposition-based methods examined. Among the competing signal representations, VMD produced the strongest performance ($80.55 \pm 0.06\%$), followed by STFT ($80.27 \pm 0.28\%$), sparse coding ($79.84 \pm 0.40\%$), and wavelet decomposition ($79.78 \pm 0.15\%$). EMD showed substantially lower performance

(72.65 ± 0.10%), indicating that the adaptive sifting process yielded comparatively less discriminative representations for this EMG classification task.

Table 3. Summary of the overall classification accuracy obtained by each representation.

Method	Classification Accuracy (%)
LSDL	**81.01 ± 0.11**
Raw	80.82 ± 0.09
VMD	80.55 ± 0.06
STFT	80.27 ± 0.28
Sparse Coding	79.84 ± 0.40
Wavelet	79.78 ± 0.15
EMD	72.65 ± 0.10

Overall, these findings indicate that recursive support localisation preserves discriminative neuromuscular information at least as effectively as substantially more computationally intensive decomposition techniques, while avoiding the iterative optimisation procedures required by methods such as EMD, VMD, and sparse coding. In conjunction with the computational efficiency analysis presented in the following section, these results show that the LSDL offers a favourable balance between classification performance and computational cost for real-time EMG pattern recognition.

11.9. Computational Efficiency Analysis

Beyond classification performance, the practical suitability of each signal representation for real-time computation was assessed through computational profiling. Because real-time systems operate under strict latency constraints, computational efficiency is an equally important consideration alongside classification accuracy. Using the UCI EMG Data for Gestures dataset, timing measurements were obtained after completion of all offline optimisation procedures. Consequently, the reported execution times reflect online inference only and indicate the computational cost encountered during real-time deployment.

For LSDL and wavelet, participant-specific decomposition selection was treated as a one-time offline calibration stage and therefore was excluded from runtime measurements. Online execution began only after the optimal decomposition had been identified and fixed. Each timing measurement included the complete online processing pipeline, spanning signal representation generation, peak localisation (LSDL only), feature extraction, feature vector construction, and LDA inference. Offline processes, including decomposition-region optimisation, dictionary learning, and parameter selection, were excluded because they are performed once during system calibration.

To minimise operating system scheduling effects, each method was executed repeatedly on identical EMG windows, and runtime statistics were computed from the resulting distributions. Median execution time was adopted as the primary measure of central tendency, whereas the 95th percentile quantified worst-case execution behaviour. Processing throughput, measured as windows per second, and computational cost relative to the LSDL were also computed. The summary in Table 4 shows the measured computational performance for each signal representation.

Computational Results

The LSDL required a median execution time of 1.111 ms per one-second EMG window, corresponding to a processing throughput of approximately 901 windows per second. This runtime was only marginally higher than direct processing of the raw EMG signal (0.525 ms), demonstrating that recursive support localisation introduces relatively little

computational overhead, despite performing recursive decomposition and peak localisation before feature extraction.

Table 4. Summary of the measured online computational performance for each competing signal representation.

Method	Median Online Time per 1 s Window	95th Percentile	Throughput	Relative Cost vs. LSDL
Raw	0.525 ms	0.576 ms	1907 windows/s	0.47×
Wavelet	0.920 ms	1.223 ms	1088 windows/s	0.83×
LSDL	**1.111 ms**	**1.303 ms**	**901 windows/s**	**1.00×**
STFT	1.947 ms	2.649 ms	514 windows/s	1.75×
VMD	4.352 ms	5.811 ms	230 windows/s	3.92×
Sparse Coding	5.837 ms	6.188 ms	171 windows/s	5.25×
EMD	24.639 ms	32.775 ms	41 windows/s	22.18×

Among the decomposition-based approaches, the wavelet transform showed the lowest computational cost (0.920 ms) and slightly outperformed the LSDL in execution speed. However, the LSDL achieved higher classification accuracy while maintaining a comparable runtime, indicating a favourable balance between computational efficiency and predictive performance.

STFT required approximately 1.75 times the computational cost of the LSDL because of repeated Fourier-domain transformations. The iterative optimisation procedures used by VMD and sparse coding resulted in substantially greater computational demands, requiring approximately 3.9 and 5.3 times the runtime of the LSDL, respectively. EMD imposed the greatest computational burden, with a median processing time of 24.639 ms, representing more than a 22-fold increase relative to the LSDL.

The 95th percentile runtimes closely tracked the corresponding median values for all methods, indicating stable execution with limited variability. The LSDL showed particularly consistent runtime behaviour, increasing from 1.111 ms to only 1.303 ms under near-worst-case execution, suggesting predictable latency characteristics that are desirable for embedded real-time control systems.

Overall, these findings show that the LSDL occupies an advantageous position within the computational performance spectrum. Although marginally slower than direct processing and conventional wavelet decomposition, it substantially outperformed more computationally intensive adaptive decomposition techniques while simultaneously achieving the highest classification accuracy. Consequently, the LSDL provides an effective compromise between discriminative performance and computational efficiency, supporting its suitability for latency-sensitive myoelectric pattern-recognition applications.

To complement the empirical timing analysis, the theoretical computational complexity of each signal representation is summarised in Table 5.

The empirical runtime measurements closely followed the expected theoretical computational behaviour, where methods based on direct linear transforms (raw, wavelet and the LSDL) exhibited the lowest execution times, whereas optimisation-driven approaches such as EMD, VMD, and sparse coding incurred substantially greater computational overhead due to their iterative convergence procedures. Although the LSDL introduces recursive localisation relative to the raw signal representation, its computational cost remained close to linear in practice while delivering superior classification performance, reinforcing its suitability for real-time signal processing.

Table 5. Computational complexity table.

Method	Approximate Computational Complexity
Raw	O(N)
LSDL	O(KN), where K denotes the number of recursive decomposition levels
STFT	O(NlogN)
Wavelet	(O(N))
EMD	Approximately $O(IN)$, where I denotes the number of sifting iterations
VMD	Approximately $O(IK\ N\log\ N)$, where K is the number of modes and I is the number of optimisation iterations
Sparse Coding	Approximately $O(ITM)$, dominated by iterative sparse optimisation, where T is the dictionary size, M is the target sparsity level and I is the number of optimisation iterations

Alongside the signal-processing capabilities of the LSDL, Table 6 shows the various benefits of the LSDL from a multitude of perspectives.

Table 6. Perspective comparison table.

Perspective	Benefits of AIL/LSDL
Signal	Localises informative support directly in amplitude space; reveals weak latent structure; preserves transient morphology; captures sparse discriminative remnants; and enables simultaneous extraction of temporal, informational, persistence, and spectral geometry from a single recursive process. It is effective for nonstationary and transient-rich signals.
Implementation	Simple recursive thresholding formulation; modular architecture; easy integration with existing DSP pipelines; basis-free operation, with no learned dictionary or wavelet family required; compatibility with classical machine-learning and deep-learning pipelines; and natural extensibility to multimodal fusion.
Hardware	Thresholding and support masking are lightweight operations. They require minimal memory for support representation and are well suited to FPGA and DSP implementation. Peak extraction is compatible with embedded systems. In addition, the use of recursive local operations makes the approach suitable for streaming architectures.
Computation	Avoids computationally intensive optimisation and reconstruction procedures; eliminates iterative inverse-problem solving; has lower complexity than sparse coding and compressed sensing; support contraction reduces downstream feature dimensionality; the admissibility constraint prevents pathological recursion; and feature extraction is efficient on the sparse retained support.
Real-time Processing	Recursive thresholds can operate online, and causal local computations are feasible. Their evolution is naturally streamable, and reduced retained support lowers the real-time processing burden. They are suitable for adaptive monitoring, anomaly detection, biomedical streaming, and transient event surveillance.
Representation Learning	Generates multi-geometric latent manifolds without learned bases; the support filtration itself induces representational structure; geometry-dependent optimality enables task-specific representations; and the method is complementary to spectral and deep representations rather than replacing them.
Robustness	Recursive support contraction suppresses nuisance structure, and perturbation stability is demonstrated under bounded noise. Persistence geometry identifies stable signal structures across thresholds, while the admissibility floor prevents over-localisation collapse.
Interpretability	Threshold evolution is physically interpretable; support geometry is directly observable; persistence lifetimes explain feature stability; and localisation trajectories provide insight into signal organisation, unlike opaque latent embeddings.
Scalability	The same framework is transferable across ECG, EEG, vibration, acoustics, radar, seismic, multimodal physiology, and transient-event systems, and no domain-specific basis redesign is required.
Theoretical Value	Provides a recursive support-filtration interpretation of signal structure; unifies sparse support, information geometry, persistent topology, and spectral organisation within a single framework; and introduces a geometry-driven signal representation rather than a purely transform-driven representation.

12. Conclusions

The results position recursive support localisation as a mathematically well-defined support-filtration process that progressively reorganises signal structure through nested amplitude-support contractions. Across both salient-support and residual-support branches, localisation shows predictable threshold convergence, monotonic support contraction, peak topology simplification, and non-expansion of energy, consistent with the proposed theoretical framework. Rather than serving as a conventional thresholding heuristic, the LSDL induces a hierarchy of support manifolds whose evolution reveals increasingly concentrated signal structure while preserving a finite and interpretable localisation trajectory. These findings provide the operator-theoretic basis for viewing recursive support evolution as a general signal representation mechanism, from which higher-order information, persistence, spectral, and discriminative geometries may subsequently emerge.

Future work should examine adaptive threshold trajectories, theoretical convergence properties under broader signal classes, and extensions of the support-filtration formalism to multivariate and multimodal signal representations. Establishing links between recursive support evolution and broader geometric, topological, and information-theoretic frameworks may further clarify the generality of support-based representation learning.

Funding: This research received no external funding.

Data Availability Statement: The original contributions presented in this study are included in the article. Further inquiries can be directed to the corresponding author.

Acknowledgments: Generative artificial intelligence (AI) tools based on large language models (LLMs) were used to assist with the editing, refinement, and presentation of several figures included in this manuscript. These tools were used solely to improve visual quality and consistency. All scientific content, mathematical formulations, analyses, interpretations, and conclusions were conceived, verified, and approved by the author, who take full responsibility for the content of this work.

Conflicts of Interest: The authors declare no conflict of interest.

Appendix A

Table A1. Formalism focus contrast.

Step	Formalism Focus	Main Mathematical Objects	Main Theoretical Claim Tested	Main Simulation/Validation
1	**Operator-theoretic peak localisation**	$\mathcal{L}_k^U, \mathcal{L}_k^L, \mathcal{P}_k$	LSDL is a finite nonlinear amplitude-peak localisation operator	threshold trajectory, peak-count decay, energy non-expansion, finite stopping
2	**Sparse informative support geometry**	$S_k, \rho_k, C_k, G_k, H_k$	recursive localisation contracts support while concentrating informative structure	support density decay, localisation gain rise, entropy contraction
3	**Perturbation robustness**	$\delta, \gamma(\tau), J(S, \widetilde{S}), \Xi_k$	support and peak geometry remain stable under bounded perturbation	Jaccard overlap, peak survival, energy deviation, robustness trajectory
4	**Discriminative separability**	$S_W, S_B, \mathcal{D}(k), RI(k)$	admissible localisation improves class geometry	RI, LDA/SVM/RF classification, PCA separation, threshold optimisation
5	**Information localisation**	H_k, I_k, JS, MI	localisation increases information concentration and class information divergence	entropy reduction, MI increase, JS divergence trajectories

Table A1. *Cont.*

Step	Formalism Focus	Main Mathematical Objects	Main Theoretical Claim Tested	Main Simulation/Validation
6	**Persistence geometry**	$b(p), d(p), \ell(p), E_{\text{pers}}$	persistent peaks encode threshold-stable structure	persistence lifetimes, persistence entropy, persistence overlap
7	**Spectral-temporal geometry**	$X_k(\omega), P_k(\omega), H_\Omega, I_\Omega$	localisation reorganises oscillatory structure	spectral entropy, spectral RI/MI/JS, dominant-frequency persistence
8	**Cross-geometric fusion**	$\Phi_T, \Phi_I, \Phi_P, \Phi_\Omega, \Psi_k$	multi-geometric fusion yields nonlinear latent manifolds	fused-feature classification, upper/lower fusion, nonlinear classifier gains

Proof of Section 3.4. Consider first the upper branch. Let

$$i \in S_{k+1}^U.$$

By definition of the upper-support set,

$$a_i \geq \tau_{k+1}^U.$$

Assumption 3 gives

$$\tau_{k+1}^U \geq \tau_k^U.$$

Combining both equations yields

$$a_i \geq \tau_{k+1}^U \geq \tau_k^U,$$

and hence

$$i \in S_k^U.$$

Since every element of S_{k+1}^U also belongs to S_k^U,

$$S_{k+1}^U \subseteq S_k^U.$$

Now consider the lower branch. Let

$$i \in S_{k+1}^L.$$

By definition,

$$0 < a_i \leq \tau_{k+1}^L.$$

Assumption 4 gives

$$\tau_{k+1}^L \leq \tau_k^L.$$

Therefore,

$$0 < a_i \leq \tau_{k+1}^L \leq \tau_k^L,$$

which implies

$$i \in S_k^L.$$

It follows that

$$S_{k+1}^L \subseteq S_k^L.$$

The cardinality inequalities follow because cardinality is monotone with respect to set inclusion on a finite domain.

For either branch $b \in \{U, L\}$, the inclusion

$$S_{k+1}^b \subseteq S_k^b$$

implies

$$\mathbf{1}_{\{i \in S_{k+1}^b\}} \leq \mathbf{1}_{\{i \in S_k^b\}}$$

for every $i \in \Omega$.

Finally, because P_k^b and P_{k+1}^b are diagonal binary masking matrices, their product retains only indices belonging to both supports:

$$P_{k+1}^b P_k^b = \operatorname{diag}\left(\mathbf{1}_{S_{k+1}^b} \odot \mathbf{1}_{S_k^b}\right),$$

where $\odot$ denotes component-wise multiplication. Since

$$S_{k+1}^b \subseteq S_k^b,$$

their intersection is S_{k+1}^b, and therefore

$$P_{k+1}^b P_k^b = P_{k+1}^b.$$

The projection matrices are diagonal and hence commute, giving

$$P_k^b P_{k+1}^b = P_{k+1}^b P_k^b = P_{k+1}^b.$$

□

Corollary A1. *Monotonic support-density contraction.*

Define the retained-support density of branch $b \in \{U, L\}$ at depth k as

$$\rho_k^b = \frac{|\, S_k^b \,|}{N}.$$

Then,

$$0 \leq \rho_{k+1}^b \leq \rho_k^b \leq 1.$$

Proof. The result follows by dividing the cardinality inequality in Proposition 1 by the fixed positive signal length N. □

Corollary A2. *Irreversibility of support removal.*

For either branch $b \in \{U, L\}$, if

$$i \notin S_k^b$$

at some depth k, then

$$i \notin S_j^b \text{for every} j > k.$$

Proof. For $j > k$, repeated application of Proposition 1 gives

$$S_j^b \subseteq S_{j-1}^b \subseteq \cdots \subseteq S_k^b.$$

Therefore, no index absent from S_k^b can belong to a later support set. □

This property is important conceptually because it distinguishes the LSDL trajectory from an unconstrained sequence of independently thresholded representations. The recursion imposes a consistent ordering in which support membership can transition from retained to removed but not in the reverse direction.

Corollary A3. *Finite support stabilisation.*

As Ω is finite, each branch can undergo at most N strict support contractions. Consequently, there exists an index

$$k_{\text{stab}}^b \leq \min(K, N)$$

such that either the recursion terminates before k_{stab}^b or

$$S_{k+1}^b = S_k^b \text{for all } k \geq k_{\text{stab}}^b$$

unless a later threshold crosses an additional observed amplitude level.

More precisely, let

$$\mathcal{V}(x) = \{a_i : i \in \Omega, a_i > 0\}$$

denote the finite set of distinct positive amplitudes in the signal, and let

$$M = \mid \mathcal{V}(x) \mid \leq N.$$

Then, the support of either branch can change at no more than M threshold-crossing events.

Proof. Every strict contraction removes at least one index from the retained support. Since the support initially contains no more than N indices and removed indices cannot re-enter by Corollary 2, there can be at most N strict contractions. □

A sharper statement follows from the fact that support membership changes only when the threshold crosses one or more observed amplitude values. Since the signal contains only M distinct positive amplitudes, there are no more than M distinct support transitions. Between successive threshold crossings, the support remains unchanged even if the numerical threshold continues to evolve.

Remark A1. *Weak and strict contraction.*

Proposition 1 guarantees weak contraction:

$$S_{k+1}^b \subseteq S_k^b.$$

It does not imply that every recursion step produces a strict reduction in support. Strict contraction,

$$S_{k+1}^b \subsetneq S_k^b,$$

occurs only when the interval traversed by the threshold contains at least one observed signal amplitude.

For the upper branch,

$$S_{k+1}^U \subsetneq S_k^U$$

if and only if there exists at least one index i satisfying, subject to the adopted boundary convention,

$$\tau_k^U \leq a_i < \tau_{k+1}^U.$$

For the lower branch,

$$S_{k+1}^{L} \subsetneq S_{k}^{L}$$

if and only if there exists at least one index i satisfying

$$\tau_{k+1}^{L} < a_i \leq \tau_{k}^{L}.$$

Consequently, plateau regions in the empirical support-density trajectory are compatible with the theoretical framework. They indicate that the threshold has evolved without crossing a new observed amplitude level rather than that the recursive localisation property has failed.

Remark A2. *Filtration interpretation.*

The term filtration is used here in the order-theoretic sense of a nested family of support sets indexed by recursion depth:

$$S_0^b \supseteq S_1^b \supseteq \cdots \supseteq S_K^b.$$

This construction should not be interpreted as claiming that the present formulation is equivalent to a full persistent-homology filtration involving arbitrary simplicial complexes or homological invariants. Rather, the LSDL trajectory supplies a finite amplitude-support filtration from which survival-based and persistence-inspired descriptors can subsequently be derived.

Remark A3. *Dependence on the lower-branch definition.*

The lower-branch contraction result depends critically on defining the retained lower support as

$$S^{L}(\tau) = \{i : 0 < a_i \leq \tau\}$$

together with a non-increasing threshold trajectory. If instead the lower branch were defined as

$$\{i : a_i \geq \tau\}$$

or as the complement of the upper support, the direction of the required threshold monotonicity and the resulting inclusion relations would change.

Appendix B. Unified Mathematical Notation

Table A2. Signal, operator and recursive localisation notation.

Symbol	Definition
$x(t)$	Continuous-time signal
$\mathbf{x}$	Discrete signal vector
x_n	Signal value at sample n
N	Number of signal samples
n	Sample index
$\mathbf{x}_{\text{ref}}$	Reference signal used to construct the amplitude domain
M	Maximum absolute signal amplitude
τ	Localisation threshold
τ_k^U, τ_k^L	Upper and lower thresholds at recursion depth k
τ_1^U, τ_1^L	Initial thresholds
α	Threshold-update parameter

Table A2. *Cont.*

Symbol	Definition
k	Localisation depth
K_{rec}	Maximum recursion horizon
$K_{\max}$	Maximum allowable recursion depth
B	Localisation branch (U, L)
$L_\tau^U(\cdot)$	Upper-support-localisation operator
$L_\tau^L(\cdot)$	Lower-support-localisation operator
$L_\tau^B(\cdot)$	General branch localisation operator
$L_\tau(\mathbf{x};\mathbf{x}_{\text{ref}})$	Reference-conditioned localisation operator
S_k^U, S_k^L	Upper and lower retained-support sets
m_k^B	Binary localisation mask
M_k^B	Diagonal projection (masking) matrix
$M_{0:k}^B$	Cumulative localisation mask
$\mathbf{x}_k^B$	Localised signal
P_k^B	Peak-support topology
$P_\tau^B(\cdot)$	Peak localisation operator
findpeaks$(\cdot)$	Peak detection operator
$\mathbf{1}_A$	Indicator function
$\odot$	Hadamard product
$\mathcal{I}$	Signal index set
$\mathcal{A}^+$	Distinct positive amplitude levels
J_k	Performance metric at recursion depth k
$k^\star$	Optimal localisation depth
arg max	Maximising argument
$\subseteq, \supseteq$	Set inclusion relations

Table A3. Support geometry.

Symbol	Definition
upp$(\cdot)$	Support operator
S_k	Retained-support set
P_k	Peak-support set
ρ_k	Support density
η_k	Peak density
E_0	Total signal energy
E_k	Localised signal energy
C_k	Energy concentration ratio
Γ_k	Mean retained energy density
$p_n^{(k)}$	Normalised support weight
H_k	Support entropy
$\widetilde{H}_k$	Normalised support entropy
$\mathcal{S}_k$	Hoyer sparsity index
G_k	Localisation gain
$\mathcal{M}_k$	Informative support manifold
$\|\cdot\|_1, \|\cdot\|_2, \|\cdot\|_\infty$	Manhattan, Euclidean and infinity norms
log $(\cdot)$	Natural logarithm

Table A4. Perturbation stability.

Symbol	Definition
$\widetilde{\mathbf{x}}$	Perturbed signal
ε	Additive perturbation
δ	Perturbation bound

Table A4. *Cont.*

Symbol	Definition
$\widetilde{S}_k$	Perturbed support
$\widetilde{P}_k$	Perturbed peak-support set
$\widetilde{E}_k$	Perturbed localised energy
J_k	Jaccard support similarity
R_k	Peak-survival ratio
D_k	Energy-deviation ratio
Σ_k	Composite stability score

Table A5. Discriminative geometry.

Symbol	Definition
c	Class index
C	Number of classes
N_c	Samples in class c
$\mathbf{z}_{i,k}^{(c)}$	LSDL feature vector
$\phi_k(\cdot)$	Feature embedding map
d	Feature dimension
$\widetilde{S}_k$	Median retained-support cardinality
$S_{\min}$	Minimum support floor
$\mathcal{A}$	Admissible localisation set
μ_c	Class centroid
μ	Global centroid
S_W	Within-class scatter matrix
S_B	Between-class scatter matrix
Λ_k	Fisher-style separability
Λ_0	Raw baseline separability
$\mathrm{tr}(\cdot)$	Matrix trace
RI	Resolution Index
$k_{RI}^{\star}$	RI-optimal localisation depth
$\tau^{\star}$	Optimal threshold

Table A6. Information geometry.

Symbol	Definition
I_k	Information concentration ratio
H_0	Original support entropy
Ω_k	Energy–information concentration
D_k	Information density
Y	Class-label random variable
Z_k	Feature representation
MI_k	Mutual information
JS_k	Jensen–Shannon divergence
$I(\cdot;\cdot)$	Mutual-information operator

Table A7. Persistence geometry.

Symbol	Definition
$b(p)$	Birth depth
$d(p)$	Death depth
$l(p)$	Persistence lifetime

Table A7. *Cont.*

Symbol	Definition
$a_p(k)$	Peak-amplitude trajectory
$\pi_E(p)$	Persistence energy
r_p	Normalised persistence weight
H_Π	Persistence entropy
I_Π	Persistence concentration
$\Pi(\mathbf{x})$	Persistence representation
$\psi(\mathbf{x})$	Persistence feature vector
$l_{\max}$	Maximum persistence lifetime
$\bar{l}$	Mean persistence lifetime
Λ_Π	Persistence separability

Table A8. Spectral geometry.

Symbol	Definition
$X(\omega)$	Fourier spectrum
$\hat{X}_k(\omega)$	Localised Fourier spectrum
$P_k(\omega)$	Spectral-power density
Ω_k	Spectral support
$\rho_{\Omega,k}$	Spectral-support density
$H_{\Omega,k}$	Spectral entropy
$\widetilde{H}_{\Omega,k}$	Normalised spectral entropy
$I_{\Omega,k}$	Spectral information concentration
$G_{\Omega,k}$	Spectral localisation gain
$\omega_k^\star$	Dominant frequency
$\zeta_k(\cdot)$	Spectral embedding
$\Lambda_{\Omega,k}$	Spectral separability

Table A9. Unified multi-geometric representation.

Symbol	Definition
Φ_T	Time–amplitude (support) geometry
Φ_I	Information geometry
Φ_P	Persistence geometry
Φ_Ω	Spectral geometry
Ψ_k^U	Upper-branch multi-geometric representation
Ψ_k^L	Lower-branch multi-geometric representation
Ψ_k^{fusion}	Upper-lower fused representation
Ψ_{LSDL}	Unified LSDL representation
$k_{RI}^\star$	RI-optimal localisation depth
$k_{MI}^\star$	MI-optimal localisation depth
$k_{\text{clf}}^\star$	Classifier-optimal localisation depth
$C(\Psi)$	Cross-validated classifier performance
Φ_0	Raw baseline representation
$[\cdot]$	Feature concatenation operator

Table A10. Comparative representation frameworks.

Symbol	Definition
$X(t,\omega)$	Short-time Fourier Transform
$w(\cdot)$	STFT analysis window
$W(a,b)$	Continuous wavelet coefficient
a, b	Wavelet scale and translation
$\psi(\cdot)$	Mother wavelet

Table A10. *Cont.*

Symbol	Definition
IMF_m	m-th intrinsic mode function
M_{IMF}	Number of intrinsic mode functions
$r(t)$	Residual component (EMD)
D_{dict}	Sparse dictionary
$\boldsymbol{\alpha}$	Sparse coefficient vector
λ	Sparsity regularisation parameter
F_k	Filtration element
K_{fil}	Number of filtration levels
(b_i, d_i)	Birth–death coordinates
l_i	Persistence lifetime
X, Y, Z	Information Bottleneck variables
β	Information Bottleneck trade-off parameter
z_L	Deep latent representation
$f_l(\cdot)$	Deep-network mapping
L	Number of network layers
$\circ$	Function composition
K_{VMD}	Number of VMD modes
N_{iter}	Number of optimisation iterations
OMP	Orthogonal Matching Pursuit

References

1. Allen, J. Short term spectral analysis, synthesis, and modification by discrete Fourier transform. *IEEE Trans. Acoust. Speech Signal Process.* **1977**, *25*, 235–238. [CrossRef]
2. Bengio, Y.; Courville, A.; Vincent, P. Representation Learning: A Review and New Perspectives. *IEEE Trans. Pattern Anal. Mach. Intell.* **2013**, *35*, 1798–1828. [CrossRef] [PubMed]
3. Boashash, B. (Ed.) *Time-Frequency Signal Analysis and Processing: A Comprehensive Reference*, 2nd ed.; Academic Press: Amsterdam, The Netherlands, 2016.
4. Cohen, L. *Time-Frequency Analysis*; Prentice Hall Ptr: Englewood Cliffs, NJ, USA, 1995.
5. Daubechies, I. *Ten Lectures on Wavelets*; Society for Industrial and Applied Mathematics (SIAM): Philadelphia, PA, USA, 1992.
6. Gabor, D. Theory of Communication. *J. Inst. Electr. Eng.—Part III Radio Commun. Eng.* **1946**, *93*, 429–457. [CrossRef]
7. Atkinson, I.C.; Kamalabadi, F. Basis selection for wavelet processing of sparse signals. *Signal Process.* **2008**, *88*, 2340–2345. [CrossRef]
8. Mallat, S.G. A theory for multiresolution signal decomposition: The wavelet representation. *IEEE Trans. Pattern Anal. Mach. Intell.* **1989**, *11*, 674–693. [CrossRef]
9. Nsugbe, E. Particle Size Distribution Estimation of a Powder Agglomeration Process Using Acoustic Emissions. Ph.D. Thesis, Cranfield University, Cranfield, UK, 2018.
10. Nsugbe, E.; Samuel, O.W.; Asogbon, M.G.; Li, G. Contrast of multi-resolution analysis approach to transhumeral phantom motion decoding. *CAAI Trans. Intell. Technol.* **2021**, *6*, 360–375. [CrossRef]
11. Aharon, M.; Elad, M.; Bruckstein, A.M. K-SVD: An Algorithm for Designing Overcomplete Dictionaries for Sparse Representation. *IEEE Trans. Signal Process.* **2006**, *54*, 4311–4322. [CrossRef]
12. Edelsbrunner, H.; Letscher, D.; Zomorodian, A. Topological Persistence and Simplification. *Discret. Comput. Geom.* **2002**, *28*, 511–533. [CrossRef]
13. Fourier, J. *Théorie Analytique De La Chaleur*; Firmin Didot Père et Fils: Paris, France, 1822.
14. Kullback, S.; Leibler, R.A. On Information and Sufficiency. *Ann. Math. Stat.* **1951**, *22*, 79–86. [CrossRef]
15. Nsugbe, E. Novel uterine contraction signals decomposition for enhanced preterm and birth imminency prediction. *Intell. Syst. Appl.* **2022**, *16*, 200123. [CrossRef]
16. Olshausen, B.A.; Field, D.J. Emergence of simple-cell receptive field properties by learning a sparse code for natural images. *Nature* **1996**, *381*, 607–609. [CrossRef] [PubMed]
17. Perea, J.A.; Harer, J. Sliding Windows and Persistence: An Application of Topological Methods to Signal Analysis. *Found. Comput. Math.* **2014**, *15*, 799–838. [CrossRef]
18. Roweis, S.T.; Saul, L.K. Nonlinear Dimensionality Reduction by Locally Linear Embedding. *Science* **2000**, *290*, 2323–2326. [CrossRef] [PubMed]

19. Shannon, C.E. A Mathematical theory of communication. *Bell Syst. Tech. J.* **1948**, *27*, 379–423. [CrossRef]
20. Nsugbe, E.; Sanusi, I. Towards an affordable magnetomyography instrumentation and low model complexity approach for labour imminency prediction using a novel multiresolution analysis. *Appl. AI Lett.* **2021**, *2*, e34. [CrossRef]
21. Nsugbe, E.; Connelly, S. Multiscale depth of anaesthesia prediction for surgery using frontal cortex electroencephalography. *Healthc. Technol. Lett.* **2022**, *9*, 43–53. [CrossRef] [PubMed]
22. Nsugbe, E.; Phillips, C.; Fraser, M.; McIntosh, J. Gesture Recognition for Trans-Humeral Prosthesis Control Using EMG and NIR. *IET Cyber-Syst. Robot.* **2020**, *2*, 122–131. [CrossRef]
23. Nsugbe, E.; Al-Timemy, A.H. Shoulder girdle recognition using electrophysiological and low frequency anatomical contraction signals for prosthesis control. *CAAI Trans. Intell. Technol.* **2021**, *7*, 81–94. [CrossRef]
24. Axler, S. *Linear Algebra Done Right*, 3rd ed.; Springer: Cham, Switzerland, 2015; ISBN 978-3-319-11079-0.
25. Conway, J.B. *A Course in Functional Analysis*, 2nd ed.; Springer: New York, NY, USA, 1990; ISBN 978-0-387-97245-9.
26. Krilova, N.; Kastalskiy, I.; Kazantsev, V.B.; Makarov, V.A.; Lobov, S. *EMG Data for Gestures [Dataset]*; UCI Machine Learning Repository: Irvine, CA, USA, 2019. [CrossRef]
27. Jaccard, P. Étude comparative de la distribution florale dans une portion des Alpes et des Jura. *Bull. Société Vaudoise Sci. Nat.* **1901**, *37*, 547–579. [CrossRef]
28. Bishop, C.M. *Pattern Recognition and Machine Learning*; Springer: New York, NY, USA, 2006.
29. Duda, R.O.; Hart, P.E.; Stork, D.G. *Pattern Classification*, 2nd ed.; John Wiley & Sons: New York, NY, USA, 2001.
30. Fisher, R.A. The use of multiple measurements in taxonomic problems. *Ann. Eugen.* **1936**, *7*, 179–188. [CrossRef]
31. Rilling, G.; Flandrin, P.; Gonçalvès, P. On empirical mode decomposition and its algorithms. In Proceedings of the IEEE-EURASIP Workshop on Nonlinear Signal and Image Processing (NSIP), Grado, Italy, 8–11 June 2003.
32. Nazari, M.; Sakhaei, S.M. Successive variational mode decomposition. *Signal Process.* **2020**, *174*, 107610. [CrossRef]

Disclaimer/Publisher's Note: The statements, opinions and data contained in all publications are solely those of the individual author(s) and contributor(s) and not of MDPI and/or the editor(s). MDPI and/or the editor(s) disclaim responsibility for any injury to people or property resulting from any ideas, methods, instructions or products referred to in the content.